2016

Acoustic Behavior Of Soil Reinforced With Grass Roots

Blake Armstrong
University of Mississippi

ACOUSTIC BEHAVIOR OF SOIL REINFORCED WITH GRASS ROOTS

A Thesis
presented in partial fulfillment of requirements
for the degree of Master of Science
in the Department of Geological Engineering
The University of Mississippi

by

BLAKE O. ARMSTRONG

May 2016

ABSTRACT

Civil engineering practice has shown that vegetative roots on slopes and streambanks can substantially increase shear strength of soil and reduce erosion. Research has been done to understand and quantify the effect. Most studies have been conducted on slopes and streambanks with woody vegetation. Past research has used a perpendicular root model to predict increase in cohesion, or shear strength, due to the mobilization of roots' tensile strength. Acoustics can be used to monitor internal changes of soil by interacting with soil particles and interstitial fluids. Compressional wave, or p-wave, velocity can be used to predict changes in effective stress and bulk density which can be related to geotechnical parameters such as cohesion and porosity. A literature review has concluded that an acoustic based apparatus capable of predicting increased cohesion due to grass root growth would be beneficial to geotechnical engineers and soil scientists. The goals of this study include: measuring changes in the acoustic response of soil reinforced with grass roots, modeling and measuring the effect of grass root reinforcement on the soil cohesion, and relate soil cohesion to p-wave velocity in soil reinforced with grass roots. For a laboratory experiment, two types of Bermuda grass (*Cynodon dactylon*) and Bahia grass (*Paspalum notatum*) were planted with a bare soil quadrant for control. Acoustic measurements during a year of grass root growth showed a 90% increase in p-wave velocity. A comparison of the modeled acoustic response using independently measured root density and cohesion (from direct shear tests) to in-

situ measured p-wave velocity was explored. Two models were presented to explain the increase in p-wave velocity: increase in cohesion with no settlement and increase in cohesion including settlement. For the case with no settlement, the required root cohesion to explain the velocity increase was from 500 to 40,000 kPa. With the inclusion of settlement the range of required root cohesion was from 50 to 25,000 kPa.

DEDICATION

This thesis is dedicated to my family for all of their support throughout my education, to my mother and father for raising me to believe that I could do anything with true dedication, and to my brother for inspiring me to pursue engineering. I also want to dedicate this thesis to my love Angelica for standing by me and keeping me focused and motivated.

LIST OF ABBREVIATIONS AND SYMBOLS

NCPA	National Center for Physical Acoustics
USDA	United States Department of Agriculture
NRCS	Natural Resources Conservation Service
MASW	multichannel analysis of surface waves
JET	jet erosion test
HET	hole erosion test
SET	slot erosion test
EFA	erosion function apparatus
LDV	laser-doppler vibrometer
TDR	time domain reflectometer
FLAC	fast lagrangian analysis of continua
CPT	cone penetrometer tests
SSCC	suction stress characteristic curve
SWCC	soil-water characteristic curve
RD	root density
RAR	root area ratio
RLD	root length density
$RCSA$	mean cross-sectional area of a single root

d_r	mean diameter of roots
L_R	length of the root
M_R	mass of the roots
V	volume of sample
c	total cohesion of soil reinforced by grass roots
c'	cohesion of soil
c_r	cohesion due to the presence of grass roots
ϕ	internal friction angle of the soil
V_p	compressional wave velocity
ρ_b	bulk density
ρ_d	dry density
ρ_g	grain density
ρ_w	density of water
ρ_a	density of air
K_{eff}	effective bulk modulus
K_o	bulk modulus of the grains
K_{matrix}	bulk modulus of the skeletal matrix
K_{pore}	bulk modulus of the porespace
K_{water}	bulk modulus of water
K_{air}	bulk modulus of air

G_{eff}	effective shear modulus
G_{matrix}	shear modulus of the skeletal matrix
G	shear modulus of grains
ν	Poisson's ratio of grains
σ'	total effective stress
σ	overburden stress
σ'_s	soil suction stress
σ_{co}	apparent tensile stress at the saturated state
n_c	grain coordination number
n	porosity
e	void ratio
α, n_v	van Genuchten's empirical fitting parameters
S	degree of saturation
S_e	effective saturation
θ	volumetric moisture content
θ_r	residual volumetric moisture content
θ_s	saturated volumetric moisture content
ψ	matric suction
h	depth of the testing point
g	gravitational acceleration

q_c	cone tip resistance
τ	undrained shear strength from direct shear test
$S_u(fv)$	undrained field vane shear strength
t_r	tensile strength of roots
a, b	empirical fitting parameters for power law relationship
x	transducer spacing

ACKNOWLEDGEMENTS

I'd like to acknowledge: my research adviser Dr. Craig Hickey, Dr. Zhiqu Lu for helping us get this project started, Dr. Louis Zachos and Dr. Joel Kuszmaul my academic advisers, Dr. Sara Brown for providing me the opportunity to continue my education and Dr. Zhen Guo for being on my committee. Thanks to the United States Department of Agriculture (USDA) for the funding under Award 58-6408-1-608. I'd also like to acknowledge the USDA Agricultural Research Service, National Sedimentation Laboratory for assistance throughout this experiment, Dr. Daniel Wren for the soil and access to the drying trailer and grinder, and Mick Ursic for access to the direct shear machine. I'd also like to acknowledge NCPA's machine shop for building the box, J. D. Heffington for help building and performing tests, and Leti Wodajo for help with various challenges along the way.

TABLE OF CONTENTS

LIST OF TABLES

LIST OF FIGURES

CHAPTER I: INTRODUCTION

1.1 OVERVIEW

In the last 50 years, designs of critical watershed infrastructure have evolved to accommodate the steady increase in demand for fresh water and other natural resources. Dams have assisted in providing an economic supply of fresh water, flood management, and soil conservation (Richardson, 2001). Overtopping erosion accounts for 34 % of all earthen dam failures. Grass roots have commonly been used to strengthen slopes and spillways, decrease the erodibility of embankment surfaces and streambanks. New technologies for monitoring the performance of existing dams must be developed to secure the availability of water resources.

Most traditional methods for characterizing soil erosion involve invasive methods and laboratory tests. Flume tests have been used to study overtopping on grass-covered soils by running water on the soil surfaces (Powledge et al., 1989). In 1990, a jet erosion test (JET) was developed to characterize erosion resistance on spillways (Hanson and Cook, 2004). The erodibility of the soil is characterized by the critical shear stress and the erodibilty coefficient. The critical shear stress is the minimum stress that must be applied to a soil for erosion to take place. The erodibility coefficient describes the rate of erosion due to hydraulic stresses in excess of the critical stress. Increasing the shear strength of soil can help decrease erodibility.

The presence of grass roots has been known to increase the cohesion (c) which is an indicator of the shear strength of soil (De Baets et al., 2008). Wu et al. (1979)

developed a simple perpendicular root model to predict increased cohesion in soils due to the presence of roots. Grass root reinforcement adds tensile strength of the roots to the soil's shear strength. Root area ratio (RAR) and the tensile strength of the root (t_r) are the main components of cohesion due to grass roots (c_r). It has also been shown that an increase in root density (RD) increases the magnitude of shear strength in soils (Tengbeh, 1989).

Typical engineering methods of measuring mechanical behavior of soils are invasive. These methods include laboratory test from core samples, cone penetrometer, field shear vane, tensiometers, and many others. In recent years acoustic methods have been developed to study soil wetting, compaction, and other processes (Berkenhagen et al., 1998; Lu et al., 2004; Whalley et al., 2012). These acoustic methods utilize the mechanics of stress waves to measure soil properties. Unsaturated soils are considered granular materials, or porous media. The soil consists of a skeletal matrix of soil particles and two pore fluids, water and air. The mechanical behavior of the media can be defined by the grain properties (bulk and shear moduli and density), the external and inter-particle forces (overburden pressure, matric suction, and cohesion), and the makeup of the porespace (porosity and saturation).

The acoustic approach has the benefit of being non-invasive and can be performed in both the field and laboratory. Acoustic waves traveling through soil interact with the soil particles and interstitial fluids. Acoustic deformations are small strain phenomena on the order of microns. Introducing small propagating waves does not alter the fabric of the soil, so the propagation is considered a constant-fabric

deformation of the soil and can therefore be used to monitor ongoing internal changes of the soil. Some of the properties that affect the acoustic response include: bulk and shear moduli of the particles, grain density, effective stress, cohesive forces, matric suction, saturation and porosity. These can be related using Biot(1962)-Gassmann(1951) and Hertz(1882)-Mindlin(1949) theories.

Biot-Gassmann theory of p-waves uses fluid separation to define the stress waves in porous medium that is partially saturated with two fluids, water and air. Since the pore contents of unconsolidated sediments have practically no shear resistance, the effective shear modulus of the soil is equal to the shear modulus of the skeletal matrix. Hertz-Mindlin theory of granular material treats soil as a skeletal matrix based on the packing of grains. The grains have external and inter-particle forces that make up the effective stress.

Effective stress is made up of three components: overburden pressure, soil suction, and the apparent tensile stress (or cohesive stress) (Lu and Likos, 2006). Overburden is a function of bulk density and the depth of interest. Since the depth of the measurements was constant for the experiment in this thesis, the overburden pressure is constant if there is no settlement. Soil suction stress is a function of matric suction which arises from capillary forces pulling particles together in unsaturated soil. The relation between matric suction and soil suction stress can be derived from van Genutchen's (1980) fitting parameters for a given soil-water characteristic curve. Matric suction was measured to be constant using tensiometers throughout this experiment. Apparent tensile stress is a function of cohesion and internal friction angle. As

mentioned above, cohesion is known to increase as a function of root growth. If cohesion increases, the cohesive stress increases and in turn increases the effective stress of the soil. An increase in effective stress will increase the bulk and shear moduli of the media, and the p-wave velocity will increase.

As soil sits, settlement will occur. Settlement is a reduction in the volume of the porespace, or a decrease in porosity of the soil. In clays such as smectite, the grains themselves can shrink or expand during drying or wetting, respectively. For this experiment during the development of roots, the water level in the soil remained constant, so we did not expect to experience any shrinking or expanding. If the moisture content remains constant while the porosity decreases, the saturation of the soil will effectively increase. When settlement occurs, the easily compressible air is pushed out. The porespace is then filled with less compressible water. This decreases the compressibility of the media substantially, increasing the p-wave velocity with every small increase of saturation. In this experiment the assumption was made that the soil was near full saturation and settlement occurred which assisted in the increase in p-wave velocity.

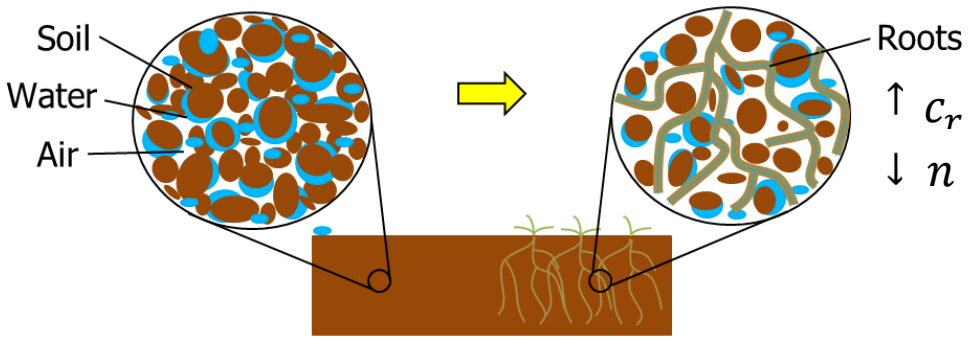

Figure 1.1 Effect of settlement and roots on geotechnical properties

This study assesses the feasibility of an acoustic method to monitor changes in the p-wave velocity of the soil as a function of grass root growth and settlement. Wu et al. (1979) made the observation that the presence of roots will increase the soil's cohesion by lending tensile reinforcement from the roots. The settlement is also assumed to increase velocity due to a decrease in porosity. Decrease in porosity with a constant moisture content increases the incompressibility of the porespace by pushing air out and replacing with less compressible water. The increase in cohesion and decrease in porosity will be reflected in the acoustic behavior of soils.

1.2 OBJECTIVES

The objectives of this laboratory experiment are listed below.

1. Assess the feasibility of measuring changes in the acoustic response of soils as a function of grass root growth and settlement.
2. Model the effect of grass root reinforcement on the cohesion of soil and the effect of settlement on the saturation of the soil.
3. Measure the effect of grass root reinforcement on the cohesion of soils and predict the effect of settlement on the saturation of the soil.
4. Relate the increase in cohesion, due to grass root reinforcement, to increases in p-wave velocity, due to grass root reinforcement, and relate increase in saturation due to decrease in porosity, or settlement, and increase in velocity.

CHAPTER II: THEORY

2.1 ACOUSTICS OF SOIL

Gassman's (1951) theory of stress waves in single fluid saturated porous medium can be used to relate the p-wave velocity in the low frequency limit to effective moduli and density of the porous medium as

$$V_p = \sqrt{\frac{K_{eff} + \frac{4}{3}G_{eff}}{\rho_b}} \tag{2.1}$$

where:

V_p = compressional wave velocity (m/s)

K_{eff} = effective bulk modulus (Pa)

G_{eff} = effective shear modulus (Pa)

ρ_b = bulk density (kg/m^3).

Biot's (1962) theory uses fluid separation to explain stress waves in a porous medium that is partially saturated with two fluids (ie. water and air). The bulk density (ρ_b) can be expressed as the three component densities weighted by degree of saturation (S) and porosity (n),

$$\rho_b = n(S\rho_w + (1-S)\rho_a) + (1-n)\rho_g. \tag{2.2}$$

Biot-Gassmann theory can be implemented to calculate effective moduli, K_{eff} and G_{eff} , of the porous material (Mavko et al., 2009) using

$$\frac{K_{eff}}{K_o - K_{eff}} = \frac{K_{matrix}}{K_o - K_{matrix}} + \frac{K_{pore}}{n(K_o - K_{pore})} \tag{2.3}$$

and

$$G_{eff} = G_{matrix} \tag{2.4}$$

where:

K_o = bulk modulus of the grains (Pa)

K_{matrix} = elastic modulus of the matrix (Pa)

K_{pore} = bulk modulus of the porespace (Pa)

G_{matrix} = shear modulus of the skeletal matrix (Pa).

The bulk modulus of the porespace filled with water and air is expressed as a weighted isostress average of the constituents

$$\frac{1}{K_{pore}} = \frac{S}{K_{water}} + \frac{1 - S}{K_{air}} \tag{2.5}$$

where:

K_{water} = bulk modulus of water (Pa)

K_{air} = bulk modulus of air (Pa).

Since soils are composed of a granular matrix, the Hertz-Mindlin theory (Hertz, 1882; Mindlin, 1949) expresses the moduli of the skeletal matrix based upon a model of a packing of spheres to be

$$K_{matrix} = \sqrt[3]{\frac{{n_c}^2(1-n)^2G^2}{18\pi^2(1-\nu)^2}\sigma'} \tag{2.6}$$

$$G_{matrix} = \frac{5 - 4\nu}{5(2 - \nu)} \sqrt[3]{\frac{3{n_c}^2(1 - n)^2 G^2}{2\pi^2(1 - \nu)^2}\sigma'} \tag{2.7}$$

where:

n_c = grain coordination number

n = porosity

G = grain shear modulus (Pa)

ν = grain Poisson's ratio

σ' = total effective stress (Pa).

The grain coordination number is six for a simple cubic packing and 12 for hexagonal close packing of identical spheres. For the current soil model the grains are assumed to be in simple cubic packing, so that the grain coordination number is assumed to be six. With this coordination number, the porosity should be about 0.48 (Cho et al., 2006). If the solid grains are assumed to be clay, then the grain Poisson's ratio and grain shear modulus are 0.14 and 1.5×10^9 Pa, respectively (Mavko et al., 2009). Under these assumptions the effective moduli are solely a function the effective stress.

2.2 SOIL STRESSES

The effective stress is traditionally defined as the difference between net overburden stress (σ) and excess pore water pressure (u) (Terzaghi, 1943),

$$\sigma' = \sigma - u. \tag{2.8}$$

Effective stress can be extended to include more specific fluid related stresses in a partially saturated soil. The generalization includes two components: soil suction stress (σ'_s) and apparent tensile stress at the saturated state caused by cohesive and physicochemical forces (σ'_{co}) (Lu and Likos, 2006) so that

$$\sigma' = \sigma + \sigma'_s + \sigma_{co}. \tag{2.9}$$

Net overburden stress is the product of bulk density, gravitational acceleration (g), and the depth below the soil surface (h),

$$\sigma = \rho_b g h. \tag{2.10}$$

In the current experiment, depth below the soil surface is the depth the transducers are buried, 0.1 m. The work of van Genuchten (1980) is commonly used to empirically fit capillary pressures and water saturations for different sediments. Soil suction stress can be derived from van Genuchten's fitting parameters for soil-water characteristic curves (SWCC) (Song et al., 2012),

$$\sigma'_s = \frac{S_e}{\alpha}\left(S_e^{\frac{n_v}{1-n_v}} - 1\right)^{\frac{1}{n_v}} \cdot 1000 \tag{2.11}$$

where:

S_e = effective saturation

α and n_v = van Genuchten empirical fitting parameters.

Effective saturation can be estimated using van Genuchten fitting parameters and matric suction

$$S_e = \frac{\theta - \theta_r}{\theta_s - \theta_r} = \left[\frac{1}{1 + \left[\alpha\left(\frac{\psi}{1000}\right)\right]^{n_v}}\right]^{\frac{n_v - 1}{n_v}} \quad (2.12)$$

where:

θ = volumetric moisture content

θ_r = residual volumetric moisture content

θ_s = saturated volumetric moisture content

ψ = matric suction (Pa).

The first equation is the definition of effective saturation, and the second uses van Genuchten's fitting method. The apparent tensile stress at the saturated state caused by cohesive and physicochemical forces can be estimated using (Song et al., 2012)

$$\sigma_{co} = \frac{c' + c_r}{tan\phi} \quad (2.13)$$

where:

c' = cohesion of soil (Pa)

c_r = cohesion due to the presence of roots (Pa)

ϕ = internal friction angle (degrees).

The stresses can be represented as a Mohr Coulomb failure envelope shown in Figure 2.1.

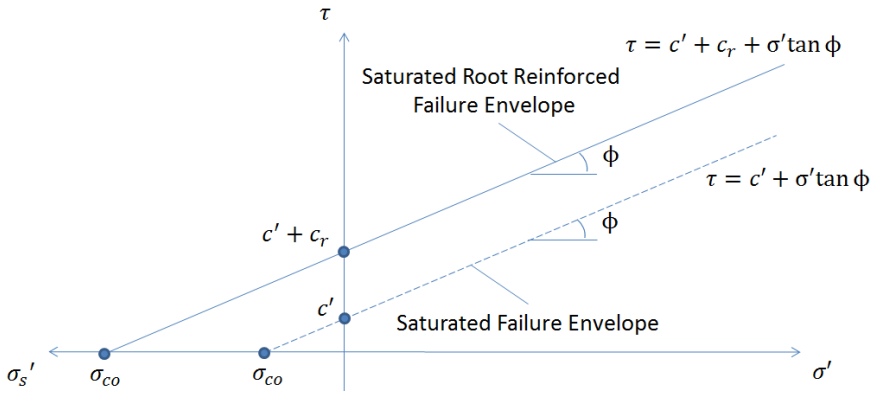

Figure 2.1 Illustration of stresses in Mohr Coulomb failure envelope

This is a linear relationship between maximum shear stress (τ) and effective normal stress (σ') in the soil at failure. The cohesion (c) is the shear stress at zero effective normal stress. In this work, the assumption is made that the cohesion is the only parameter affected by the presence of roots.

2.2 ROOT REINFORCEMENT OF SOIL

Soils reinforced with roots have been more resistant to soil erosion compared to bare soils (Pollen et al., 2005). The roots add tensile strength to resist erosion of the soil which in turn increases the soil's shear strength (τ), or cohesion (c). The model below utilizes the tensile strength of roots (t_r), the root area ratio (RAR), and the root density (RD) to predict the increase in cohesion (c) of soils. Wu et al. (1979) developed a simple perpendicular root model to evaluate cohesion due to roots (c_r). The tensile strength of roots per unit area and the angle of shear distortion (θ) are shown in Figure 2.2.

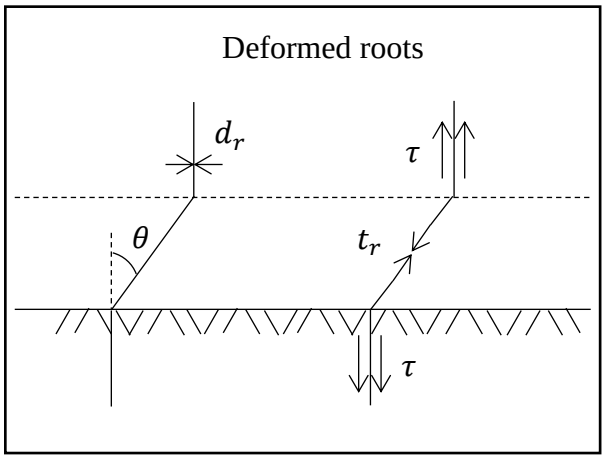

Figure 2.2 Simple perpendicular root model (Wu et al., 1979)

The tensile strength of roots is weighted by the root area ratio which is the area of the roots divided by the total area of the sample. Wu's et al. (1979) original equation to predict root cohesion is shown in Equation 2.14. The internal friction angle

of the soil is denoted by ϕ in

$$c_r = t_r RAR(sin\theta + cos\theta tan\phi). \quad (2.14)$$

Wu noticed that the values of the root cohesion showed small variation with a range of the shear distortion angle and internal friction angle (Wu et al., 1979). In the same paper that introduced the simple perpendicular root model, the equation was simplified. The term in parentheses was assumed to be a constant of 1.2 giving

$$c_r = 1.2 t_r RAR. \quad (2.15)$$

De Baets et al. (2008) measured root diameter and tested the tensile strength of roots. A power law relationship was then established between the root diameter and the root's tensile strength

$$t_r = a{d_r}^{-b}. \quad (2.16)$$

Cheng et al. (2003) measured the tensile strength of Bahia and Bermuda roots as a function of root diameter (Figure 2.3). The parameters a and b were equal to 12955 and 0.568, and 14719 and 0.877 for Bermuda and Bahia grass, respectively. The range of tensile strengths measured for Bahia grass roots is from 13000 to 25000 kPa, and the range for Bermuda grass is from 10000 to 17000 kPa.

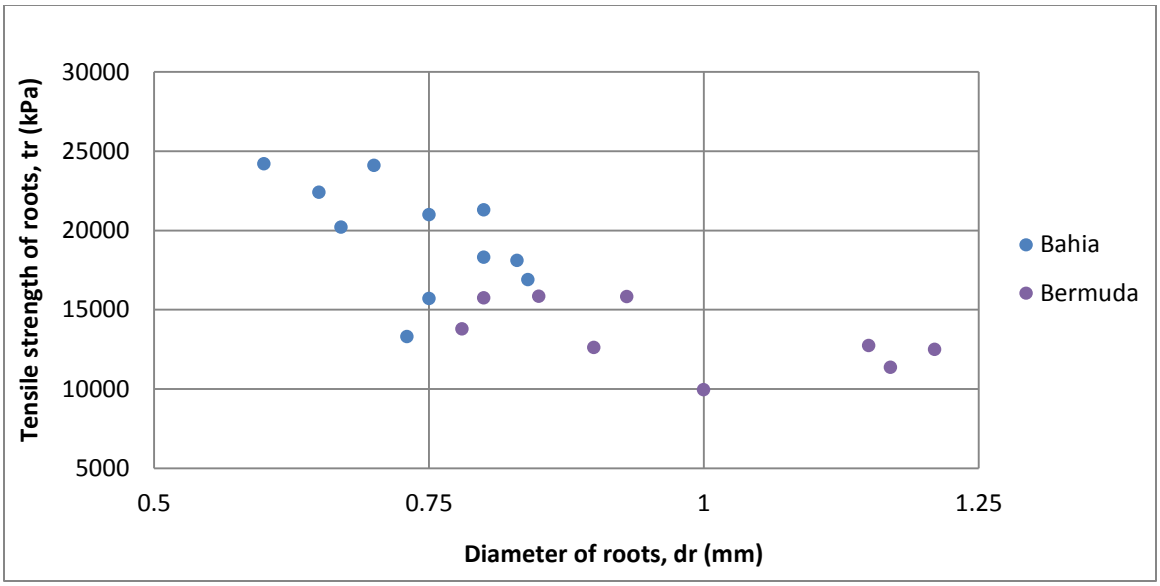

Figure 2.3 Cheng et al. (2003) power law relationship

Root density is the mass of dried roots (M_R) divided by the volume of the soil reinforced (V),

$$RD = \frac{M_R}{V}. \tag{2.17}$$

In order to relate root density to root area ratio, the assumption was made that the lengths of the roots are equal to the total length of the sample. This allows root area ratio to be equal to root volume ratio, and root density can be related to root area ratio through root tissue density,

$$\mathrm{RD} = \mathrm{RTD} \cdot \mathrm{RAR}. \tag{2.18}$$

Average root tissue density was assumed to be that of an average fine root tissue density of roots from a field-community in shallow soil and was equal to 315 kg/m³ (Birouste et al., 2014).

2.3 PARAMETERIZATION

Many parameters had to be determined through assumptions and measurements. A prepared sample of the same soil was tested before the acoustic measurements to determine geotechnical properties before sod was planted. Tests on a prepared sample of the same soil yielded an average, estimated porosity equal to 0.57. It is probable that roots can alter bulk density by filling or creating water and air voids. With the complexity of the mechanics of grass growth, the assumption was made that bulk density does not change as a function of grass root growth. The only parameters assumed to be affected are root cohesion due to the mobilization of tensile strength and porosity due to settlement.

A water characteristic curve was not measured but predicted using van Genuchten empirical parameters for silt, α and n_v, are 0.052/m and 2.003, respectively. The matric suction was measured after the sod was planted during acoustic tests using Soil Moisture tensiometers (#2710ARL06-L, www.soilmoisture.com) and remained fairly constant at 3000 Pa. Using van Genutchen's model with a constant matric suction of 3000 Pa, the resulting effective saturation was constant at 0.99.

Typical limiting volumetric moisture contents, θ_r and θ_s, for a silty clay loam are 0.10 and 0.55, respectively (Leij et al., 1996). The actual moisture content was measured after the sod was planted during acoustic tests with a Stevens HydraProbeII (#93640, www.stevenswater.com) and remained fairly constant at 0.45. Using the predicted effective saturation and the measured volumetric moisture content, the porosity is

calculated to by 0.45 which is close to the measured value of 0.47.

Low matric suction means that soil suction stress was not a major component of effective stress. The suction stress was predicted to be 3000 Pa from the measured matric suction of 3000 Pa and the fitting parameters. Since volumetric moisture content and matric suction have been measured to remain constant, soil suction stress must have been constant. If there was no settlement, overburden stress remained constant at 1800 Pa throughout the acoustic tests. If settlement was included in the model, bulk density would increase due to a decrease in porosity.

At the end of the experiment, core samples were taken from each quadrant of the same box. Direct shear tests were performed on core samples. Average total cohesion of the reinforced soil and internal friction angle were 11000 Pa and 32°, respectively. Cohesion of the soil was assumed only to change due to the presence of roots. A common assumption in the literature is internal friction angle is unaffected by root growth (Operstein et al., 2000). If there was no settlement and soil suction stress was constant, changes in effective stress was solely a function of changes in cohesion due to the presence of roots. If there was settlement and soil suction stress was constant, changes in effective stress was a function of changes in cohesion due to roots, and changes in saturation was a function of changes in porosity and moisture content.

The soil model in this thesis consisted of a solid granular matrix composed of clay minerals saturated with a mixture of air and water. A complete list of initial and final parameter values are presented in Tables 2.1 and 2.2.

Table 2.1 Initial parameters

Symbol	Parameter	Value	Comment	Vary with Grass Growth
c'	Soil cohesion	2000 Pa	Measured with direct shear tests	Yes
c_r	Root cohesion	0 Pa	Measured with direct shear tests	Yes
ϕ	Internal friction angle	32 °	Measured with direct shear tests	No
σ_{co}	Cohesive stress	3200 Pa	Calculated with Equation 2.13	Yes
ψ	Matric suction	3000 Pa	Measured with tensiometers	No
θ	Volumetric moisture content	0.45	Measured with HydraProbeII	Yes
w	Gravitational moisture content	0.32	Measured	Yes
α	van Genutchen's empirical fitting parameters	0.052 m^{-1}	Assumed constant	No
n_v		2.003		No
S_e	Effective saturation	0.99	Calculated with Equation 2.12	No
σ'_s	Soil suction stress	3000 Pa	Calculated with Equation 2.11	No
ρ_b	Bulk density	1790 kg/m³	Measured	No
g	Gravitational constant	9.81 m/s²	Assumed constant	No
h	Depth	0.1 m	Depth of transducers	No
σ	Overburden stress	1800 Pa	Calculated with Equation 2.10	No
σ'	Effective stress	7900 Pa	Calculated with Equation 2.9	Yes
ν	Poisson's ratio	0.14	Assumed constant	No
G	Grain shear modulus	1.5×10^9 Pa	Assumed constant	No
n	Porosity	0.57	Measured	Yes

Symbol	Parameter	Value	Comment	Vary with Grass Growth
n_c	Coordination number	6	Assumed constant	No
K_{air}	Air bulk modulus	1.01×10^5 Pa	Assumed constant	No
K_{water}	Water bulk modulus	2.15×10^9 Pa	Assumed constant	No
S	Saturation	0.79	Measured	Yes
K_{pore}	Bulk modulus of porespace	4.8×10^5 Pa	Calculated with Equation 2.5	Yes
G_{matrix}	Shear modulus of skeletal matrix	1.4×10^7 Pa	Calculated with Equation 2.7	Yes
K_{matrix}	Bulk modulus of skeletal matrix	9.4×10^6 Pa	Calculated with Equation 2.6	Yes
K_o	Grain bulk modulus	2.50×10^{10} Pa	Assumed constant	No
G_{eff}	Effective shear modulus	1.4×10^7 Pa	Calculated with Equation 2.4	Yes
K_{eff}	Effective bulk modulus	1.0×10^7 Pa	Calculated with Equation 2.3	Yes
ρ_g	Grain density	2550 kg/m³	Assumed constant	No
ρ_a	Air density	1.22 kg/m³	Assumed constant	No
ρ_w	Water density	1000 kg/m³	Assumed constant	No
V_p	P-wave velocity	220 m/s	Measured with time of flight	Yes

Table 2.2 Final parameters

Symbol	Parameter	Value	Comment	Vary with Grass Growth
c'	Soil cohesion	10000 Pa	Measured with direct shear tests	Yes
c_r	Root cohesion	1000 Pa	Measured with direct shear tests	Yes
ϕ	Internal friction angle	32 °	Measured with direct shear tests	No
σ_{co}	Cohesive stress	18000 Pa	Calculated with Equation 2.13	Yes
ψ	Matric suction	3000 Pa	Measured with tensiometers	No
θ	Volumetric moisture content	0.43	Measured with HydraProbeII	Yes
w	Gravitational moisture content	0.30	Measured	Yes
α	van Genutchen's empirical fitting parameters	0.052 m^{-1}	Assumed constant	No
n_v		2.003		No
S_e	Effective saturation	0.99	Calculated with Equation 2.12	No
σ'_s	Soil suction stress	3000 Pa	Calculated with Equation 2.11	No
ρ_b	Bulk density	1790 kg/m³	Measured	No
g	Gravitational constant	9.81 m/s²	Assumed constant	No
h	Depth	0.1 m	Depth of transducers	No
σ	Overburden stress	1800 Pa	Calculated with Equation 2.10	No
σ'	Effective stress	22000 Pa	Calculated with Equation 2.9	Yes
ν	Poisson's ratio	0.14	Assumed constant	No
G	Grain shear modulus	1.5×10^9 Pa	Assumed constant	No
n	Porosity	0.47	Measured	Yes

Symbol	Parameter	Value	Comment	Vary with Grass Growth
n_c	Coordination number	6	Assumed constant	No
K_{air}	Air bulk modulus	1.01×10^5 Pa	Assumed constant	No
K_{water}	Water bulk modulus	2.15×10^9 Pa	Assumed constant	No
S	Saturation	0.91	Measured	Yes
K_{pore}	Bulk modulus of porespace	1.2×10^6 Pa	Calculated with Equation 2.5	Yes
G_{matrix}	Shear modulus of skeletal matrix	2.2×10^7 Pa	Calculated with Equation 2.7	Yes
K_{matrix}	Bulk modulus of skeletal matrix	1.5×10^7 Pa	Calculated with Equation 2.6	Yes
K_o	Grain bulk modulus	2.50×10^{10} Pa	Assumed constant	No
G_{eff}	Effective shear modulus	2.2×10^7 Pa	Calculated with Equation 2.4	Yes
K_{eff}	Effective bulk modulus	1.8×10^7 Pa	Calculated with Equation 2.3	Yes
ρ_g	Grain density	2550 kg/m³	Assumed constant	No
ρ_a	Air density	1.22 kg/m³	Assumed constant	No
ρ_w	Water density	1000 kg/m³	Assumed constant	No
V_p	P-wave velocity	560 m/s	Measured with time of flight	Yes

CHAPTER III: METHODS

3.1 OVERVIEW

There were three different phases for this laboratory experiment: pre-acoustic measurements (geotechnical tests performed on prepared samples of the same soil), during-acoustic measurements (acoustic and continuous tests performed on the reinforced soil from after the sod was planted until the sample was destroyed), and post-acoustic measurements (destructive tests performed on the soil in the box and on cores taken from the box). The continuous tests performed during the acoustic tests and grass root growth consisted of measuring moisture content in the center of the quadrants and matric suction in the center as well as in each quadrant. The destructive tests performed in the box after the acoustics tests consisted of measuring field vane shear strength and cone tip resistance. Soil core samples were taken from each quadrant. Direct shear tests were performed on samples from the cores. Geotechnical tests were then performed on the samples after the direct shear tests. After the geotechnical tests, roots were washed out of the sample to measure root density. Figure 3.1 shows the quadrants after sod was planted in September of 2014 and before cores were taken in October of 2015.

Figure 3.1 a) Grass planted September 15, 2014, b) Cores taken October 16, 2015

In October of 2013 piezoelectric, bimorph transducers were built at The University of Mississippi (UM) NCPA. These work by sending an electric pulse to the source transducer's ceramic disks which bend outwardly. A stress wave is produced from this bending. The stress propagates through the soil as a p-wave and interacts with the particles and pore fluids. The stress wave bends the receiving transducer. The mechanical stress is converted to an electric signal which is shown as a waveform. Figure 3.2 shows the ceramic disks and the cables.

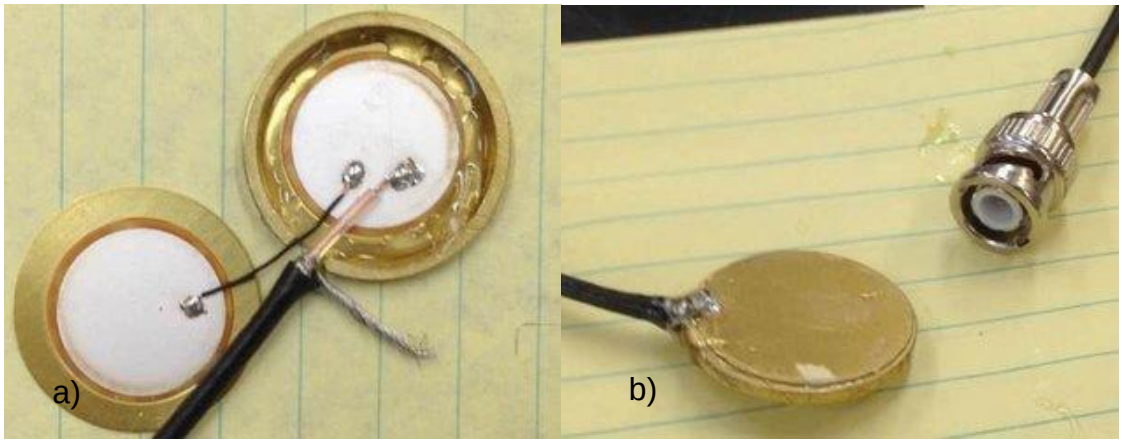

Figure 3.2 a) Inside of and b) complete bimorph transducer with BNC connector

The box was built by NCPA's machine shop in December of 2013. In January of 2014, the USDA ARS, NSL donated silty clay loam for the box. The soil was dried and ground using NSL's drying trailer and grinder. In February of 2014 a 0.06 m layer of pea gravel was placed in the bottom of the box. In March soil was added to the box and three transducers were buried in each quadrant at a depth of 0.1 m. The transducer spacing was 0.15 m. The quadrants were separated with geotextile fabric to keep roots from growing into other quadrants. Lights were hung from a rack made by the NCPA machine shop. In May water was added from the bottom of the box. The level was brought up slowly throughout May and June. At the end of June a fill valve was installed to the water reservoir to automatically keep the level constant. A tensiometer was installed in June 2014 at the center of the quadrants at a depth of 0.15 m in June 2014. The ceramic cup of the tensiometer was 0.05 m long, so the measurement ranged from 0.1 to 0.15 m in depth. Figure 3.3 shows the box at the end of July 2014 after the HydraProbeII and the first tensiometer were installed.

Figure 3.3 Box in July of 2014

From August to September seeds were planted twice without success. In September of 2014, sod was planted. Acoustic behavior began to change between each quadrant without much change in the matric suction from the center tensiometer. More tensiometers were installed in the corners of each quadrant at a depth of 0.1 m in June of 2015 to assess if the change was due to local changes in matric suction. After the conclusion of acoustics measurements in October of 2015, three field shear vane and three cone penetrometer tests were conducted in each quadrant, and three soil cores were collected from each quadrant. Direct shear tests were conducted on the cores at depths of 0.5, 0.1 and 0.2 m. After the shear tests, samples were measured and dried to measure final geotechnical properties. After samples were dried, roots were washed from each sample to measure root density. Figure 3.4 shows a diagram of all the tests conducted on the soil during and after the acoustic tests. Table 3.1 explains the symbols, instrumentation, parameters and units.

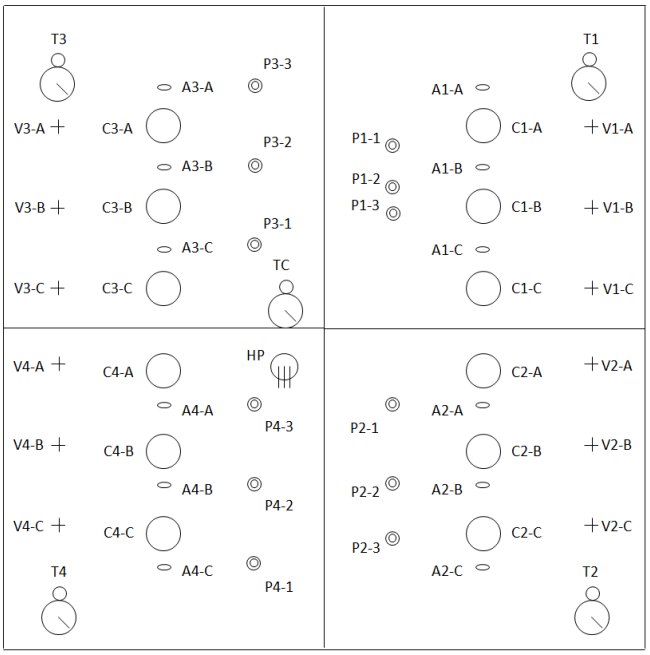

Figure 3.4 Diagram of tests conducted in box

Table 3.1 Symbols for diagram, tests conducted, parameters measured and units

Symbol	Instrumentation	Parameter	Units
A	Bimorph transducer	P-wave velocity	m/s
C	Geotechnical tests	Bulk density	kg/m³
		Dry density	kg/m³
		Gravitational moisture content	kg/kg
		Porosity	
		Void ratio	
		Degree of saturation	
	Direct shear test	Shear strength	kPa
		Cohesion	kPa
		Internal friction angle	degrees
	Root washing	Root density	kg/m³
		Root area ratio	%
HP	HydraProbeII	Volumetric moisture content	m³/m³
		Conductivity	S/m
		Dielectric permittivity	F/m
		Soil temperature	°C (°F)
P	Pentrologger	Cone tip resistance	kPa
T	Tensiometer	Matric suction	kPa
V	Shear vane test	Field vane shear strength	kPa

3.2 SAMPLE PREPARATION AND TESTS

The container was filled with a silty clay loam soil donated from USDA ARS, NSL. Pipette analysis was conducted by NSL to determine the percentages of sand, silt, and clay. The soil consisted of 1% sand, 67% silt and 32% clay as shown in the soil triangle in Figure 3.6.

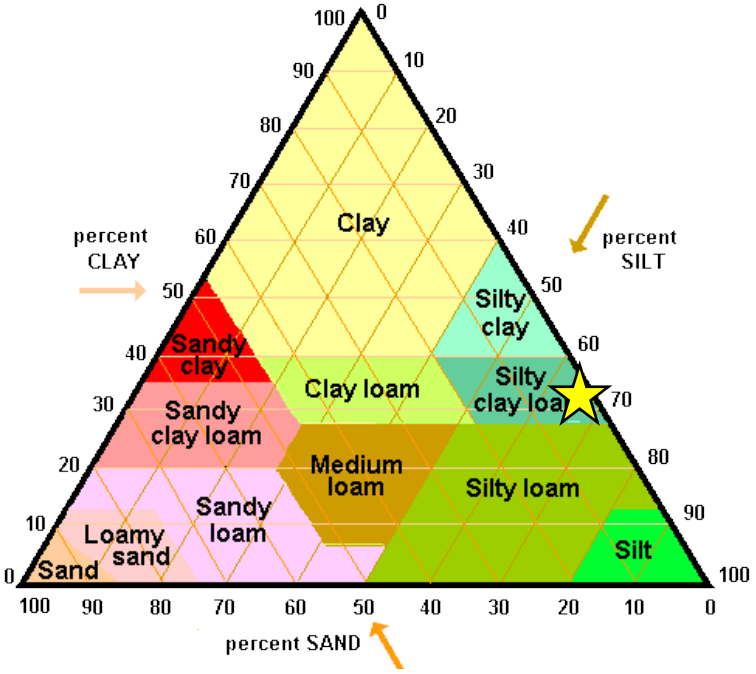

Figure 3.6 Classification of soil sample

The mineralogy of the clay is unknown, but after the experiment when the clay was allowed to dry, shrinking was noticed. This means the clay was a type of fat clay such as smectite. The clay was also considered a high plasticity clay according to the Unified Soil Classification and Symbols (USCS) test.

The soil was dried, ground, and compacted into the box (1.2 x 1.2 x 0.6 m) in 0.025 m layers with a metal plate. There were a total of 12 layers per quadrant to reach the depth of 0.3 m. Acoustic transducers were placed 0.1 m deep and 0.15 m apart during compaction. After the soil was compacted into the box, stresses in the soil were allowed to relax for two months. The water was then slowly introduced from a drain in the bottom center of the box while the soil was under tension. The water level in an external reservoir was slowly raised for a month to saturate the soil to the surface. Once saturated to the surface, the water in the reservoir was lowered slowly back to a height of 0.025 m above the top of the pea gravel layer.

Grass sod pieces were placed on top of the soil layer making sure the roots and the top soil had good contact with the prepared soil layer. The Common Bermuda sod (*Cynodon dactylon*) was donated by a commercial turf company, Tula Turf in Oxford, MS. The 007 Sumrall Bermuda grass (*Cynodon dactylon*) was collected from pasture land in Marshall County, MS, and the wild Bahia mix (*Paspalum notatum*) was collected from a roadside slope in Oxford, MS. Sunlight Supply Sun Blaze T5 grow lamps were placed 0.3 m above the top of the grass and left on 12 hr/day. The grass was cut weekly to the height of 0.15 m for the Forage Bermuda and Bahia and 0.08 m for the Common Bermuda. The grass quadrants were fertilized twice a week with Miracle-Gro LB 15-30-15 ($N - P_2O_5 - K_2O$) water soluble fertilizer to boost root growth. Other ingredients besides nitrogen, phosphorous and potash include boron, copper, iron, manganese, molybdenum, and zinc. The fertilizer does not have a deflocculating agent, so the clay bonds should not be unaltered by the fertilizer. Air

temperature was measured daily with a Temperature Humidity USB Monitor.

After acoustic tests, an AMS field vane shear tester (#59020, www.ams-samplers.com) was used to measure the undrained field vane shear strength of soil and soil-root matrices as a function of depth. Three tests were conducted for each quadrant at depth increments of 0.05 m. The largest vane (0.0254 x 0.0508 m) was used since the soil is near fully saturated. An auger was used to reach each depth increment. Figure 3.7 shows the shear vane, dummy vane, and auger utilized in the experimental setup.

Figure 3.7 a) Shear vane tester, auger, and bore holes in b) Bahia grass and c) bare soil

Cone penetrometer tests (CPT) were also conducted in each quadrant after the acoustic tests using an Eijkelkamp Pentrologger set A (#06.15.SA, www.en.eijkelkamp.com) to acquire cone tip resistance of soil as a function of depth. The largest cone (5 cm^2) was utilized since the soil was near fully saturated. The resolution of the data was 0.01 m. The Pentrologger was bolted to the grow light frame in order to keep the Pentrologger still while testing. A cored drill was used to bore the cone tip into the soil at a constant rate of 0.02 m/s. Figure 3.8 shows the Pentrologger attached to the light frame, the test area with boreholes, and the cone tip after going through the soft soil.

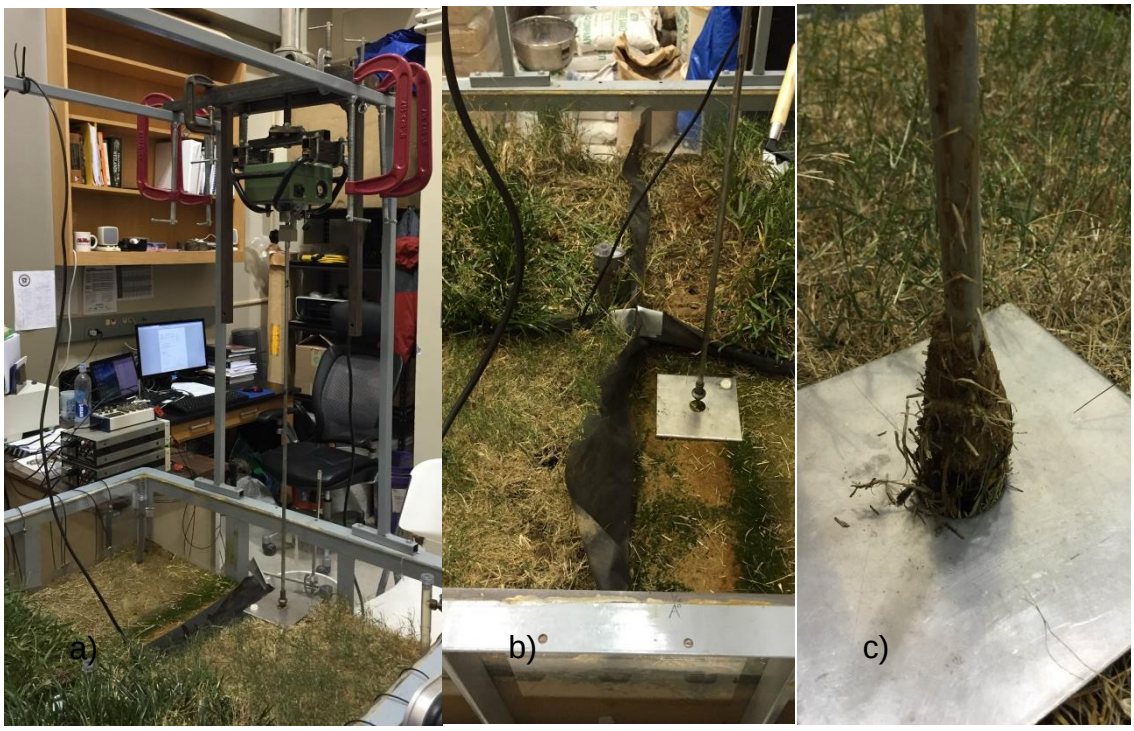

Figure 3.8 a) Penetrologger bolted to light rack, b) boreholes, and c) cone tip covered in soft soil

3.3 CORE SAMPLE MEASUREMENTS

After the acoustic tests, three cores 0.064 m x 0.31 m were taken from each grass soil matrix and the bare soil. 0.025 m x 0.064 m samples were sub-sectioned from the cores at 0.05, 0.1, and 0.2 m depths.

Direct shear tests were conducted using American Society of Testing and Materials' (ASTM) standard test method for direct shear tests of soils under consolidated drained conditions (ASTM D3080 / D3080M-11). In order to build a Mohr Coulomb failure envelope, three shear strengths were needed from the same depth under three different normal stresses, so the assumption was made that the soil was laterally homogeneous. This allowed a failure envelope, cohesion and internal friction angle to be measured as a function of depth for each quadrant. The machine is shown in Figure 3.9.

Figure 3.9 USDA NSL's direct shear test machine

The shear box had a height of 0.025 m and a diameter of 0.0635 m. The samples were sheared at 0.0635 mm/min. The rate was slow enough to allow for pore water pressure to dissipate. Normal stresses applied were 1.5, 4.6, and 7.7 kPa. Failure was defined by maximum shear stress or shear stress at 20 % relative lateral displacement, whichever came first. Mohr Coulomb failure envelopes, or shear strength versus normal stress, were obtained at three depths to determine total cohesion as a function of depth. Root cohesion was then calculated equal to the difference of the cohesion of the grass root reinforced soil and the cohesion of the bare soil.

After direct shear tests, the soil samples were weighed to determine bulk density. The samples were placed in an oven at 105 °C for 24 hr. The samples were weighed again to determine dry density. Particle density was assumed to be that of clay 2550 kg/m³. From the densities, gravitational water content, void ratio, porosity, and degree of saturation were calculated.

After the samples were dried, each root reinforced sample was washed to

separate the roots from the soil using NRCS hand sieving method (Franks et al., 2000). Samples were placed in water and stirred to help the roots disperse from the soil. The roots floated to the top and were decanted onto a 0.5 mm sieve. The process was repeated three or more times until all of the roots were on the sieve. The roots were washed on the sieve to remove any soil as shown in Figure 3.10.

Figure 3.10 Root washing

Roots were rinsed off the sieve into a pan with a small jet of water. The roots and water in the pan were poured onto filter paper. The pan was rinsed, and the rest of the roots were poured onto the filter paper again to ensure no roots were left. The water drained from the filter paper, and the roots air dried overnight. The weights of the roots were recorded. Root density was calculated using Equation 2.14.

3.3 MEASUREMENT OF P-WAVE VELOCITY

The acoustic sensors consist of bimorph transducers built at NCPA and placed at a depth of 0.1 m. Each quadrant had three sensors at a spacing (x) of 0.15 m. One transducer performed as the source and the other two as receivers to measure two sets of time of flight measurements in each quadrant. Figure 3.11a illustrates the input negative, half cycle pulse of 6 kHz that vibrates into the source transducer (the orange, bottom line). The created stress waves travel through the soil and are recorded by the receiving transducer (the blue, top line). The time measurement (Δt) annotated is referred to as the first arrival time or travel time. Figure 3.11b shows a side view of the transducer spacing, and Figure 3.11c shows a picture of a transducer.

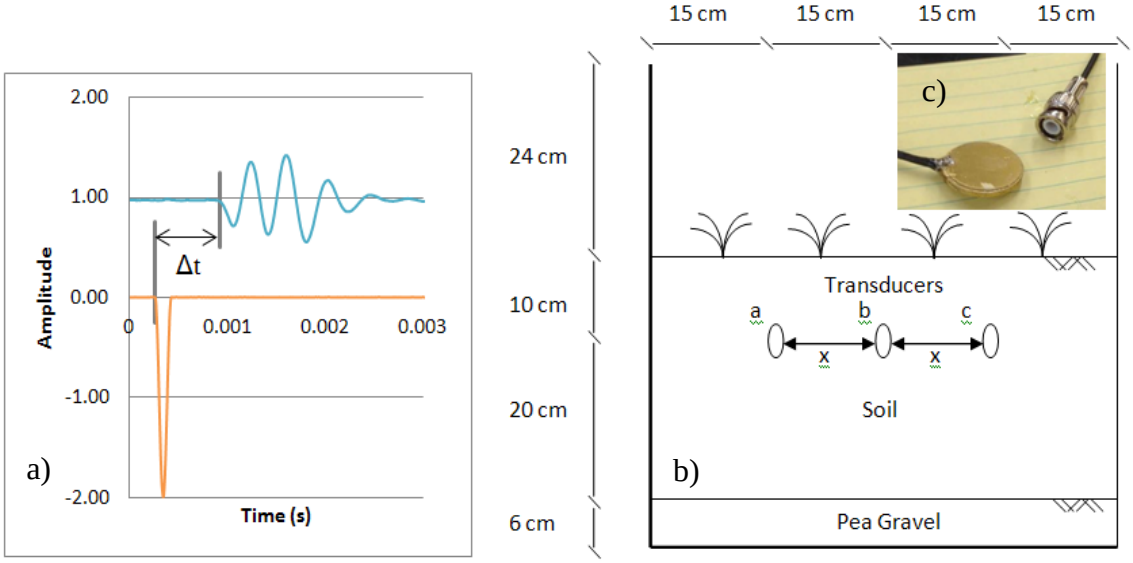

Figure 3.11 a) Time of flight measurements, b) box diagram and c) transducer picture

Using the measured travel time and the known separation between transducer

pairs, the compressional wave velocity (V_p) were calculated using Equation 3.1,

$$V_p = \frac{x}{\Delta t}. \tag{3.1}$$

Since the velocity of soils can change due to changes in temperature, moisture content, relaxation of stress and other properties not associated with grass growth, a control was required. The bare soil acoustic velocities were used as the baseline control for the experiment.

CHAPTER IV: RESULTS

4.1 MEASUREMENTS DURING ACOUSTIC TESTS

Throughout the acoustic measures as grass roots developed, volumetric moisture content and matric suction were measured with a HydraProbeII and tensiometers, respectively. Temperature and dielectric properties of the soil were measured with a HydraProbeII in the center of the box. The instrument converts the dielectric properties to volumetric moisture content based off of empirical relationships for specific soil types. Figure 4.1 shows volumetric moisture content from September 2014 to October 2015. Saturated volumetric moisture content for a silt loam is approximately 0.46 m^3/m^3 (Leij et al., 1996). This soil had high water retention properties since volumetric moisture content is around 0.45 m^3/m^3. A change from 0.45 to 0.43 m^3/m^3 is not considered a large decrease. This decrease most likely occurred due to evapotranspiration.

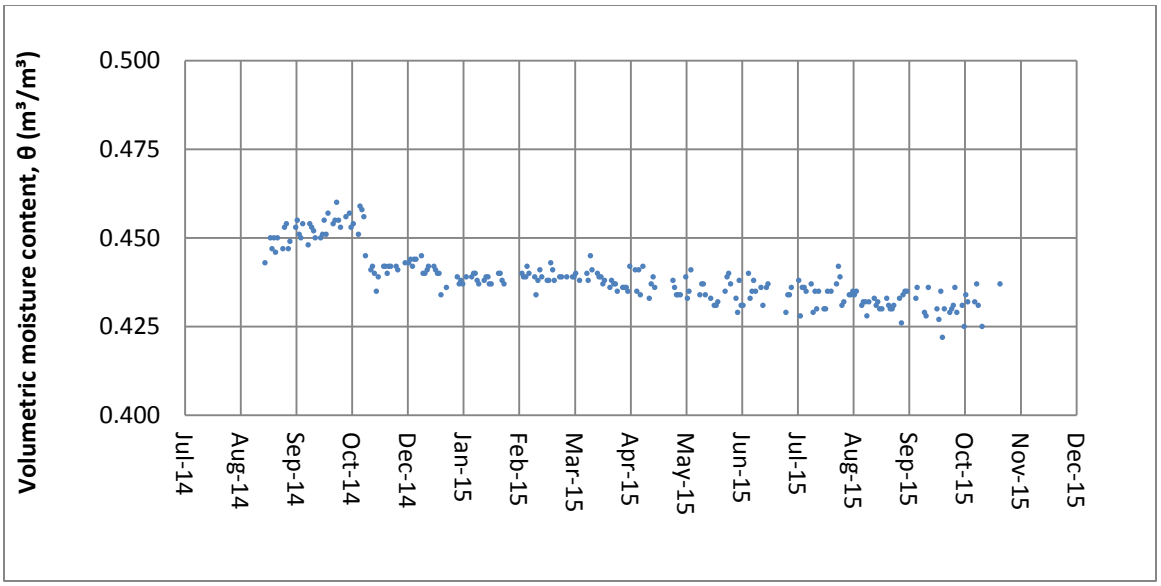

Figure 4.1 Volumetric moisture content, $\boldsymbol{\theta}$ (m^3/m^3) since planting grass

Average matric suction measured in between the quadrants at a depth of 0.15 m is shown in Figure 4.2.

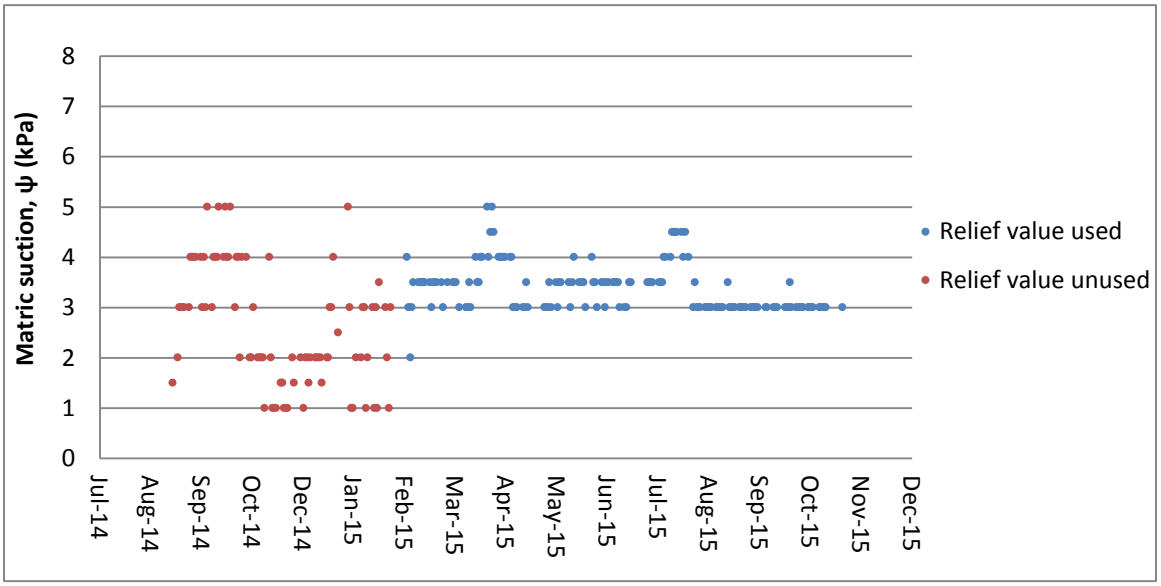

Figure 4.2 Average matric suction, $\boldsymbol{\psi}$ (kPa) at a depth of 0.1 to 0.15 m since planting grass

A pressure relief valve on the tensiometer was not used for the months denoted

in the red in Figure 4.2. The larger variation in readings was due to pressure that was built up in the tensiometer itself, not based on the matric suction in the soil. During proper operation, average fairly constant matric suction was measured at 3 kPa. Average matric suction remained low due to the soil having an average degree of saturation greater than 90 %. Local matric suction, shown in Figure 4.3, was also measured for each grass type with tensiometers at a depth of 0.1 m.

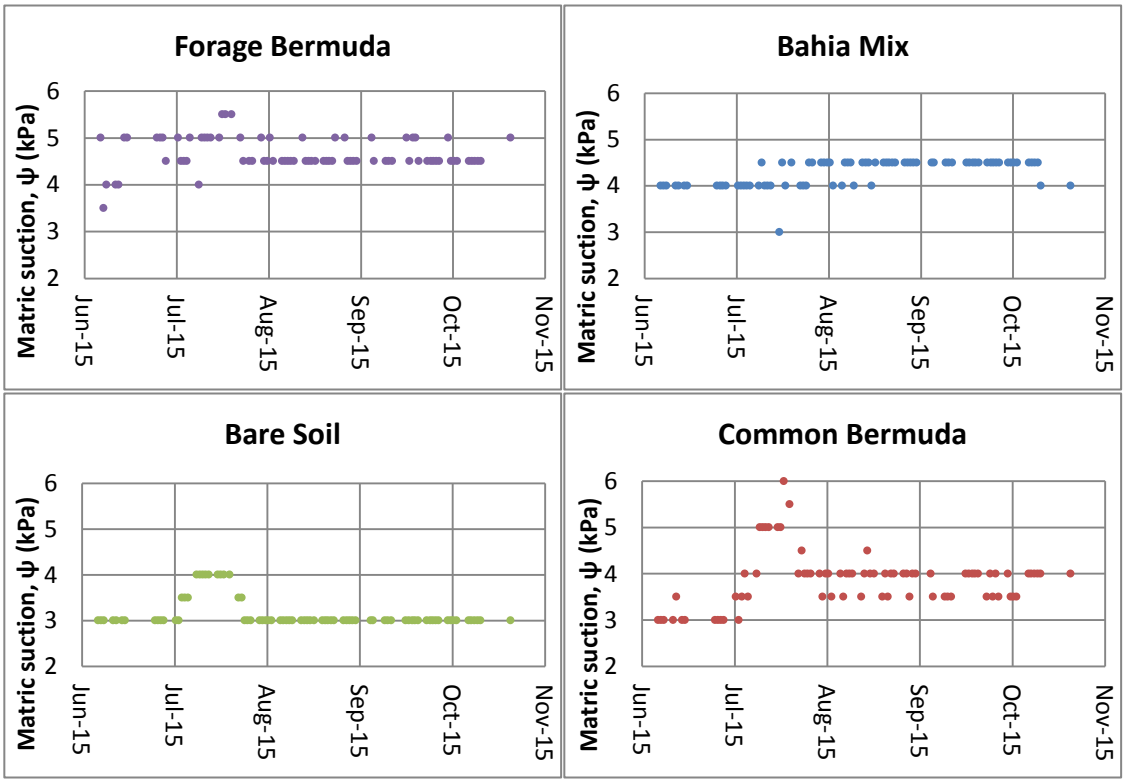

Figure 4.3 Local matric suction, ψ (kPa) at depth of 0.05 to 0.1 m

Local matric suction for each of the grass types agreed with the average matric suction measured in between the quadrants. The matric suction was very low, 3 to 5 kPa, due to the soil being close to full saturation. From August through October the matric suction is basically constant for all quadrants.

4.2 MEASUREMENTS AFTER ACOUSTIC TESTS

4.2.1 Measurements in Box

After acoustic tests, destructive measurements were conducted on the soil in the box, and core samples were taken from the quadrants for further tests. Cone tip resistance (q_c) and field vane shear strength ($S_u(fv)$) were measured in each quadrant during October 2015. Three cone penetrometer tests were conducted per quadrant (Figure 4.4). The results were the average of the three trials (Figure 4.5).

The bare soil had the lowest cone tip resistance. This could be due to the lack of root resistance to penetration. The Forage Bermuda had the highest resistance. The resistance was appropriate since the roots seemed to be well developed in that quadrant. The Bahia grass's root system was much more developed, but the resistance was not as high as the other grasses.

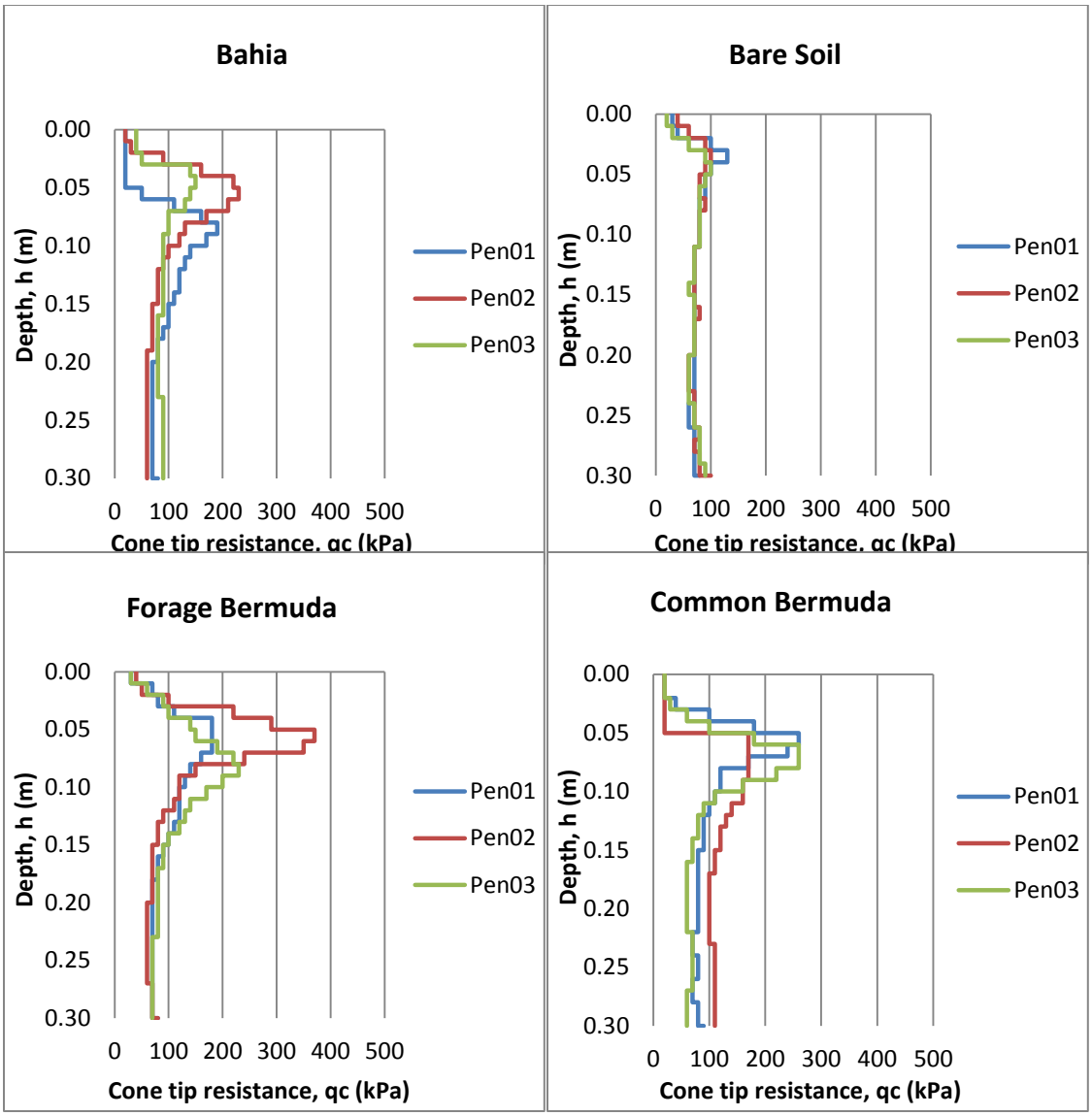

Figure 4.4 Cone tip resistance, $\boldsymbol{q_c}$ (kPa) as a function of depth, $\boldsymbol{h}$ (m) for each quadrant

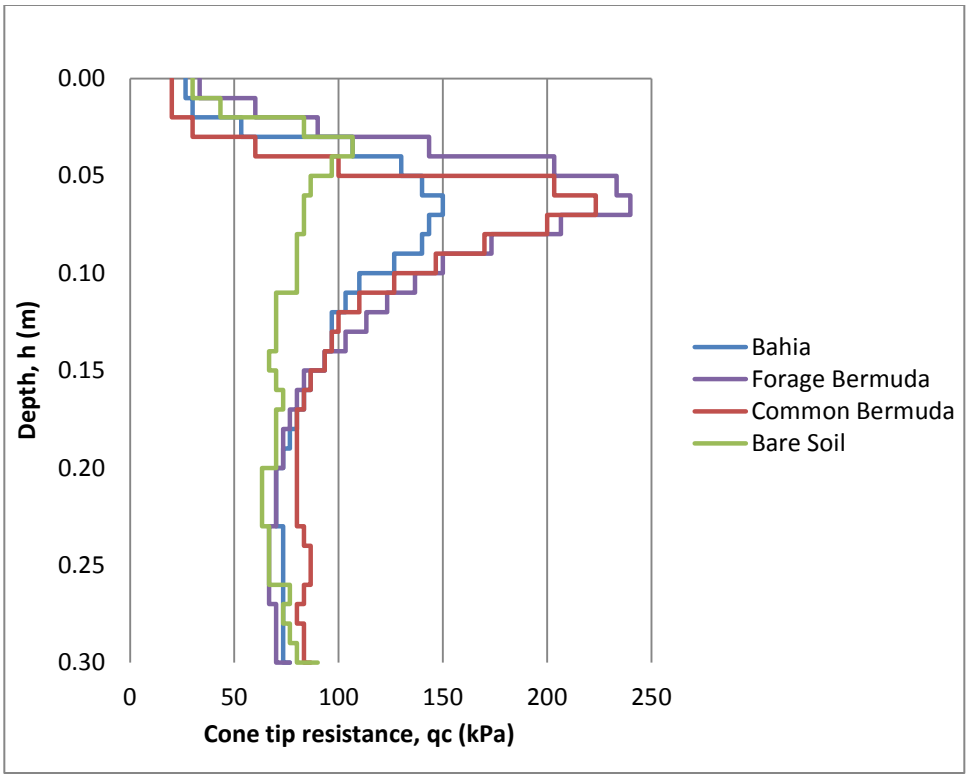

Figure 4.5 Cone tip resistance, $\boldsymbol{q_c}$ (kPa) as a function of depth, $\boldsymbol{h}$ (m)

One would reason that more roots would translate to higher resistance by the roots. The Common Bermuda grass had a higher resistance than expected. The Common Bermuda could have been due to grass being pushed down by the cone. A cone covered in grass would have had higher resistance than a bare cone. Below the depth of 0.2 m, the cone tip resistance in the root reinforced soil was similar to the bare soil.

Also in October 2015, three shear vane tests were conducted in each quadrant in five centimeter depth increments (Figure 4.6). The average results of the three trials are shown in Figure 4.7.

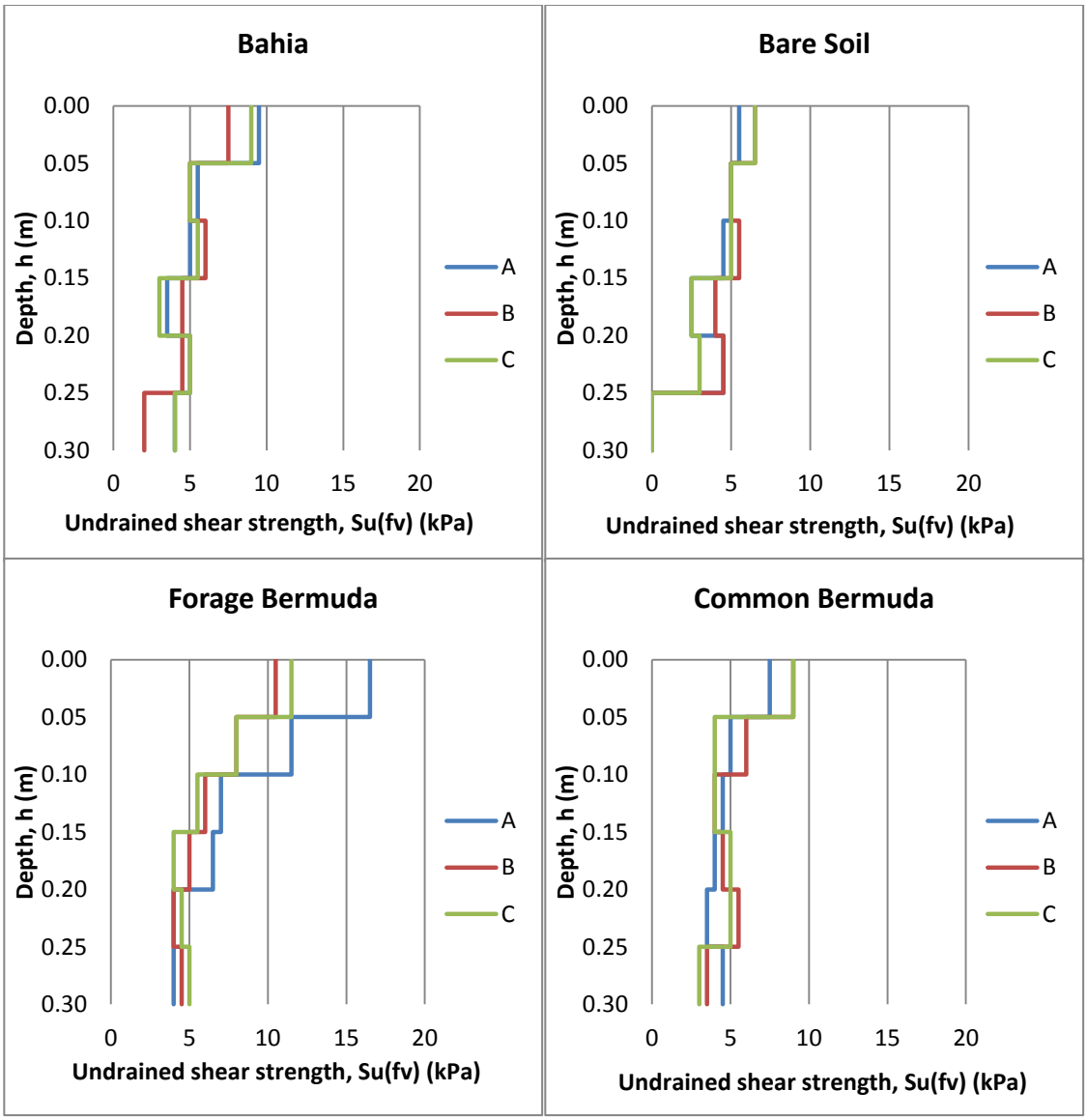

Figure 4.6 Undrained shear strength, $\boldsymbol{S_u(fv)}$ (kPa) as a function of depth, $\boldsymbol{h}$ (m) for each quadrant

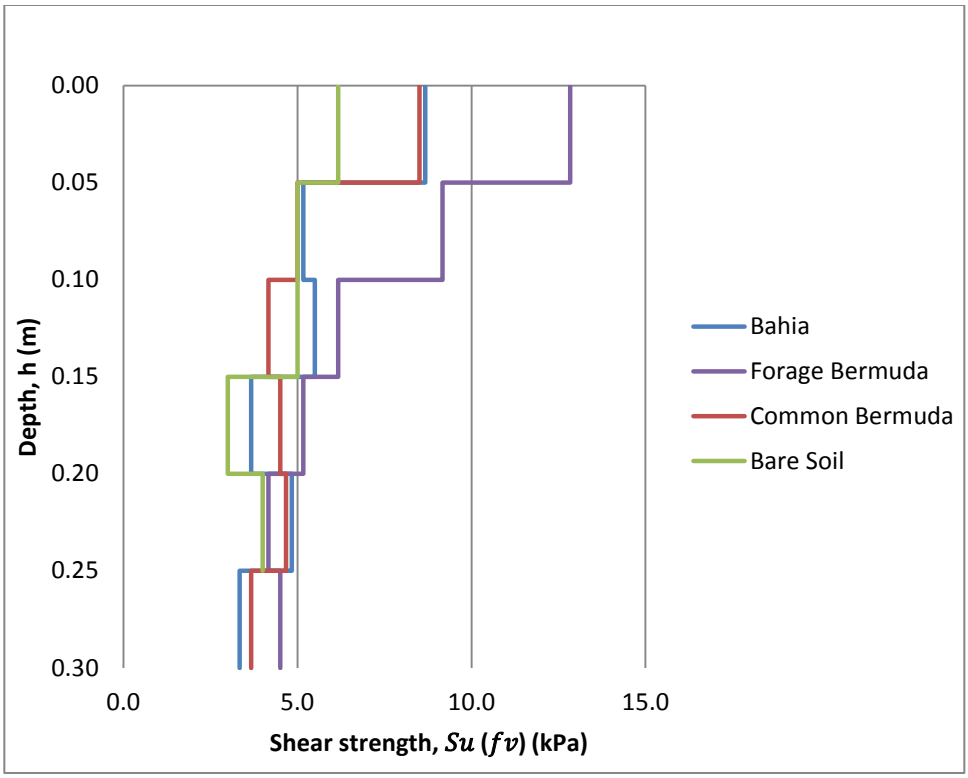

Figure 4.7 Undrained field vane shear strength, $S_u(fv)$ (kPa) as a function of depth, h (m)

The bare soil had on average less field vane shear strength than the soil reinforced with grass roots. The Forage Bermuda had the highest shear resistance at every depth. However, shear strength values were low in general due to the high degree of saturation in the unconsolidated silty clay loam. Shear vane test shear strength in remolded, undrained, soft silty clay typically range from 1 to 12 kPa (Kwong et al., 2001). Values were within typical values according to the literature. For the bare soil, the shear strength was fairly constant as a function of depth. For the grass root reinforced soil, the shear strength decreased as a function of depth.

4.2.2 Direct Shear Tests

Direct shear tests of soils under consolidated drained conditions were conducted to measure cohesion and internal friction angle on 36 samples. Three cores were taken from each quadrant, and subsamples were taken from 0.05, 0.1 and 0.2 m depths of each core. Within the quadrants, the soil and roots were assumed to be laterally uniform at each depth. The assumption allowed for Mohr-Coulomb failure envelopes to be constructed from the three samples taken from three different cores at constant depths within the quadrants. Normal stresses placed on the samples during the tests were chosen to represent overburden stresses in the soil at 0.1, 0.3 and 0.5 m and were calculated to be 1.5, 4.7, and 7.7 kPa. The results of the tests are shown in Figures 4.8 through 4.11.

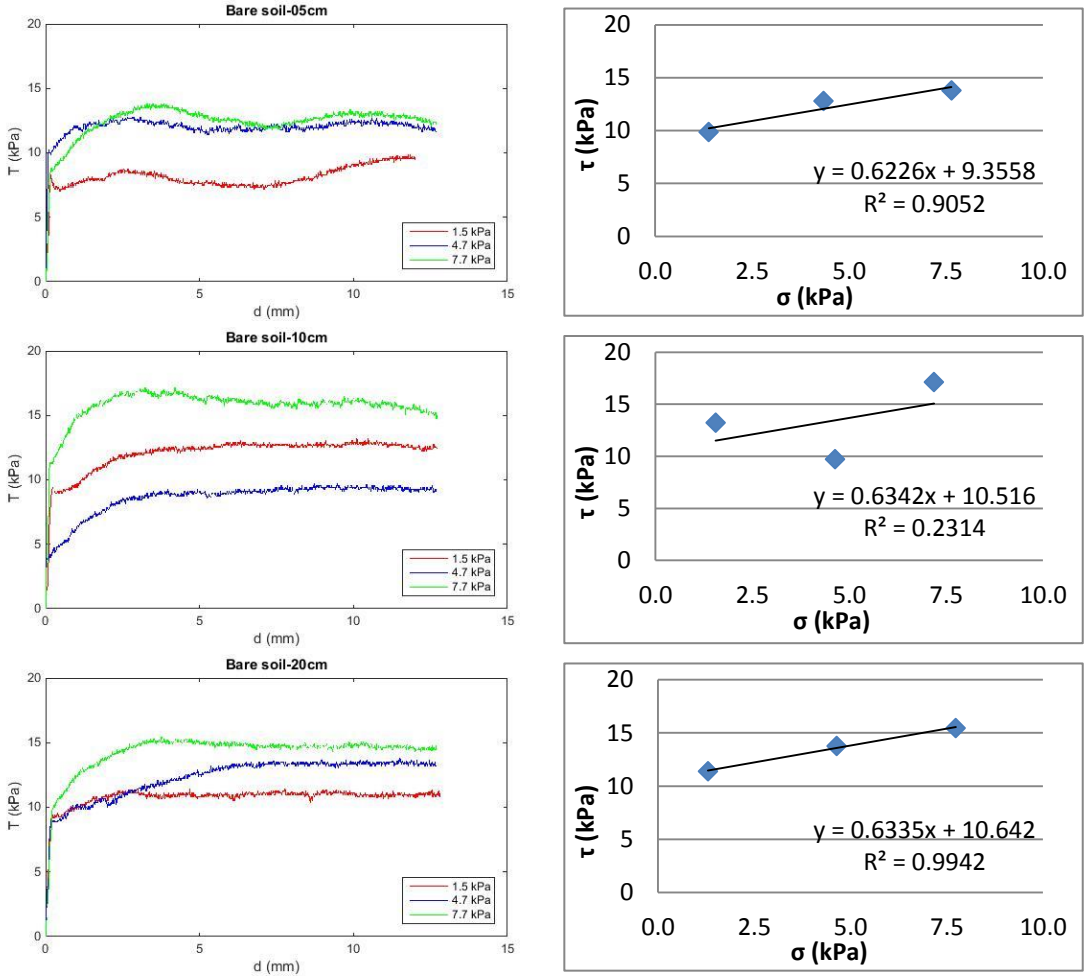

Figure 4.8 Bare Soil shear stress, $\boldsymbol{\tau}$ (kPa) versus lateral displacement, $\boldsymbol{d}$ (mm) and shear stress, $\boldsymbol{\tau}$ (kPa) versus normal stress, $\boldsymbol{\sigma}$ (kPa) from 0.05, 0.1, and 0.2 m depths

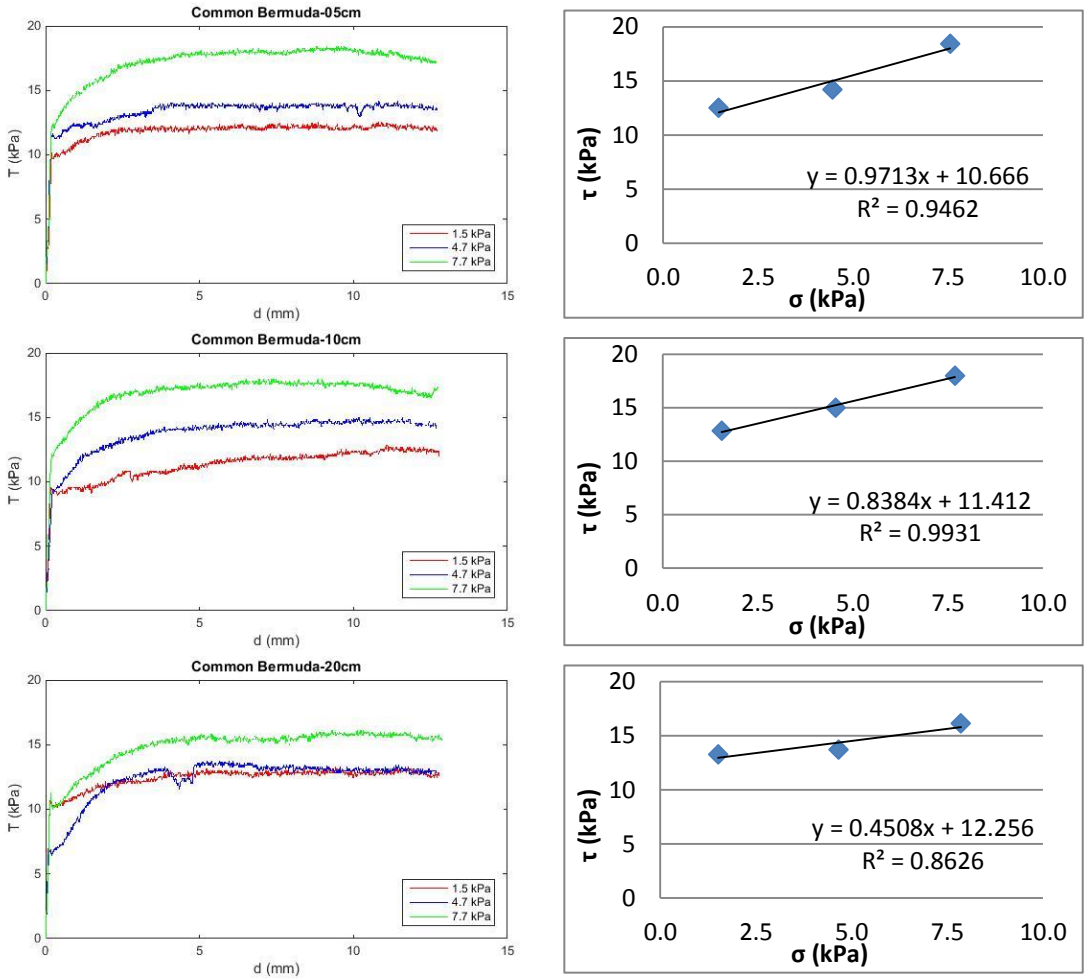

Figure 4.9 Common Bermuda Shear stress, $\boldsymbol{\tau}$ (kPa) versus lateral displacement, $\boldsymbol{d}$ (mm) and shear stress, $\boldsymbol{\tau}$ (kPa) versus normal stress, $\boldsymbol{\sigma}$ (kPa) from 0.05, 0.1, and 0.2 m depths

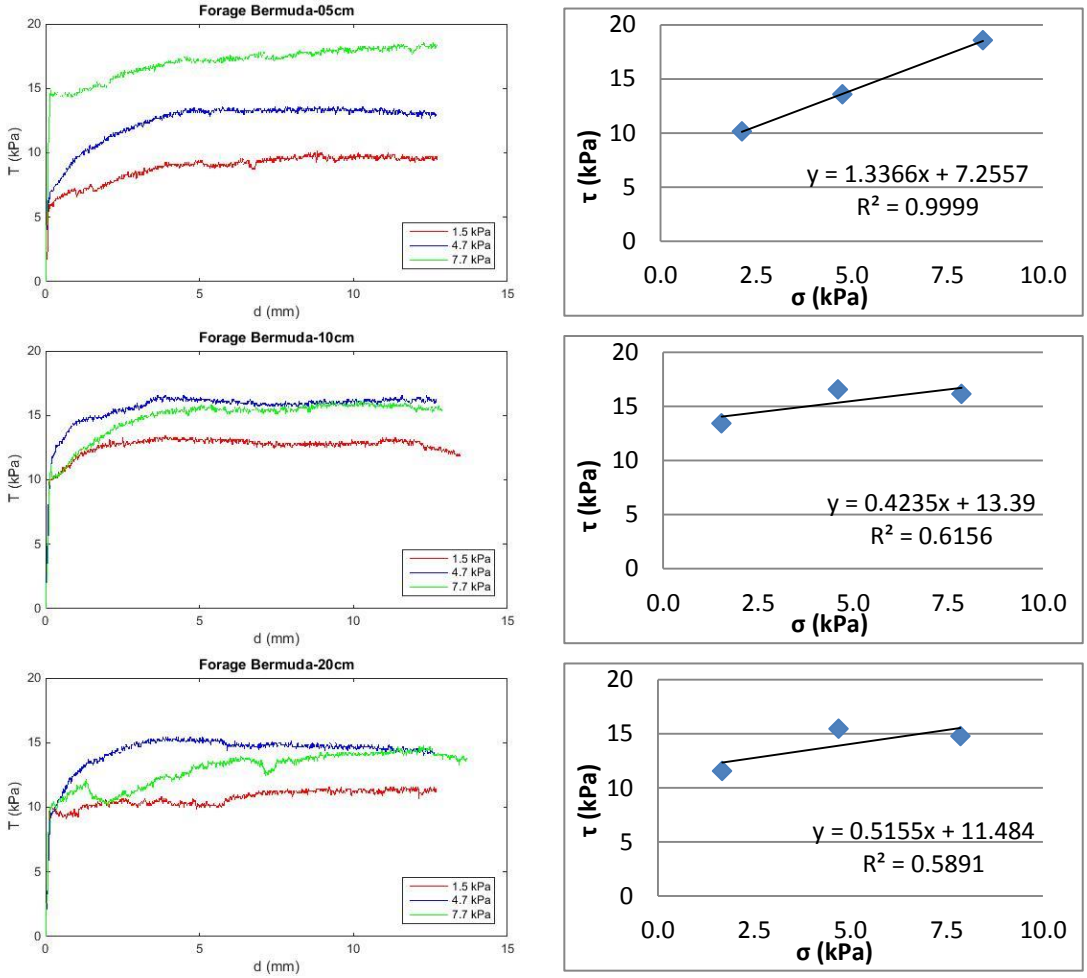

Figure 4.10 Forage Bermuda shear stress, $\boldsymbol{\tau}$ (kPa) versus lateral displacement, $\boldsymbol{d}$ (mm) and shear stress, $\boldsymbol{\tau}$ (kPa) versus normal stress, $\boldsymbol{\sigma}$ (kPa) from 0.05, 0.1, and 0.2 m depths

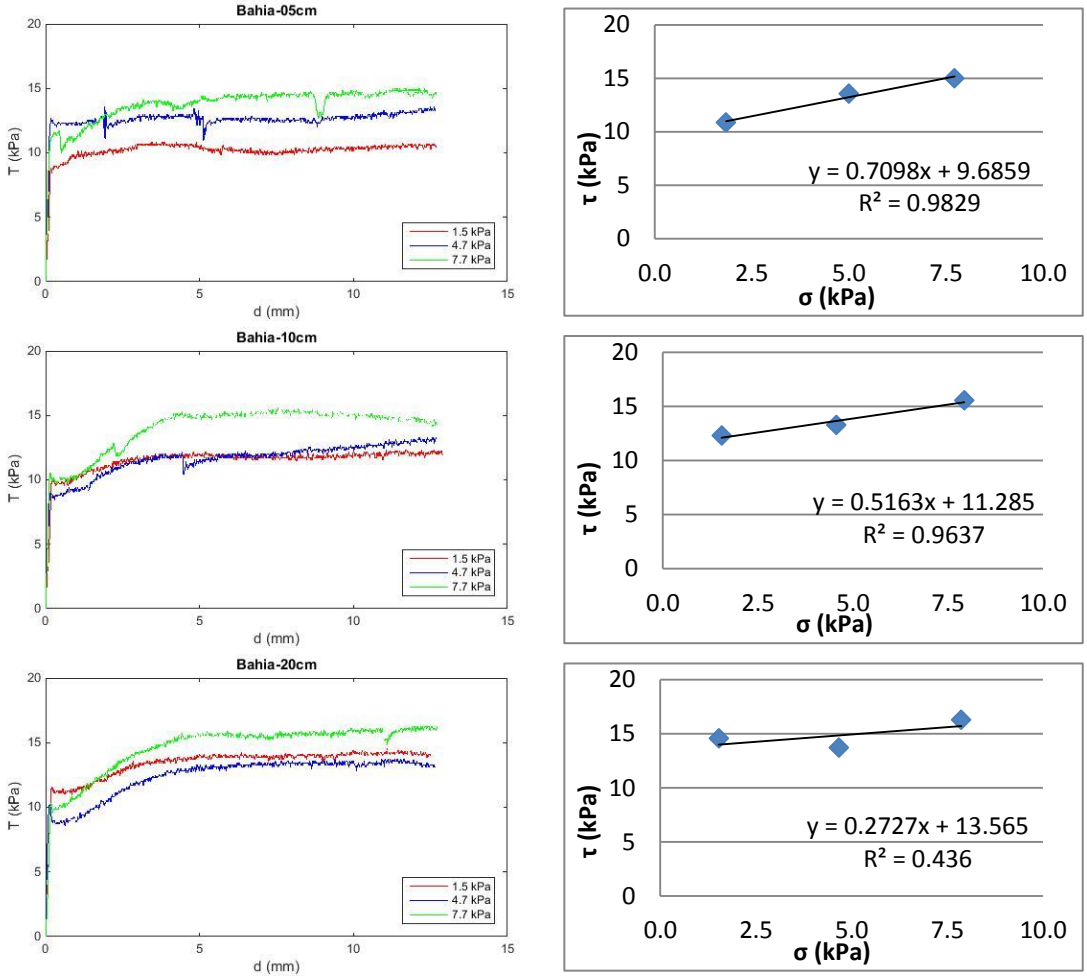

Figure 4.11 Bahia shear stress, $\boldsymbol{\tau}$ (kPa) versus lateral displacement, $\boldsymbol{d}$ (mm) and shear stress, $\boldsymbol{\tau}$ (kPa) versus normal stress, $\boldsymbol{\sigma}$ (kPa) from 0.05, 0.1, and 0.2 m depths

Peak shear stress occurred within the first 5 mm of displacement in the majority of the tests. Residual strength was the same as peak strength suggesting the failure was ductile and not brittle due to the high degree of saturation of the soil. Peak shear stress was between 10 and 20 kPa for all samples. Some of the shear stress-displacement curves had brief dips of shear stress possibly due to the breaking of roots. The shear stress of the soil quickly regained strength after that phenomenon. The cohesion of the soil and roots as a function of depth is shown in Figure 4.12.

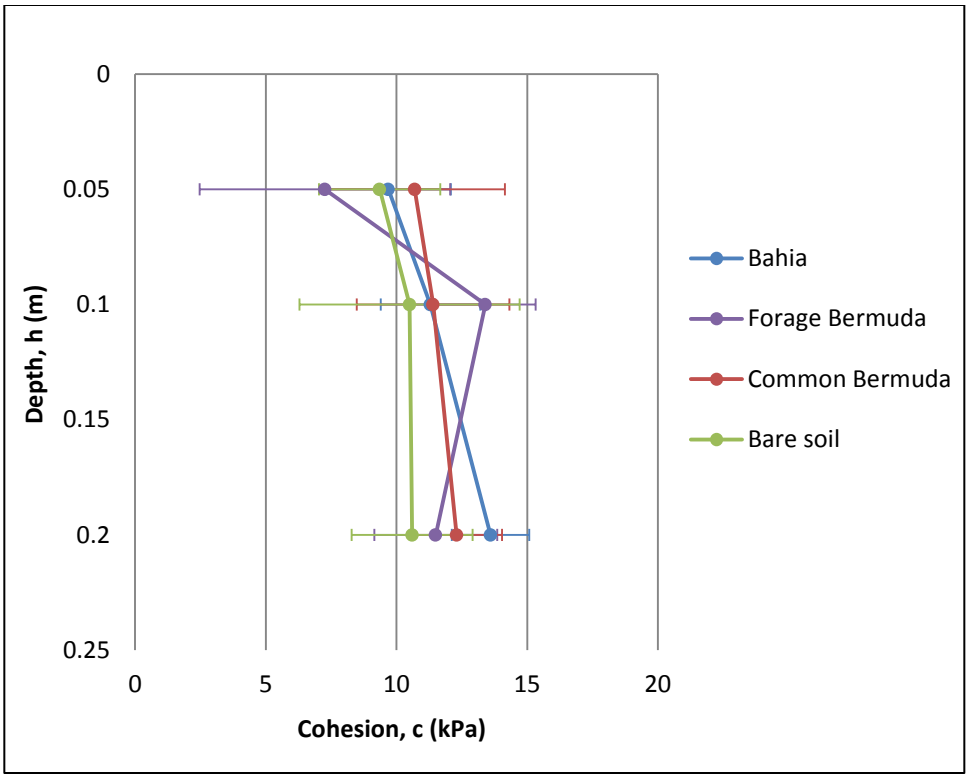

Figure 4.12 Cohesion, $\boldsymbol{c}$ (kPa) as a function of depth, $\boldsymbol{h}$ (m) for each soil and roots

Measured cohesion values were low due to the soil being saturated. The range of cohesions was also small. Minnesota Department of Transportation, Pavement Design, 2007 suggest a range of cohesions for a saturated silty clay loam are from 10 to 20 kPa. The average total cohesion measured was 11 kPa. The bare soil does, on average, have lower cohesion than the soils reinforced with roots.

Even with roots the cohesion did not increase significantly as expected. One possible explanation could be that the friction between the roots and the soil was very weak. Instead of the roots' tensile strength being mobilized to the fullest leading to the roots breaking, the roots simply pulled out of the saturated soil. Pullout occurs at a much lower shear stress for roots less than 3 mm in diameter in saturated soils (Pollen et al.,

2005). The suggestion was made that the fertilizer might have worked as a deflocculant pushing clay particle apart and weakening the shear strength of the soil. Further investigation into the fertilizer proved there was no deflocculating agent. Internal friction angle results are shown in Figure 4.13.

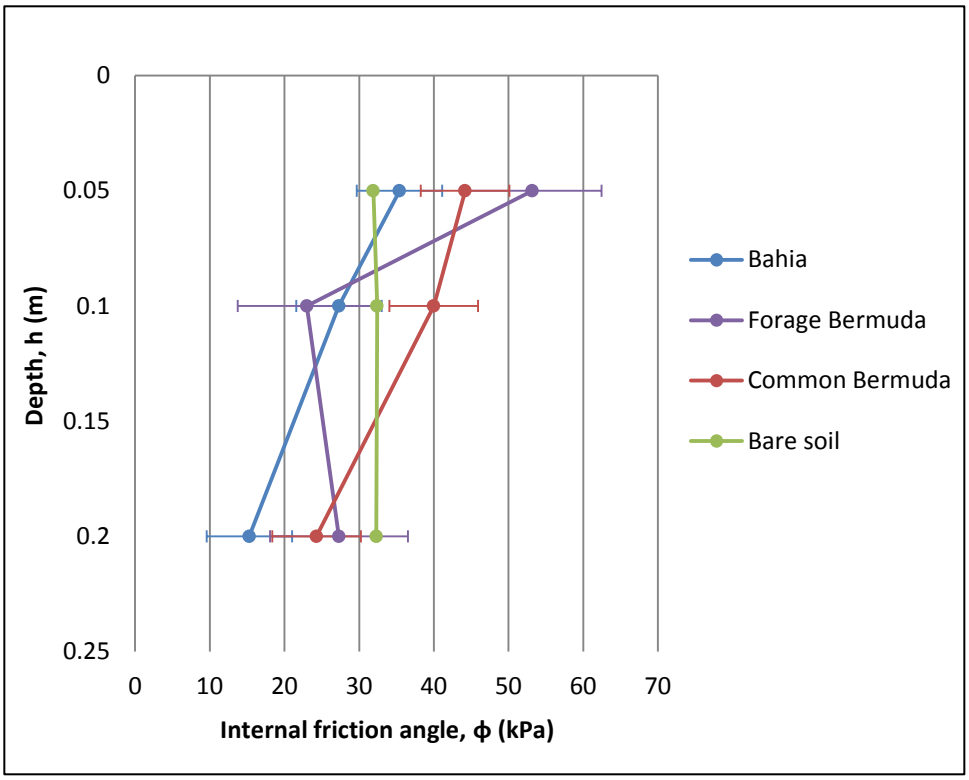

Figure 4.13 Internal friction angle, $\boldsymbol{\phi}$ (degrees) and a function of depth, $\boldsymbol{h}$ (m) for each soil and roots

According to Operstein et al. (2000) internal friction angle is not affected by root reinforcement. The direct shear test results were quite scattered for the root reinforced soil. At 0.05 m depth, the internal friction angles for the grass quadrants are greater than that of the bare soil. At 0.2 m, the internal friction angle in the bare soil is greater than that of the grass quadrants. The root density measured at these depths were within experimental error of each other, so one cannot say that there were more

roots that increased or decreased internal friction angle. Minnesota Department of Transportation, Pavement Design, 2007 suggests that a typical range of internal friction angle for a silty clay loam is from 18 to 32 º. The average internal friction angle between all of the soil and grass types was 32 º.

The internal friction angle was high for this soil type. A possible explanation has to do with the locations where the cores were taken. The test with the highest normal stress was conducted on a sample that was taken directly on top of a tuft of roots. The test with the lowest normal stress was conducted on a sample that was taken from an area that did not have as many roots. The result was a steep increase in shear stress as a function of normal stress, or steep internal friction angle, which led to a lower cohesion value.

Another possible explanation could be that the sub-samples taken in the first 0.05 m of the soil could have contained topsoil that was coarser than the soil below. Coarse grained soils are known to have higher internal friction angles than fine grained soils due to interlocking of grains.

4.2.3 Geotechnical Tests

After direct shear tests were conducted the, 36 samples were weighed, dried, and weighed again to get bulk density, dry density, porosity, void ratio, gravitational moisture content, and degree of saturation. The table below has the average values and the standard deviations of the geotechnical parameters for each quadrant. The values were averaged from three sub-samples taken from three cores in four quadrants. The

averages were from nine measurements from each quadrant.

Table 4.1 Geotechnical parameters taken after the acoustic measurements

Quadrant	ρ_b kg/m³	±	ρ_d kg/m³	±	n %	±	e m³/m³	±	w %	±	S %	±
Bahia	1819	18	1357	19	47	1	0.88	0.03	34	1	99	3
Bare soil	1783	31	1330	30	48	2	0.93	0.08	34	1	96	5
Forage Bermuda	1822	33	1365	23	46	1	0.87	0.03	34	1	98	5
Common Bermuda	1783	59	1323	52	48	1	0.92	0.04	35	1	95	3
Average	1802	35	1344	31	47	1	0.90	0.05	34	1	97	4

The values matched typical silty clay loam properties according to Minnesota Department of Transportation, Pavement Design, 2007. The soil was a near saturated silty loam and classified to have average to high porosity. In the bare soil the bulk density increased slightly with depth, but this was not far above the experimental error of the test.

4.2.4 Root Washing

After the samples were dried and weighed, roots were washed from the soil samples and dried overnight. The volumes of the soil-root samples were recorded as well as the weight of the dried roots. Root density was measured for each sub-sample from each core. The results are shown in Figure 4.14.

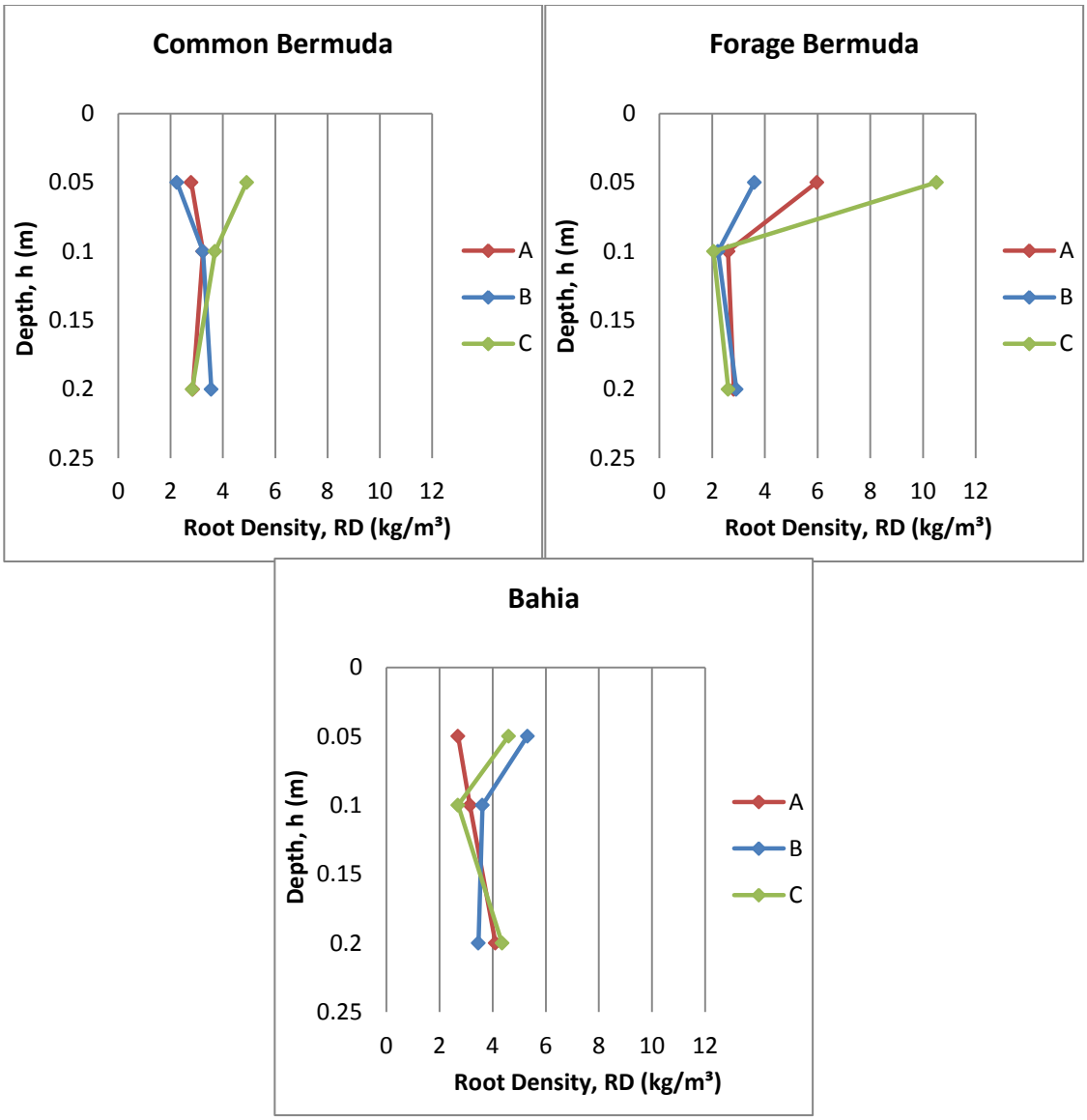

Figure 4.14 Root density, $\boldsymbol{RD}$ (kg/m³) as a function of depth, $\boldsymbol{h}$ (m) for each core sample

The average measured root density was 3.7 kg/m³ which agrees with De Baets et al. (2008). Root density was expected to decrease as a function of depth, but it seems that the roots were mainly present in the first 0.05 m of the soil. The Common Bermuda had the lowest roots density on average. The Forage Bermuda had the largest root density and largest variation at 0.05 m due to the tuft of roots where core C was

taken as discussed at the end of section 4.2.2. Root density had the smallest variation at a depth of 0.1 m for all grasses.

A logarithmic relationship could not be established between root density and cohesion as suggested in Tengbeh (1989). The relationship between shear strength and root density was explored, but no logarithmic relationship could be established. This was most likely due to the small range of shear strength and root density values measured.

4.3 P-WAVE VELOCITY MEASUREMENTS

Compressional wave velocity was measured with bimorph transducers for over 13 months as grass roots developed. There were two sets of time of flight measurements per quadrant as mentioned in section 3.4. The acoustic tests were conducted from when the sod was planted until the destructive measurements were taken. Results are presented in Figure 4.15.

Initially the p-wave velocity in the bare soil was the highest. The bare soil velocity values between the transducer pairs were approximately 30 m/s apart when the sod was planted. This was thought to be due to small variations in the sensor placement. If the sensor spacing was different between transducer pairs, the assumed distance in the time of flight calculation would have given different velocities. After the experiment, sensor spacing was measured to be the correct distance of 0.15 m. Another explanation may be differences in local compaction when soil was placed in the box. Velocity was fairly constant in the bare soil until it increased 100 m/s from July to October. The increase is predicted to be from settlement or an increase in soil cohesion.

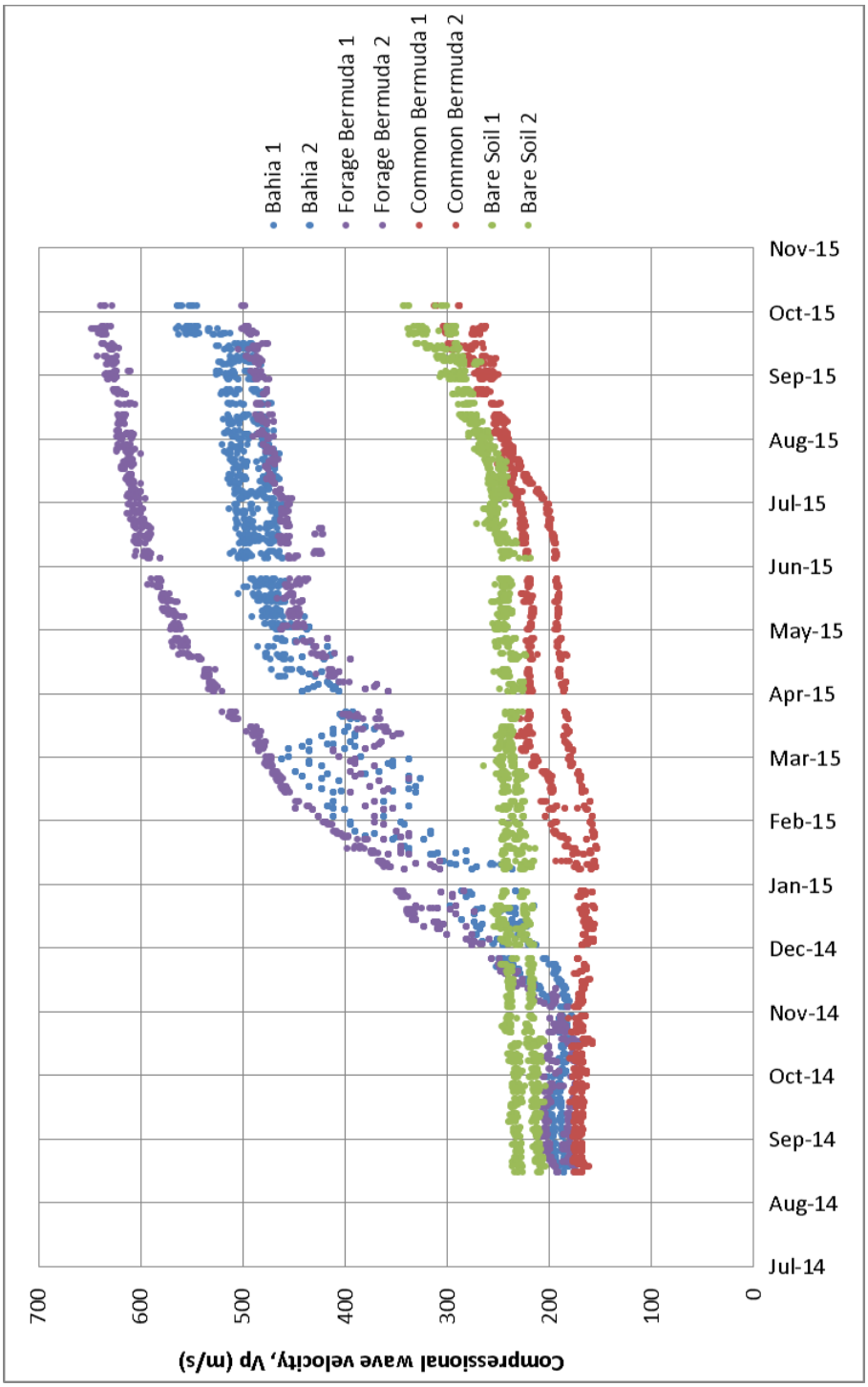

Figure 4.15 P-wave velocity, $\boldsymbol{V_p}$ (m/s) as a function of grass root growth

Initial p-wave velocities in the Common Bermuda were the lowest and more consistent between transducer pairs than the bare soil. However in January, a local phenomenon occurs that separates the velocity by about 50 m/s. This could have been due to roots growing in between one of the transducer pairs more than the other. During this time, both velocities increased slightly which could have been a sign that roots were developing in the soil at the depth of the transducers. After the short increase, the velocities become fairly constant until August when the pairs come back together and begin to increase in the same way as the bare soil velocities. The velocity in the Common Bermuda behaved similarly to the bare soil velocity. The final velocity of the bare soil and Common Bermuda ranged from 290 to 350 m/s. Visual inspection and subsequent measurement of root density suggested that the Common Bermuda was not growing well.

The initial velocities in the Bahia and Forage Bermuda were about 20 to 60 m/s less than the velocities of the bare soil. This could have been due to difference in compaction between the quadrants. The velocity in both quadrants started to increase in December due to grass root growth. During this time, the velocity values were apart by up to 100 m/s. The Bahia velocities came back together in May possibly due to root spreading homogeneously, but the Forage Bermuda velocities were about 130 m/s apart even at the end of the experiment suggesting the roots grew more heterogeneously. The velocity in both quadrants increased until June when the rate of increase in velocity slowed. This could have been to a slowing of the root development. For most of the experiment the Forage Bermuda and the Bahia velocities were twice as high as

the bare soil and Common Bermuda velocities suggesting more root growth. The final velocity in the Bahia and the Forage Bermuda ranged from 500 to 640 m/s.

To summarize, the volumetric moisture content remained constant and close to fully saturated. The soil had low average matric suction which is typical for saturated soils. Average cone tip resistance and undrained field vane shear strength were highest in the grass quadrants in the first 0.05 to 0.1 m. Direct shear test results were consistent between the quadrants most likely due to the soil being saturated and the roots getting pulled out instead of mobilizing the full their tensile strength. Root density varies the most in the first 0.05 m of the soil and was consistent with the literature. P-wave velocities in root reinforced soil increased up to 90 % compared to the bare soil velocities.

CHAPTER V: DISCUSSION AND MODELLING

5.1 OVERVIEW

Compressional wave velocity was measured with bimorph transducers for over 13 months as grass roots developed. There were two sets of time of flight measurements per quadrant as described in section 3.4. The velocity in the Forage Bermuda and Bahia started to increase in December of 2014. The velocity increased until about June, 2015 when the rate of increase slowed down due to slower root growth. Velocity in the Common Bermuda remained relatively constant throughout the experiment until July when both the bare soil and Common Bermuda started to increase due to settlement or increased total cohesion. The majority of the Common Bermuda sod was yellow throughout the experiment. Visual inspection and subsequent measurement of root density suggests that the Common Bermuda was not growing well. For most of the experiment the Forage Bermuda and the Bahia velocities were twice as high as the bare soil and Common Bermuda velocities.

The measured velocities varied between transducer pairs in each quadrant due local heterogeneity of the soil within the measurement volume. In order to account for variability between transducer pairs, the measurements were averaged. The average velocities measured for each grass type are shown in Figure 5.2.

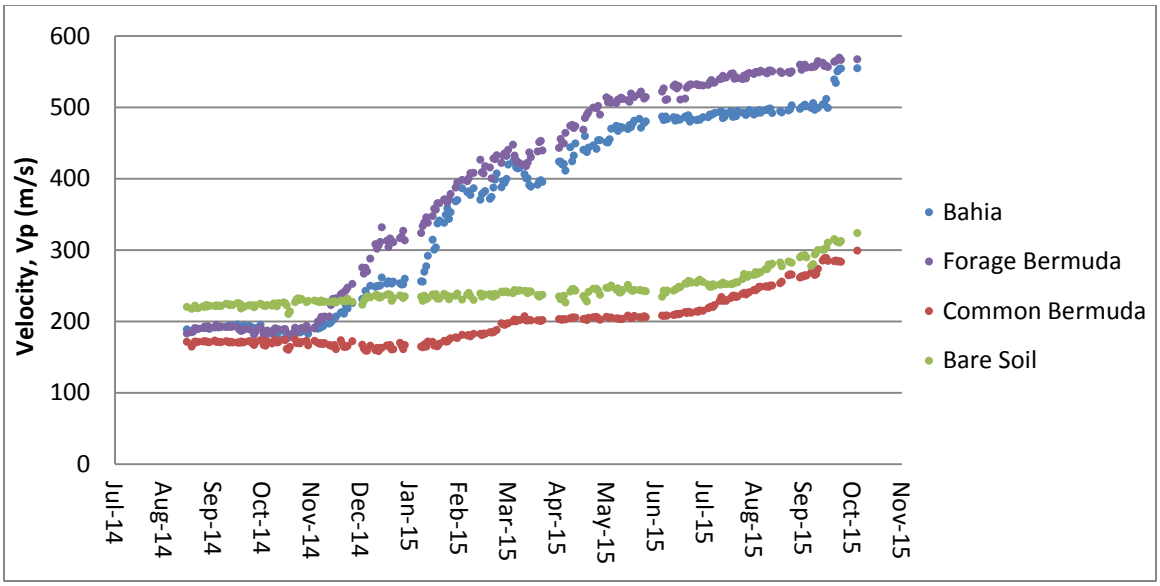

Figure 5.2 Average p-wave velocity, $\boldsymbol{V_p}$ (m/s) as a function of time

A code was written in MATLAB® to invert the velocity data and predict cohesion and porosity as a function of time. Coordination number, volumetric moisture content, matric suction, soil cohesion, porosity, grain shear modulus and other properties were measured and assumed in this model. The values are shown in Table 2.1. The porosity measured agrees with typical porosities found in the literature for a simple cubic pack (Cho et al., 2006). Equations 2.1 through 2.13 were used in this model.

5.2 BARE SOIL ANALYSIS

On May 21, 2014 water was introduced to the bottom of the soil. As described in section 3.1 the water level was raised slowly in order to keep the soil under tension. If the soil was not under tension then air voids could become trapped in the soil allowing for large voids. By June 10, 2014 the water level had reached the top of the sample. At the beginning of August 2014, the water level was lowered in 0.05 m increments until the water was 0.05 m above the gravel at the bottom of the soil. Compressional wave velocities were measured until October 26, 2015. The average velocities between transducer pairs measured in the bare soil are shown in Figure 5.4. The initial velocity in the dry soil was about 150 m/s when wetting began. Once the soil was wet to the surface the velocity increased up to 200 m/s. As the water level was lowered back down to the bottom of the soil layer, the velocity increased slightly to 220 m/s. After the sod was planted, the velocity stayed relatively constant until it started to increase in July. This increase was due to settlement or an increase in soil cohesion.

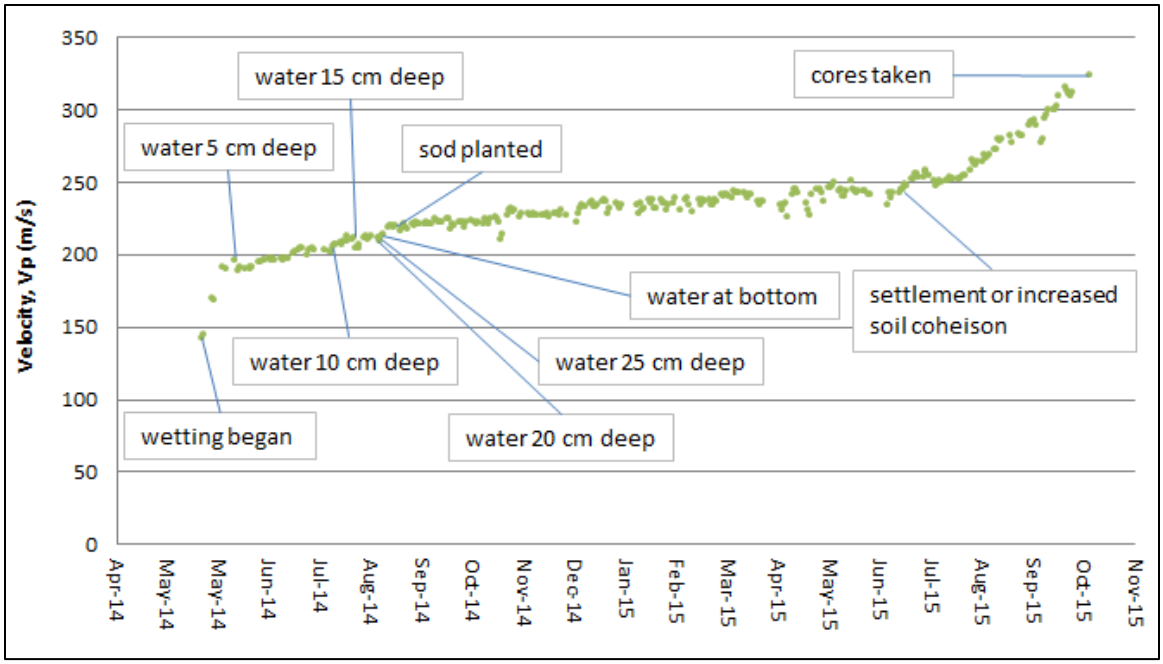

Figure 5.3 Average p-wave velocity, $\boldsymbol{V_p}$ (m/s) in the bare soil as a function of time

The change in acoustic behavior in the bare soil was modeled under two scenarios. The first case considered the increase in velocity was due to settlement, or a decrease in porosity. The cohesion was assumed to be constant at 2 kPa from direct shear tests on prepared soil samples. The measured time dependent moisture content and acoustic velocity were used to predict porosity shown in Figure 5.4. Moisture content is shown in black, and the predicted porosity of the bare soil is green.

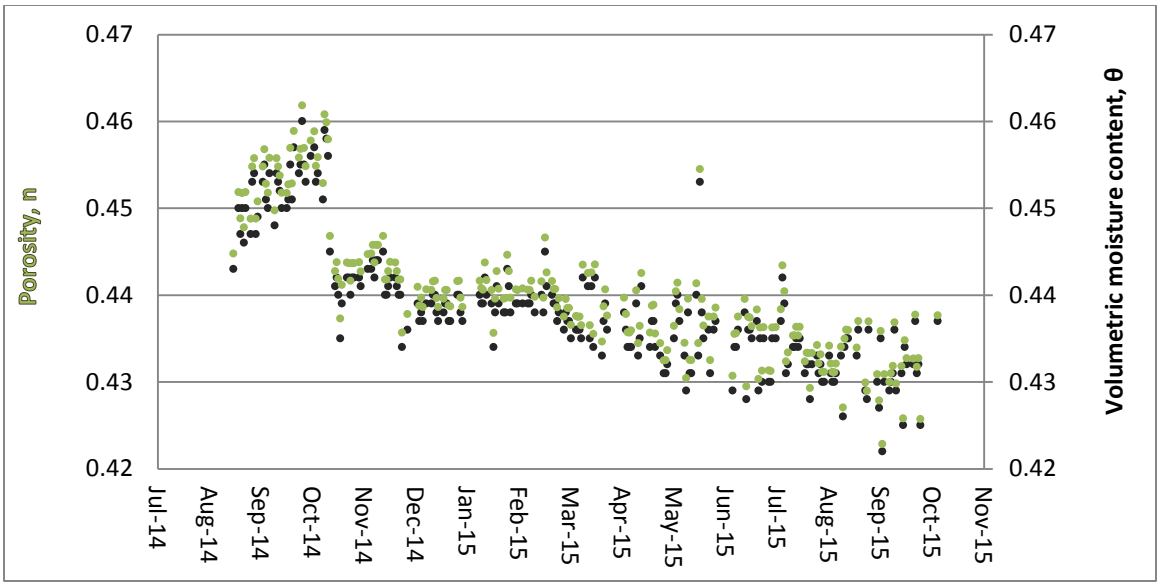

Figure 5.4 Bare soil porosity, $\boldsymbol{n}$ and volumetric moisture content, $\boldsymbol{\theta}$ as a function of time

According to Swiss Standard (1999), inorganic silts with slight plasticity can have a range in porosity from 0.21 to 0.56. The predicted porosity was within this range, but on the higher end which is typical for a nearly saturated silty clay loam. The initial porosity measured on prepared samples and the final porosity measured on cores were 0.57 and 0.47, respectively. The increase in moisture content and porosity at the beginning (Figure 5.4) may have been due to local wetting considering the water level was not altered. The sharp decrease in moisture content was possibly due to a fan drying the soil surface for a few days to help the sod grow in the other quadrants.

In order to explain the change in velocity, the saturation had to remain very large, greater than 0.99. At saturations greater than 0.99, the p-wave velocity begins to behave like that in water due to the lower compressibility of the water saturated porespace. In order to achieve saturation greater than 0.99, the porosity had to be close to the moisture content. Theoretical velocity as a function of saturation is shown in

Figure 5.5. The horizontal bars on the plot show the range of saturations needed to explain the p-wave velocities in each quadrant.

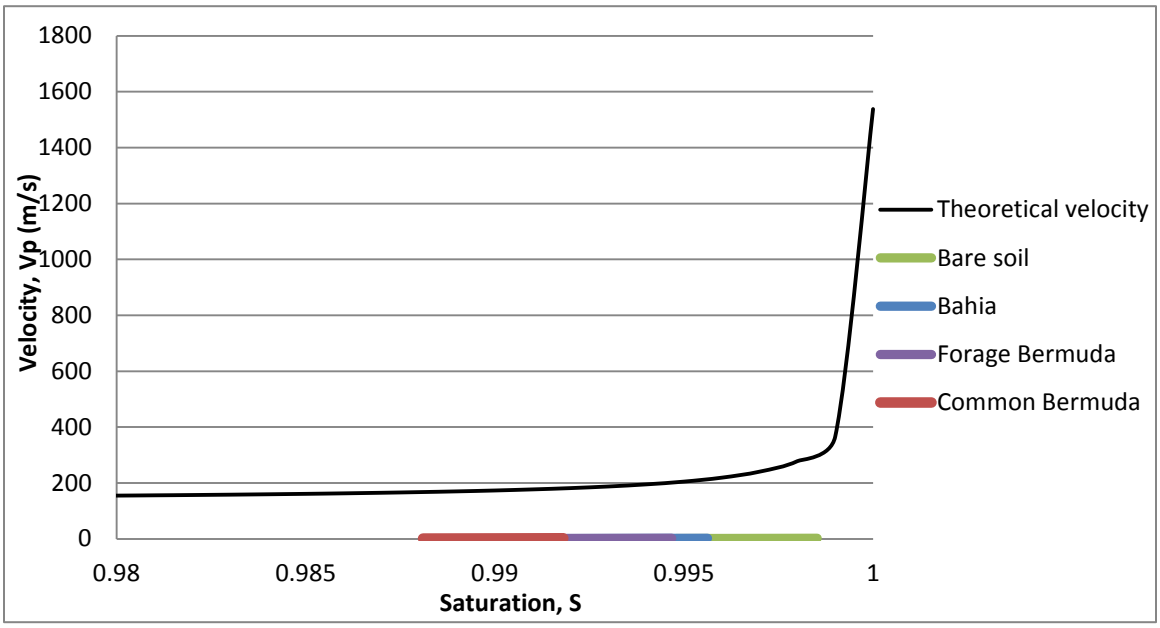

Figure 5.5 Velocity, $\boldsymbol{V_p}$ (m/s) as a function of saturation, $\boldsymbol{S}$

The analysis was generalized to allow the soil cohesion to increase from 2 to 10 kPa based on values measured destructively on prepared samples (initial value) and cores samples (final value), respectively. In soils with large amounts of clay content, cohesion increases as a function of time and decreasing water content (Kemper et al., 1984). The increase in cohesion was assumed to be exponential and is shown in Figure 5.6.

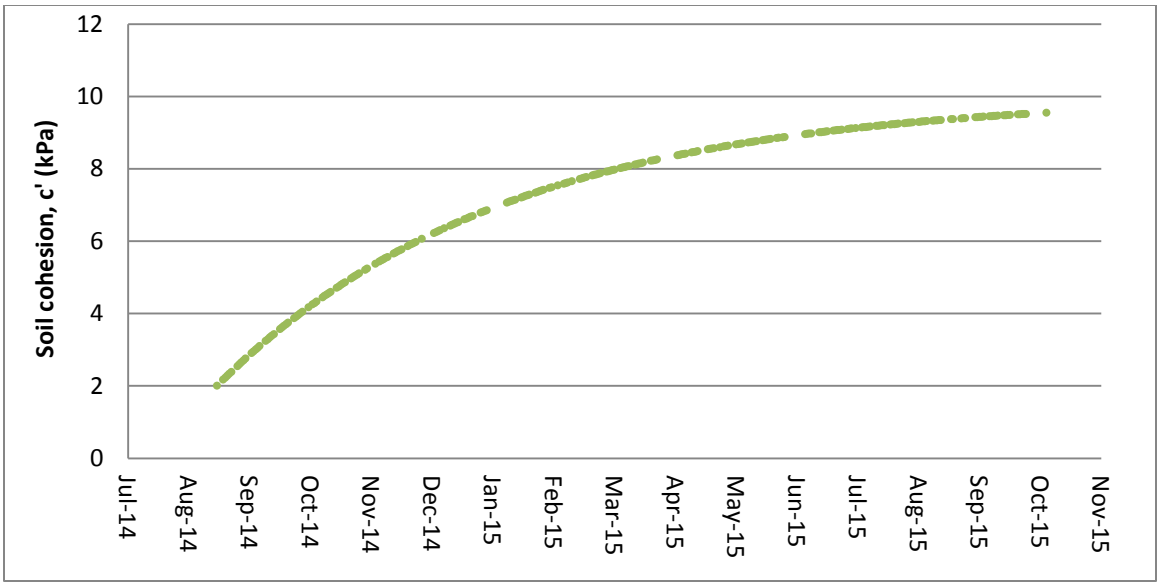

Figure 5.6 Exponential increase in soil cohesion, $\boldsymbol{c'}$ (kPa) as a function of time

Settlement analysis for the bare soil was conducted again using the time dependent soil cohesion shown above. The predicted porosity, shown in Figure 5.7, is similar to Figure 5.4. This is because the effect of the bulk modulus of the porespace was dominating over changes associated with the influence of cohesion on the bulk and shear moduli of the skeletal matrix.

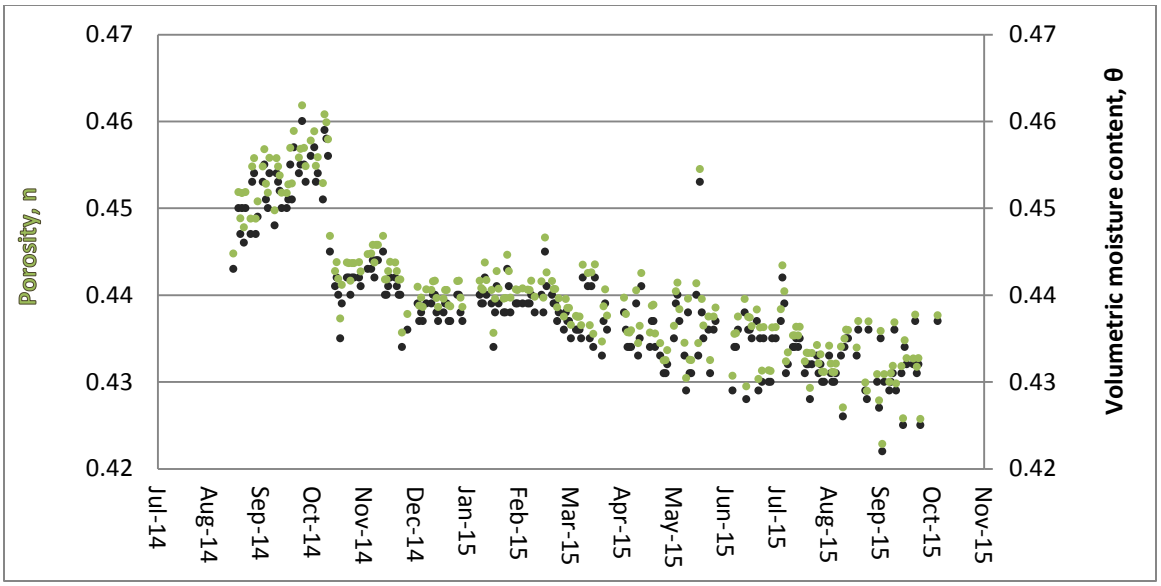

Figure 5.7 Bare soil porosity, $\boldsymbol{n}$ and volumetric moisture content, $\boldsymbol{\theta}$ as a function of time

Time dependent saturation was calculated by dividing the volumetric moisture content by the porosity (Figure 5.8). The saturation was predicted to increase from 0.9960 to 0.9985. These values are high for soils. Typically to achieve saturations over 0.99, soil must be stirred in water. The value predicted was greater than the average saturation, 0.97, measured from the cores. However, oven drying tests do not have the accuracy of measuring saturation to 0.001.

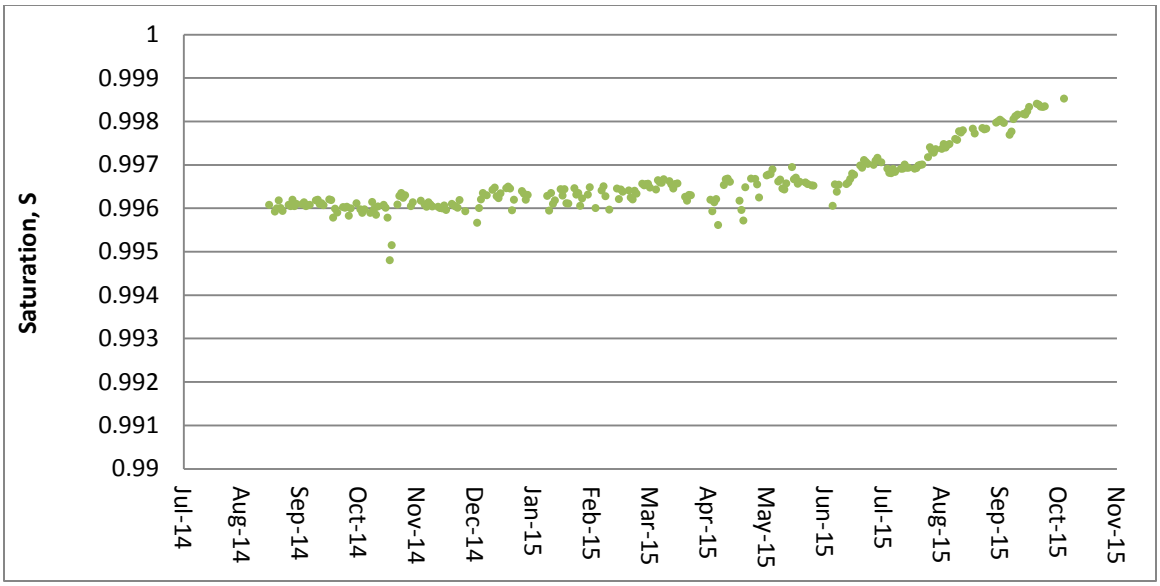

Figure 5.8 Bare soil saturation, ***S*** as a function of time

For the second scenario, there was no settlement in the bare soil. The change in velocity was solely due to an increase in soil cohesion. The porosity was assumed to be constant at a measured value of 0.47. With this constant porosity and the measured volumetric moisture content, the saturation (Figure 5.9) was less than 0.98. In this saturation range, the velocity was not nearly as sensitive to changes in saturation (Figure 5.5). The changes in p-wave velocity were no longer dominated by the bulk modulus of the porespace but are due to the bulk and shear moduli of the skeletal matrix.

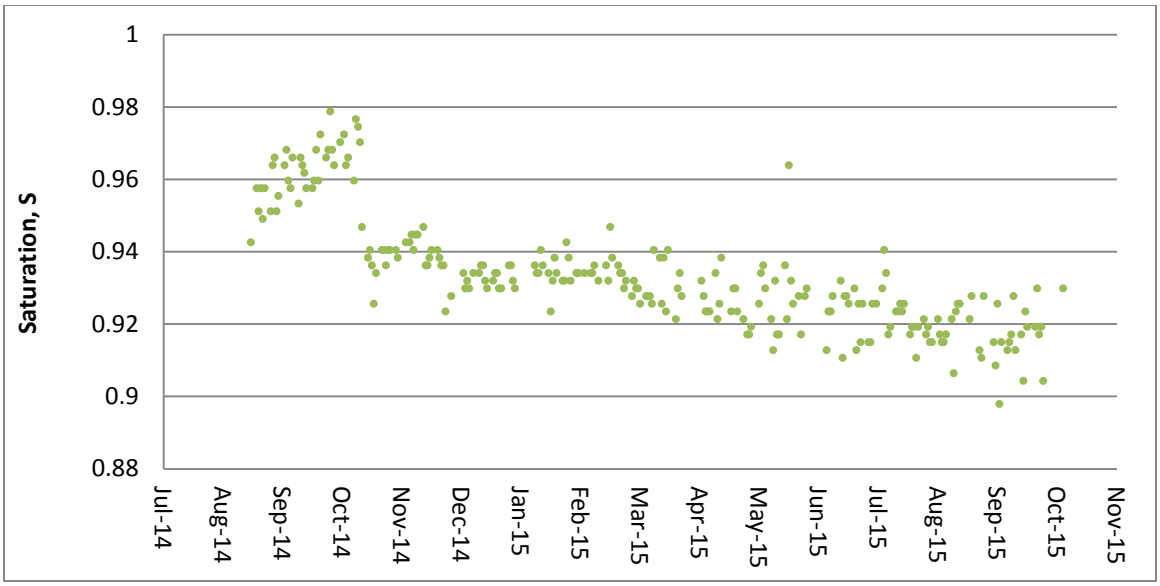

Figure 5.9 Bare soil saturation, ***S*** as a function of time

The increase in soil cohesion required to explain the change in velocity is shown in Figure 5.10. The predicted soil cohesion approached 1 MPa, which was greater than 10 kPa measured on soil cores at the end of the experiment. Minnesota Department of Transportation, Pavement Design, 2007 suggests for a saturated silty clay loam cohesions range from 10 to 20 kPa. According to Hertz-Mindlin and Biot-Gassmann theories, changes in p-wave velocity are proportional to the one-sixth power of changes in effective stress. Since the contributions of the matric suction and overburden were 3 and 2 kPa, respectively, the required cohesion had to be large to increase the effective stress.

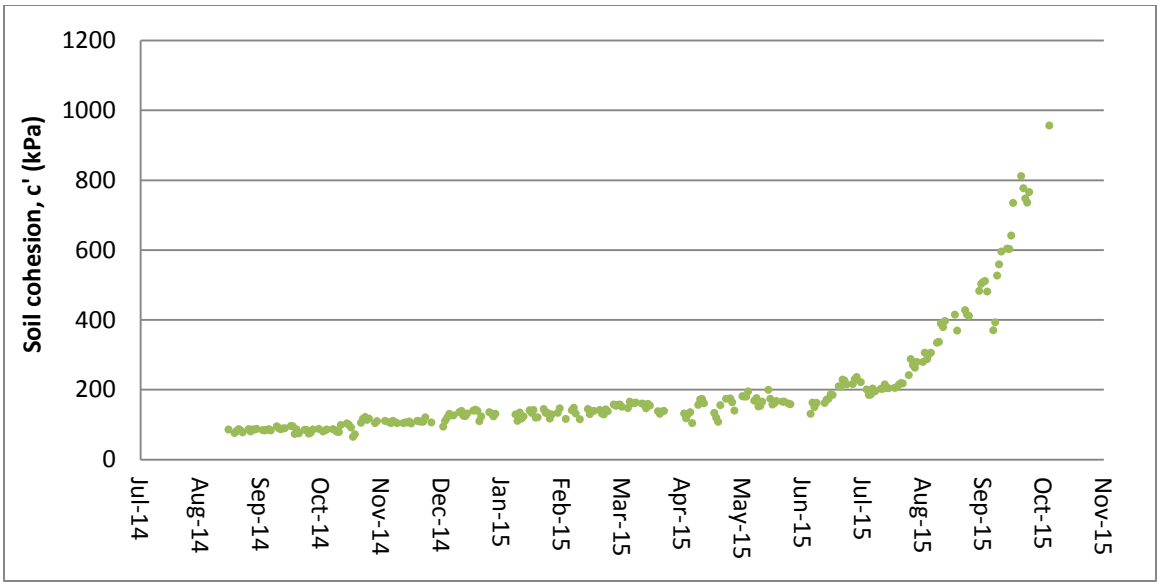

Figure 5.10 Soil cohesion, ***c'*** (kPa) as a function of time

In summary, the measured p-wave velocity of the soil can be modelled with soil saturation above 0.99 when the soil cohesion is low. In this region, the p-wave velocity is very sensitive to small changes in saturation due to the stiffening of the bulk modulus of the porespace. In case two, the change in velocity was modelled by an increase in soil cohesion associated an increase in effective stress. The increase in bulk and shear moduli of the skeletal matrix accounts for the increase in p-wave velocity. Typically soil cohesion greater than 100 kPa is not reasonable, so there must be other phenomena occurring to affect the acoustic behavior of the soil, or the acoustic model cannot be used to relate cohesion to direct shear measurements

5.3 GRASS ROOT REINFORCED SOIL ANALYSIS

To model the changes in acoustic behavior of the grass root reinforced soil quadrants, a similar approach was taken as in the bare soil. As shown in Figure 5.2, the initial velocity values in the soil before sod was planted ranged from 170 to 220 m/s. The velocity in the bare soil was the highest. This could be due to local heterogeneities of the quadrants such as compaction, patchy saturation, or other phenomena. In order to account for the differences in initial velocities, the initial grass velocities were normalized to the initial value of the bare soil velocity (Figure 5.11). This was done by adding the difference in initial grass velocities and initial bare soil velocity to the time dependent grass velocities.

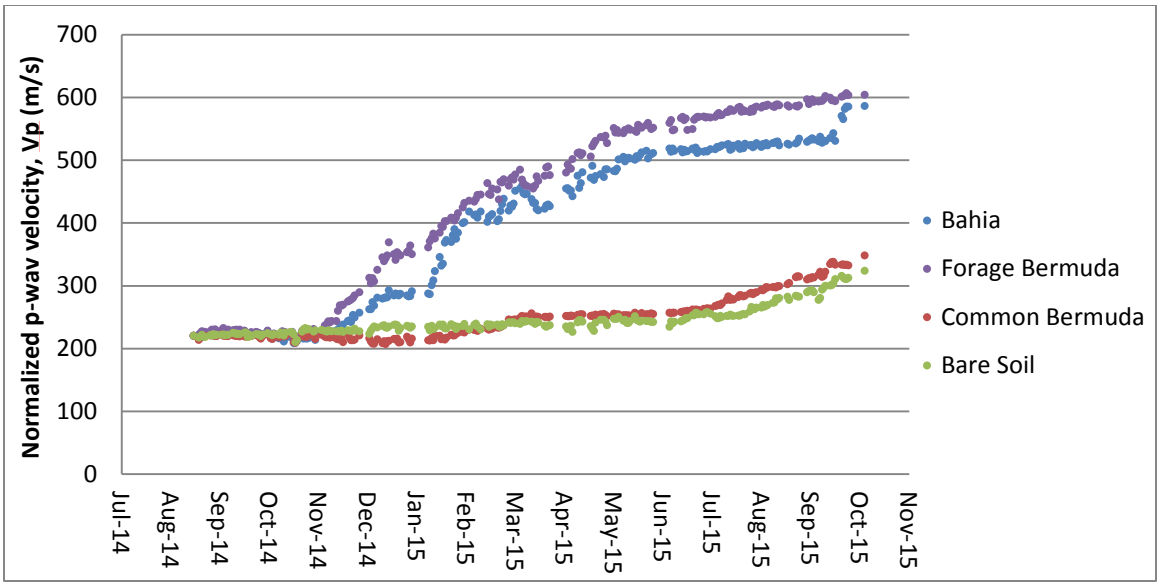

Figure 5.11 Normalized p-wave velocities, $\boldsymbol{V_p}$ (m/s) in each quadrant as a function of time

The change in p-wave velocity was modelled by two cases. The change in velocity was solely due to an increase in cohesion, and the change in velocity was due to settlement and an increase in cohesion. For the first scenario, the change in velocity was attributed to an increase in soil and root cohesion; no settlement was considered. The total cohesion is shown in Figure 5.12. The porosity was assumed to be constant at the measured value of 0.47. The bare soil cohesion would be the same as the previous analysis, shown in Figure 5.10. The total cohesion was calculated using Biot-Gassmann, Hertz-Mindlin and Wu's simple perpendicular root model. The Common Bermuda total cohesion often is about the same magnitude of the bare soil cohesion. The velocities in the Forage Bermuda and Bahia were much higher than the bare soil and Common Bermuda. In order to explain these large changes in velocities, the total cohesion had to approach 40000 kPa. Again this is a consequence of the required effective stress in the Hertz-Mindlin and Biot Gassmann theories. Typical values of

cohesion and shear strength of soils reinforced with grass roots range from 1 to 100 kPa (Wu et al., 1979, Tengbeh, 1989, Operstein et al., 2000, Pollen et al., 2005, De Baets et al., 2008, Trung, 2012).

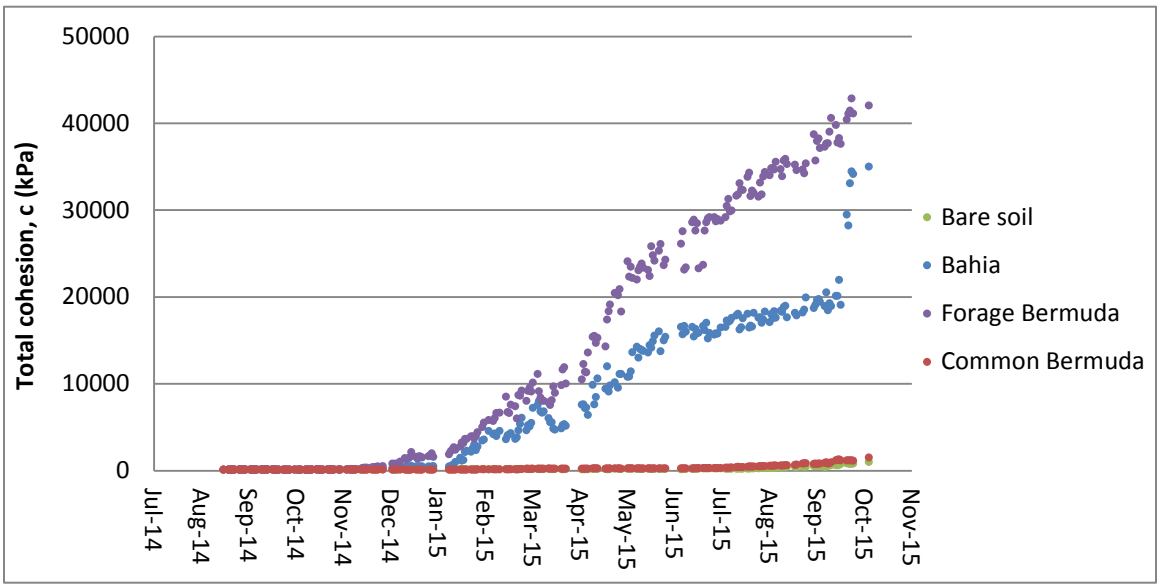

Figure 5.12 Total cohesion, ***c*** (kPa) as a function of time

Root cohesion (Figure 5.13) was calculated by subtracting the soil cohesion (Figure 5.10) from the total cohesion (Figure 5.12). In early grass root development, the velocities of the grass reinforced soil were less than the velocity in the bare soil causing root cohesion to be negative. This could have been caused by other changes in the soil before the grass roots penetrated to the depth of the transducers. However, the negative values are within experimental error. For this analysis the assumption was made that grass roots increase cohesion of the soil, so the negative root cohesion values were neglected.

The root cohesions required to explain the acoustic measurements were much larger than the measured root cohesion of 1 kPa measured using the direct shear test.

The values were also outside the range of root cohesion, 1 to 100 kPa, commonly cited in the literature. Like the previous analysis of the bare soil, if the cohesion was responsible for the changes in p-wave velocity, it was attributable to the bulk and shear modulus of the skeletal matrix.

An explanation could have been the difference in scale of the measurements. The deformation of the soil during p-wave propagation is a small strain phenomenon on the order of microns. Traditional direct shear test measurements involve large strain phenomena on the order of millimeters (Potts et al, 1987). The two different approaches might be responsible for the differences in cohesion.

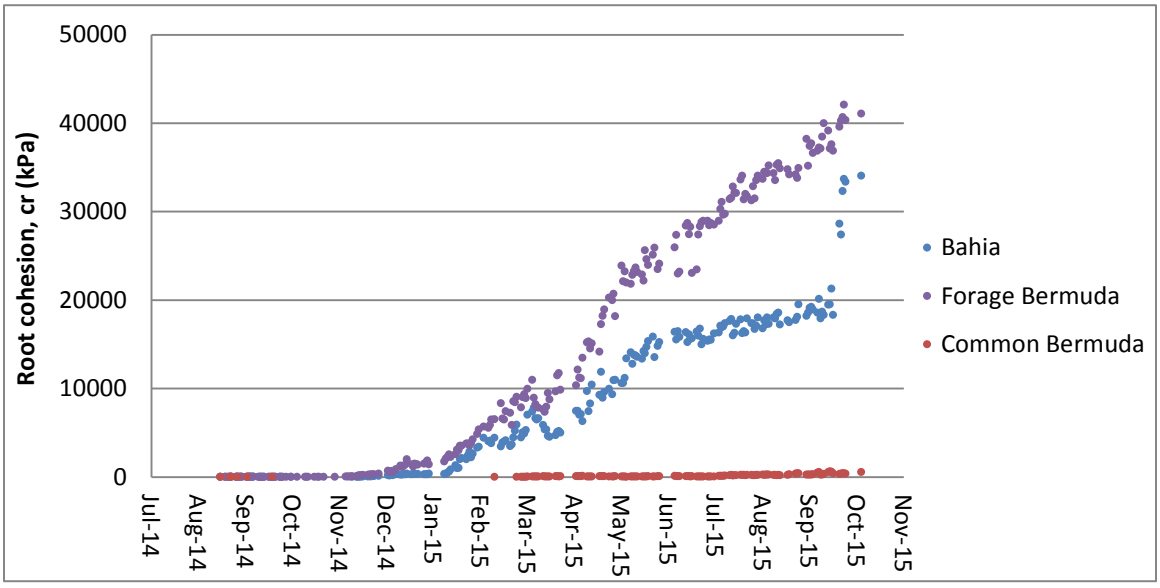

Figure 5.13 Root cohesion, c_r (kPa) as a function of time

There are two ways roots fail during direct shear tests: breakage and pull-out. Since the soil was practically saturated, the friction between the roots and the soil was less than it would have been in less saturated soil making the roots susceptible to root pull out. The maximum tensile strength of the root was not achieved lowering the

measured cohesion from the direct shear tests. P-wave propagation deforms the roots on such a small scale that pull-out or breakage is not likely. It is more likely that the roots merely flex elastically. The differences in the deformation associated with the two measurements might explain the differences in the cohesion values.

A simple perpendicular root model developed by Wu can be used to calculate the root cohesion of soils using the root area ratio and tensile strength of roots (t_r) (Equation 2.15). Upper and lower limits for the root tensile strength deduced from Cheng's et al. (2003) power law relationship between tensile strength of roots and root diameter was shown in Figure 2.3. For Bahia, the range of tensile strengths was from 13000 to 25000 kPa, and for Bermuda the range was from 10000 to 17000 kPa. The perpendicular root model and the range of tensile strengths were used to calculate a range of root area ratios from the modelled root cohesion and are shown in Figure 5.14.

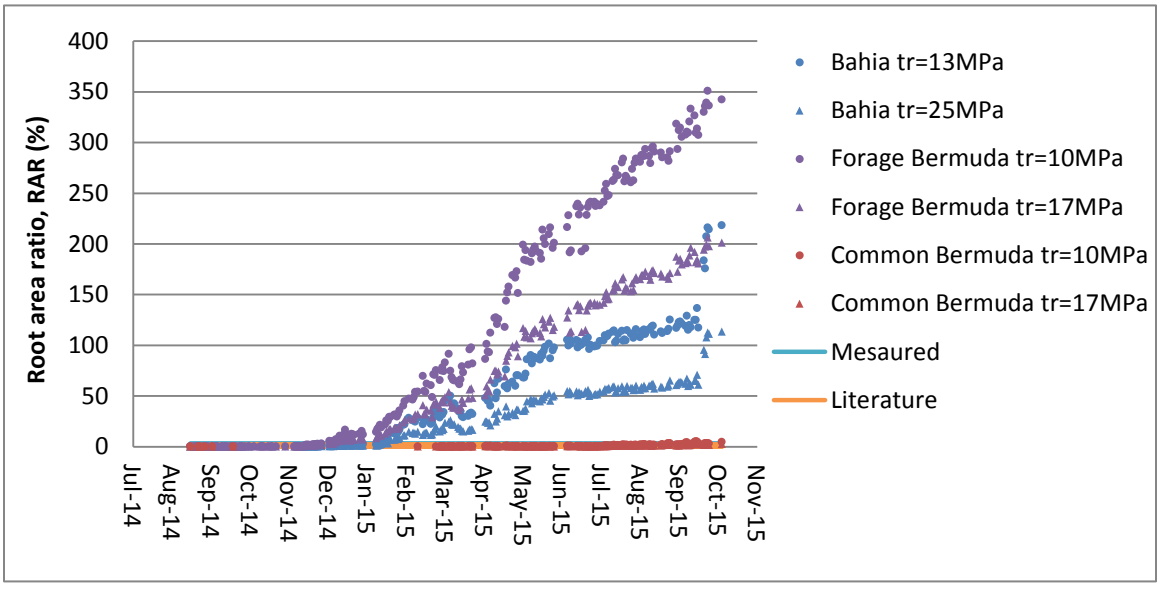

Figure 5.14 Root area ratio, ***RAR*** (%) as a function of time

Root area ratios have been published by Operstein et al. (2000), Simon et al.

(2002), and De Baets et al. (2006) and typically range from 0.001 to 2.5 % although most values are less than 1 %. The root area ratios calculated from the root density measured at the end of the experiment ranged from 0.7 to 3 %. The acoustic related values were far greater than the measured or literature values. In fact root area ratios greater than 100 % are not physical since the roots area would have to be greater than the area of the sample itself.

Using Equation 2.18, one can use root area ratio and root tissue density to predict root density. Birouste's et al. (2014) measured the average root tissue density from a field-community in shallow soil to be 315 kg/m³. This average value was assumed to be the average root tissue density of the grass roots. A range of predicted root densities are shown with the measured and literature values in Figure 5.15.

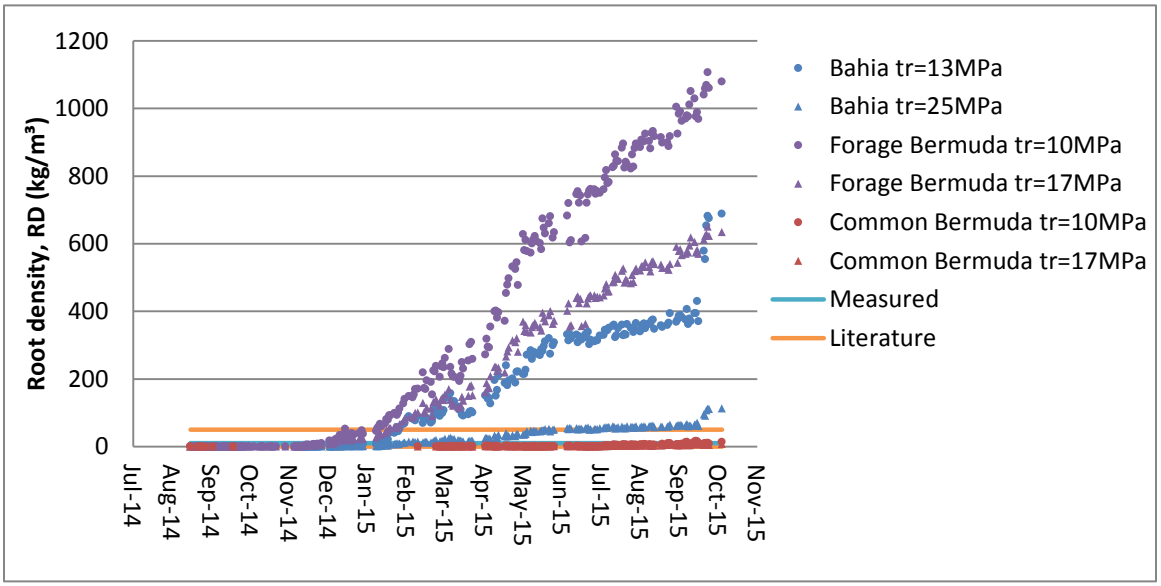

Figure 5.15 Root density, ***RD*** (kg/m³) as a function of time

According to the literature typical root densities are measured from 0.05 to 50 kg/m³ (Gyssels et al., 2005, De Baets et al., 2006, De Baets et al., 2008). Values

measured from root washing cores and drying the roots ranged from 2 to 10 kg/m³. The predicted root density for the Forage Bermuda and Bahia were greater than the values in the literature. Again this was expected due to the large predicted cohesion. The root density in the Common Bermuda agreed with the measured and literature values.

The second approach to model the acoustic velocity of the grass reinforced soil is to assume that the soil settled in the same manner as the bare soil. With the same porosity and the measured moisture content, the saturation in the grass quadrants would also behave like the saturation in the bare soil (Figure 5.8). The total cohesion for the grass reinforced soil is shown in Figure 5.16.

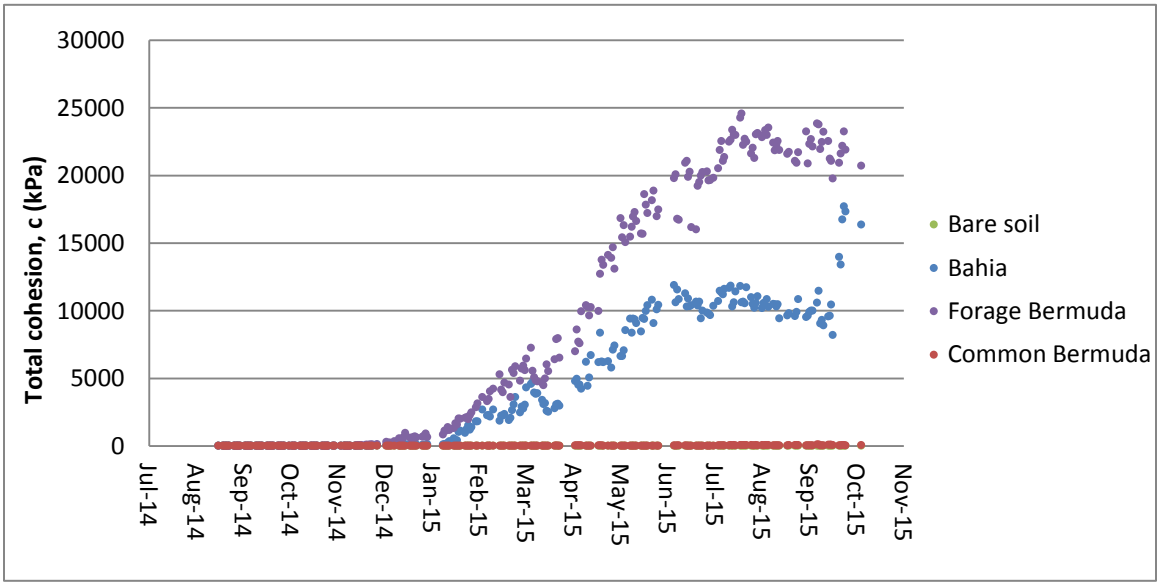

Figure 5.16 Total cohesion, ***c*** (kPa) as a function of time

The cohesion of the Common Bermuda behaved similarly to the bare soil cohesion. The Bahia and Forage Bermuda cohesions increased up to 20000 and 25000 kPa, respectively. Attributing settlement changes in the bare soil did result in much

lower total cohesion values. The soil cohesion was assumed to increase from 2 to 10 kPa as shown in Figure 5.6. The initial value was measured from prepared soil samples of the same soil, and the final value was measured from the bare soil core samples. The root cohesion (Figure 5.17) was calculated as the difference in total (Figure 5.16) and soil cohesion (Figure 5.6).

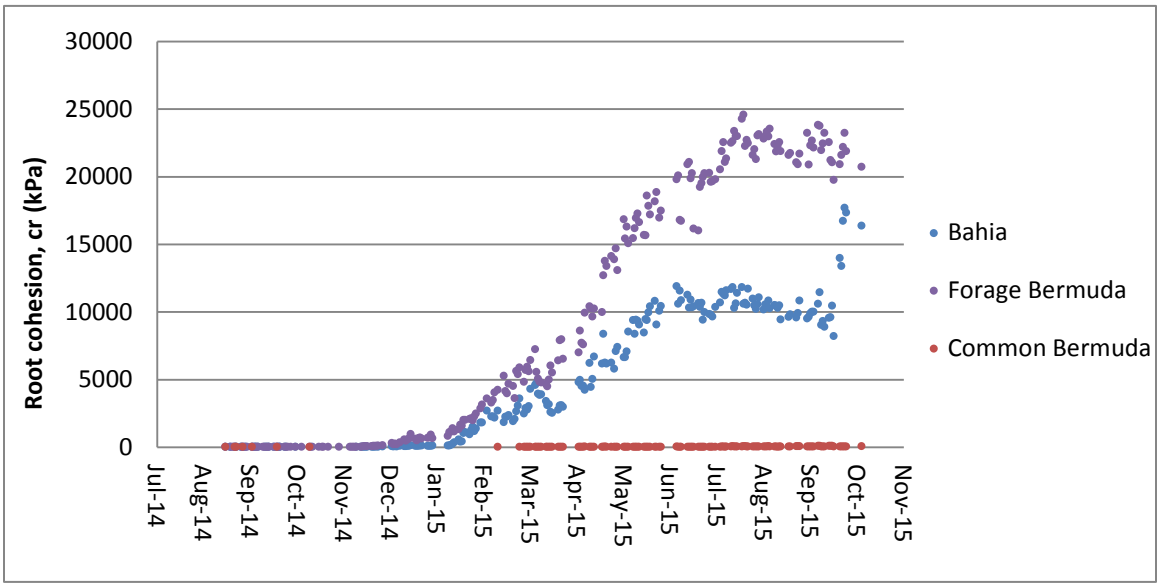

Figure 5.17 Root cohesion, c_r (kPa) as a function of time

The root cohesion was very similar to the total cohesion since soil cohesion was assumed small. Required root cohesion values in Figure 5.17 were less than what was calculated in Figure 5.13. This was due to the high saturation increasing the incompressibility of the porespace, so less cohesion was required to explain the change in velocity. The predicted root cohesion values were still greater than the range in the literature.

Using Wu's simple perpendicular root model and Cheng's range of tensile strengths of roots, a range of root area ratios were predicted (Figure 5.18). The

acoustic related values were far greater than the measured or literature values. The calculated range of root area ratios for the Forage Bermuda grass was greater than 100 % which is not physical. The Common Bermuda root area ratio was less than 1 % which is typically found in the literature.

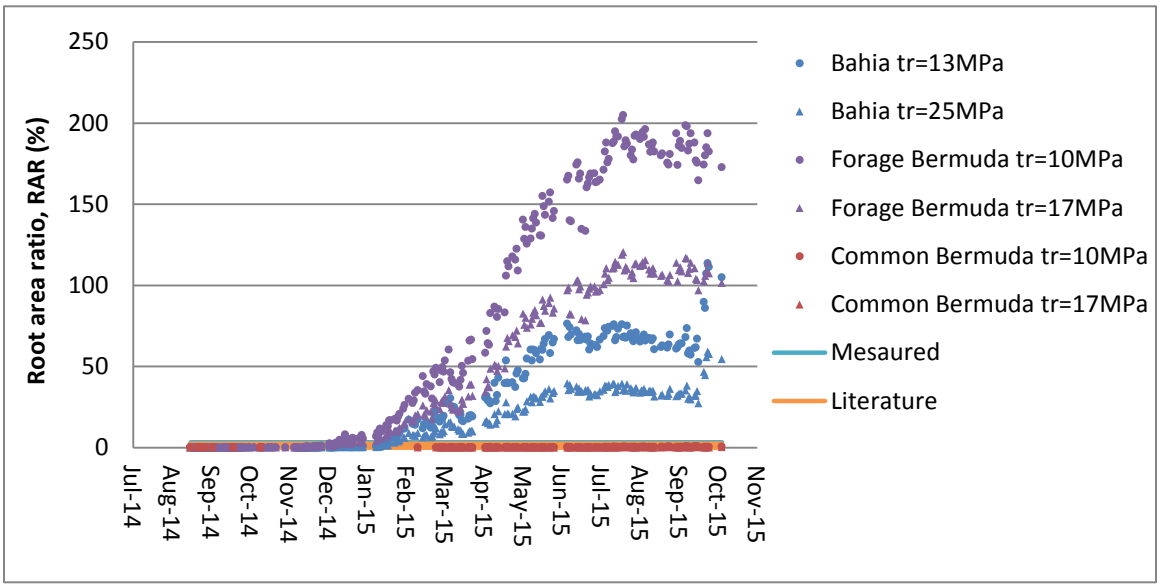

Figure 5.18 Root area ratio, ***RAR*** (%) as a function of time

Again using the same method used to generate Figure 5.15, a range of root densities were calculated from the range of root area ratios. Like the previous figure, the Forage Bermuda and Bahia root densities were high with respect to the range in the literature (De Baets et al., 2006, De Baets et al., 2008). The final Common Bermuda values agreed with the literature.

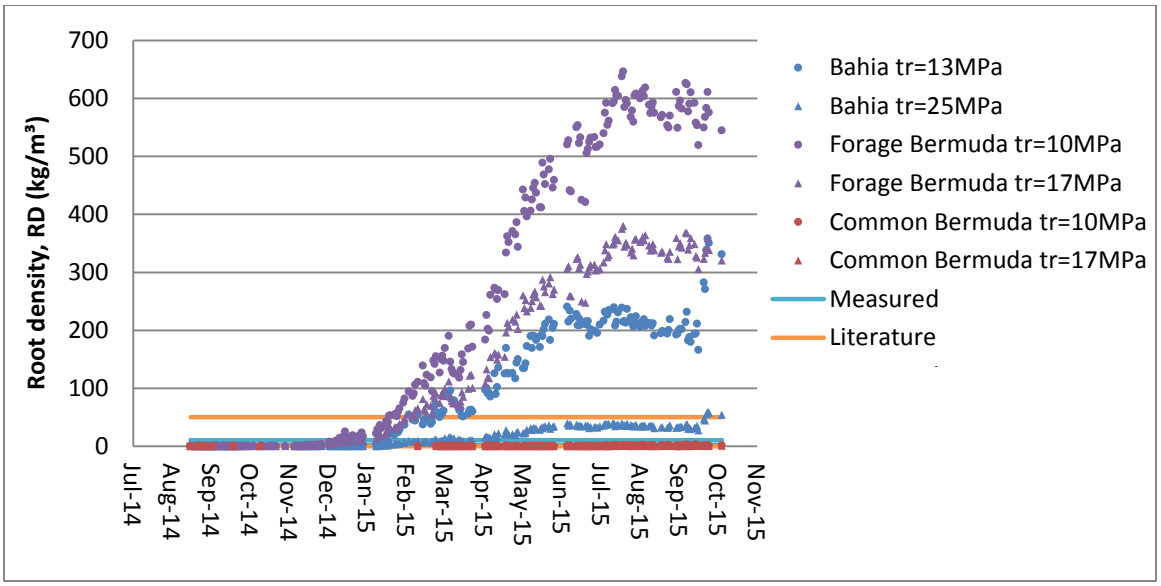

Figure 5.19 Root density, $\boldsymbol{RD}$ (kg/m³) as a function of time

There required root cohesion was modelled in two way: the first model having constant porosity with no settlement and the second model having soil settlement. Incorporating the decrease in porosity in the Bahia quadrant raised the saturation above 0.99 which lowered the required root cohesion by 20000 kPa. The high saturation made the porespace less compressible which increased the velocity requiring less effective stress via cohesion. A slight decrease in required cohesion was shown in the settlement case as a result of the velocity's high sensitivity to saturation greater than 0.99.

The required root cohesion in the Bahia grass for each case is shown in Figure 5.20. For the case with no settlement the required root cohesion was about 35000 kPa. Including soil settlement decreased the required root cohesion to about 15000 kPa. This was due to the incompressibility of the porespace described above.

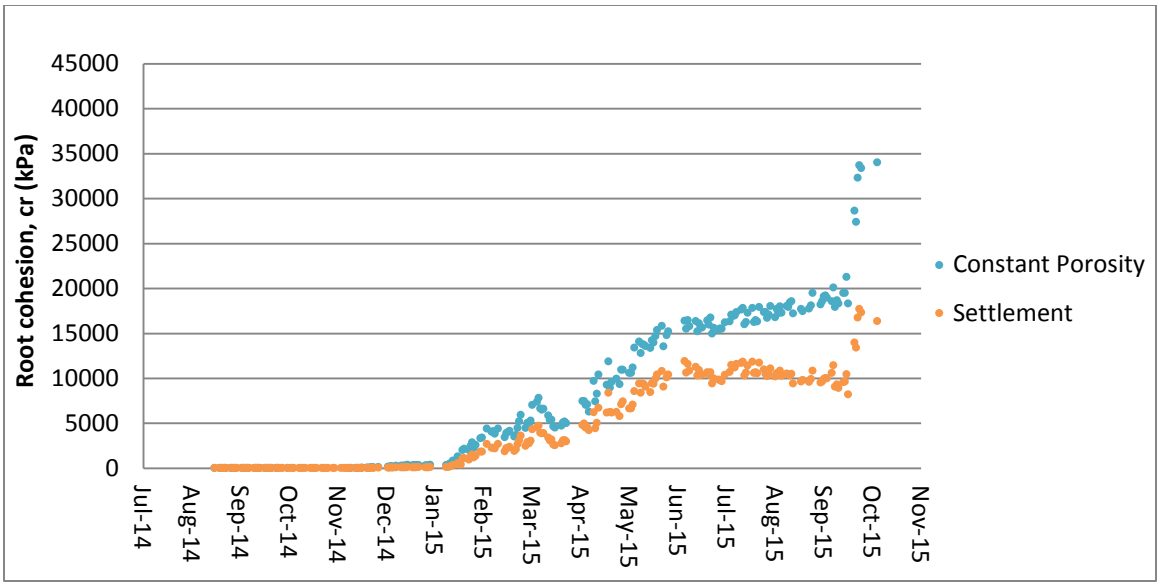

Figure 5.20 Bahia root cohesion, c_r (kPa) as a function of time

For the Forage Bermuda, accounting for settlement lowered the required root cohesion by 20000 kPa. This is shown in Figure 5.21. Later in the experiment when saturation was approaching 1.0, the required root cohesion began to stay constant if not slightly decrease.

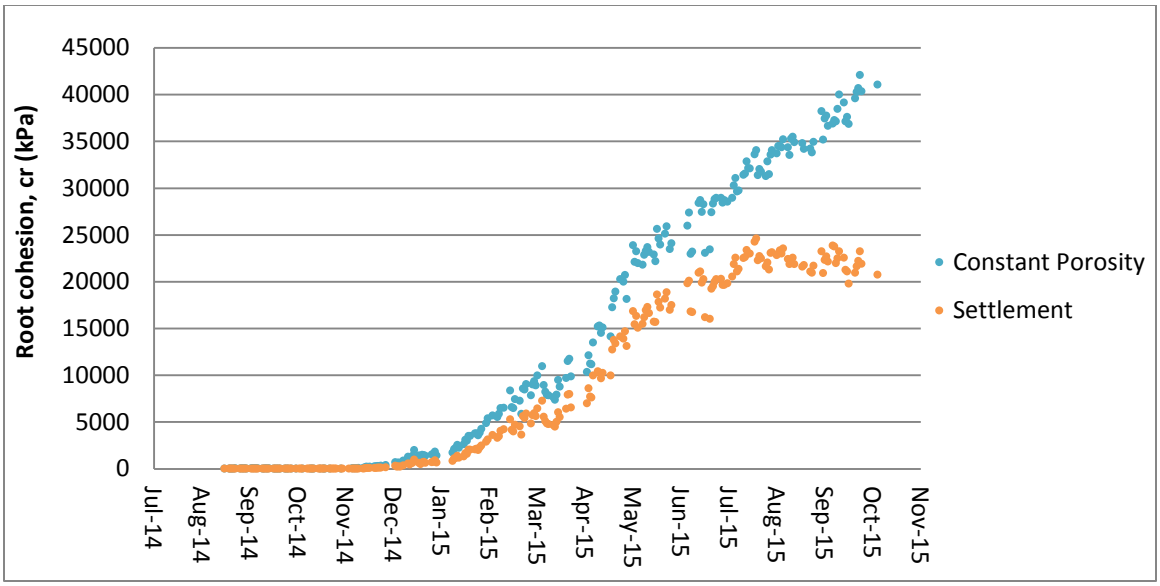

Figure 5.21 Forage Bermuda root cohesion, c_r (kPa) as a function of time

The Common Bermuda required root cohesion was much smaller due to lower p-wave velocity (Figure 5.22). Accounting for settlement, the final root cohesion predicted was in the range of values found in the literature, 1 to 100 kPa. According to the p-wave analysis the roots were slow to develop until about March of 2015. The difference between the root cohesion in the settlement case and no settlement case was about 500 kPa. This was again due to the incompressibility of the porespace.

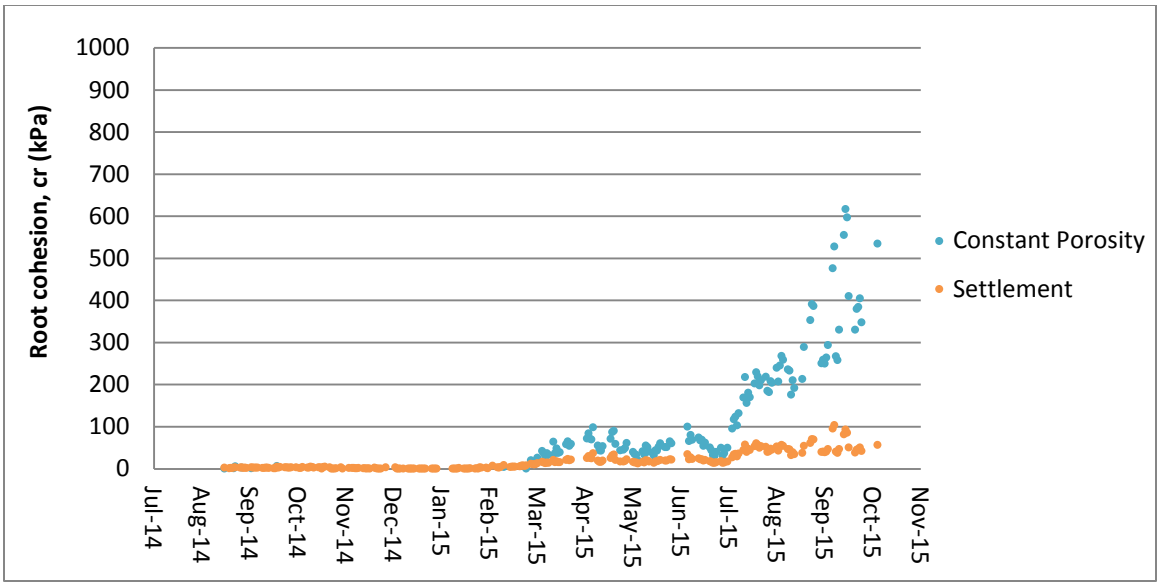

Figure 5.22 Common Bermuda root cohesion, c_r (kPa) as a function of time

In summary, two cases were considered to model the acoustic velocity of the grass root reinforced soil. In the first case porosity was assumed to be constant at the measured value of 0.47. The lower saturation required very large cohesion, root area ratio and root density values, in order to explain the velocity. In the second case settlement of the soil was considered and porosity was assumed to decrease with time. This lowered the cohesion, root area ratio, and root density required to explain the velocity. However, values predicted for the Bahia and Forage Bermuda were large compared to the values measured using the direct shear tests and literature values. Common Bermuda values agreed with the measured and literature values.

CHAPTER VI: CONCLUSION

Watershed infrastructure provides flood management, fresh water, and soil conservation. Grass has commonly been used to strengthen the surfaces of dams, slopes, and streambanks. New technologies must be developed to monitor the performance of this valuable infrastructure.

In this laboratory experiment, three types of grass were planted with one bare soil quadrant as a control. The grass roots were allowed to develop for about one year. P-wave velocity was measured throughout the experiment using bimorph transducers and a time of flight method. Other time dependent measurements consisted of volumetric moisture content and matric suction. After a year, soil core samples were taken from each quadrant. Direct shear tests were conducted on the samples to measure cohesion and internal friction angle of the soil. The samples were then dried to determine bulk density, dry density, gravitational moisture content, porosity, void ratio, and saturation. Roots were washed from the samples to measure root density.

P-wave velocity ranged from 170 – 570 m/s and increased in all quadrants including the bare soil. Velocity in two of the root reinforced soil increased up to 90% of the bare soil velocity. Volumetric moisture content decreased from 0.45 – 0.43, and matric suction was constant at 3 kPa. Direct shear measurements of soil cohesion was 10 kPa on average, and root cohesion was about 1 kPa. Measured internal friction angle ranged from 15 to 53°. Average bulk and dry density from the core samples were 1800 and 1300 kg/m^3, respectively. Gravitational moisture content and saturation were 0.34 and 0.97, respectively. Porosity and void ratio were 0.47 and 0.90, respectively.

Several modelling approaches were attempted using Biot-Gassmann and Hertz-Mindlin theories to explain the increase in p-wave velocity due to settlement and an increase in cohesion. First the bare soil quadrant was analyzed assuming the soil cohesion was negligible. The increase in p-wave velocity was solely ascribed to settlement, and therefore a reduction in porosity. Since moisture content remained relatively constant as porosity decreased, the saturation increased. When a soil is saturated above 0.99, the compressibility of the porespace has a stiffening effect on the soil, and the p-wave increases sharply. In order to explain the increases in p-wave velocity of the bare soil, saturation had to be greater than 0.99. The final measured porosity was 0.47, but the porosity required to explain the change in velocity was much closer to the final moisture content of 0.44.

A second modelling approach of the bare soil assumed that there was no settlement so that the porosity remained constant at 0.47. The increase in p-wave velocity was ascribed to an increase in soil cohesion. In the Hertz-Mindlin theory, the p-wave velocity is proportional to the one-sixth root of the effective stress. This required a change in effective stress on the order of $10^1 - 10^4$ kPa to explain the measured change in p-wave velocity. Effective stress has three components: overburden, matric suction, and cohesion. Measured overburden and matric suction were small and remained constant. This required that the large increase in effective stress had to be due to an increase in cohesion. The soil cohesion required to explain the change in velocity was 1000 kPa. The final measured soil cohesion from direct shear tests was 10 kPa on average. The change in velocity was due to the bulk and

shear moduli of the skeletal matrix in this model. To explain the change in p-wave velocity in the bare soil, either porosity was required to decrease to 0.44 or soil cohesion was required to increase to 1000 kPa.

In this thesis, the assumption was made that root growth only affected the root cohesion. The change in acoustic velocity in a grass reinforced soil may be due to changes in the soil as well as the influence of the roots. From direct shear tests on root reinforced soil core samples, root cohesion was determined to be about 1 kPa. Root density was measured to be 3.7 kg/m^3 on average.

For the first modelling approach in the grass quadrants, the porosity was assumed to be constant. The root cohesion was modelled to explain the change in velocity. P-wave propagation deforms the media on a much smaller scale than direct shear tests. The required soil cohesion was 1000 kPa as in the bare soil case. The required root cohesion to explain the change in velocity ranged from 500 – 40000 kPa.

Another attempt at modelling the increase in p-wave velocity was to account for the change in bare soil with settlement and the influence due to grass on an increase in cohesion. The time dependent behavior of the porosity of the bare soil calculated in the first case was assumed to be the behavior of the porosity in all of the quadrants. Again the soil was saturated above 0.99, so the compressibility of the porespace had a stiffening effect on the soil and the p-wave. The contribution of the bulk modulus of the porespace required much less cohesion to explain the change in velocity. The root cohesion required to explain the change in velocity was much greater than the average root cohesion measured in the direct shear tests. This suggests that cohesion predicted

from Biot-Gassmann and Hertz-Mindlin theory cannot be related to cohesion measured from direct shear tests. The final Common Bermuda root cohesion was predicted to be within the range found in the literature, 1 – 100 kPa (Wu et al., 1979; Tengbeh, 1989; Operstein et al., 2000; Pollen et al., 2005; De Baets et al.; 2008, Trung, 2012). To explain the changes in acoustic behavior of the soil, required porosity from the theory had to decrease to a value close to the moisture content, and root cohesion from the theory was required to increase up to 20000 kPa.

CHAPTER VII: FUTURE WORK

In future experiments, effort should be made to separate pore compressibility from cohesion. When measuring p-wave velocity in saturated soils, the compressibility of the porespace can dramatically affect velocity. Shear wave velocity should be measured to observe the shear modulus behavior of the skeletal matrix. This allows a measurement without the influence of the bulk modulus of the porespace.

Another way to reduce the effect of the pore compressibility would be to lower the saturation. Draining the water from the soil could replicate a wider range of field conditions on embankments or earthen dams. This would result in a lower saturation and would minimize the effect of the compressibility of the porespace. This would also increase the effect of matric suction on effective stress.

Alternate porous media models should be explored. Biot-Gassmann and Hertz-Mindlin put emphasis on effective stress and the heterogeneity of saturation in soils. P-wave velocity is proportional to the one-sixth root of effective stress. Patchy saturation is an alternative model that could be used.

Another method to independently measure cohesion should be considered. P-wave propagation is a small scale phenomena on the order of microns, and direct shear tests are large scale phenomena on the order of millimeters. P-waves cause elastic deformations of the soil, and direct shear tests cause plastic deformation of the soil. During deformation of the roots due to p-wave, roots will not pull-out or break, and during direct shear tests, roots can pull-out and break. A metal wedge method used by soil scientists could be a better alternative.

Alternate root reinforcement models should also be explored. Wu's simple

perpendicular root model has been known to overestimate root cohesion in grasses up to 100% (De Baets et al., 2008). The fiber bundle root model (Pollen and Simon, 2005) could be a more accurate model for this experimental design.

Assumptions in this thesis on the effect of root reinforcement on soil should be relaxed. Roots could possibly affect the porosity of soil by increasing or decreasing the porespace. The porespace could be increased by roots pushing particles apart or decreased by filling voids. Root tissue density could increase or decrease the bulk density by filling air voids or pulling water from the soil, respectively. Internal friction angle of the soil might also be affected by the friction on the surface of the root.

CHAPTER VIII: REFERENCES

Arnott, W. P., Sabatier, J. M. (1990). "Laser-Doppler Vibrometer Measurements of Acoustic to Seismic Coupling." Applied Acoustics, 30(4), pp. 279-291.

ASTM D3080 / D3080M-11, Standard Test Method for Direct Shear Test of Soils Under Consolidated Drained Conditions, ASTM International, West Conshohocken, PA, 2011, www.astm.org

Benahmed, N., Bonelli, S. (2012). "Investigating Concentrated Leak Erosion Behavior of Cohesive Soils by Performing Hole Erosion Tests." European Journal of Environmental and Civil Engineering, 16(1), pp. 43-58.

Berkenhagen, J. H., Hickey, C. J., Prasad, S. N., Römkens, M. J. M. (1998). "Acoustic Observation of a Clay during a Wetting-Drying Cycle." In Proceedings of the Third Symposium Bouyoucos Conference on Agroacoustics, Tishomingo, MS, pp. 77-89.

Biot, M. A. (1962). "Mechanics of Deformation and Acoustic Propagation in Porous Media." Journal of Applied Physics, 33(4), pp. 1482-1498.

Birouste, M., Zamora-Ledezma, E., Bossard, C., Pérez-Ramos, I. M., Roumet, C. (2014). "Measurement of Fine Root Tissue Density: a Comparison of Three Methods Reveals the Potential of Root Dry Matter Content." Plant and Soil, 374(1-2), pp. 299-313.

Blum, A., Flammer, I., Friedli, T., Germann, P. (2004). "Acoustic Tomography Applied to Water Flow in Unsaturated Soils." Vadose Zone Journal, 3(1), pp. 288-299.

Bonelli, S., Benahmed, N. (2010). "Piping Flow Erosion in Water Retaining Structures: Inferring Erosion Rates from Hole Erosion Tests and Quantifying the Failure Time." In IECS 2010, 8th ICOLD European Club Symposium Dam Safety-Sustainability in a Changing Environment, Innsbruck, Austria, pp. 6.

Briaud, J. L., Ting, F. C. K., Chen, H. C., Cao, Y., Han, S. W., Kwak, K. W. (2001). "Erosion Function Apparatus for Scour Rate Predictions." Journal of Geotechnical and Geoenvironmental Engineering, 127(2), pp. 105-113.

Briaud, J. L. (2005). "Erodibility of Fine Grained Soils and New Soil Test in Erosion of Soils and Scour of Foundations." In Proceedings of the Geo-Frontiers Congress, Austin, TX, pp. 1-10.

Briaud, J., Chen, H., Govindasamy, A., Storesund, R. (2008). "Levee Erosion by Overtopping in New Orleans during the Katrina Hurricane." Journal of Geotechnical and Geoenvironmental Engineering, 134(5), pp. 618–632.

Brutsaert, W., Luthin, J.N. (1964). "The Velocity of Sound in Soils Near the Surface as a Function of the Moisture Content." Journal of Geophysical Research, 69(4), pp. 643-652.

Burdine, N. (1953). "Relative Permeability Calculations from Pore Size Distribution Data." Journal of Petroleum Technology, 5(03), pp. 71-78.

Chambers, J. P., Sabatier, J. M. (2002). "Recent Advances in Utilizing Acoustics to Study Surface Roughness in Agricultural Surfaces." Applied Acoustics, 63(7), pp. 795-812.

Chen, F., Zhang, J., Zhang, M., Wang, J. (2015). "Effect of Cynodon Dactylon Community on the Conservation and Reinforcement of Riparian Shallow Soil in the Three Gorges Reservoir Area." Ecological Processes, 4(1), pp. 1-8.

Cheng, H., Yang, X., Liu, A., Fu, H., Wan, M. (2003). "A Study on the Performance and Mechanism of Soil-Reinforcement by Herb Root System." In Proceedings of Third International Vetiver Conference, Guangzhou, China, 384, pp. 390.

Cho, G. C. , Dodds, J. , Santamarina, J. C. (2006). "Particle Shape Effects on Packing Density, Stiffness, and Strength: Natural and Crushed Sands." Journal of Geotechnical and Environmental Engineering, 132(5), pp. 591–602.

Corriher, V. A., Redmon, L. A. (2011). "Bermudagrass Varieties, Hybrids and Blends for Texas." Technical Report E-320, 9(11)

De Baets, S., Poesen, J., Gyssels, G., Knapen, A. (2006). "Effects of Grass Roots on the Erodibility of Topsoils during Concentrated Flow." Geomorphology, 76(1), pp. 54-67.

De Baets, S., Poesen, J., Reubens, B., Wemans, K., De Baerdemaeker, J., Muys, B. (2008). "Root Tensile Strength and Root Distribution of Typical Mediterranean Plant Species and Their Contribution to Soil Shear Strength." Plant and Soil, 305(1-2), pp. 207-226.

De Baets, S. D., Torri, D., Poesen, J., Salvador, M. P., Meersmans, J. (2008). "Modelling Increased Soil Cohesion due to Roots with EUROSEM." Earth

Surface Processes and Landforms, 33(13), pp. 1948-1963.

Egwuonwu, C. C., Okereke, N. A. A. (2012). "Characterization of Erodibility Using Soil Strength and Stress-strain Indices for Soils in Some Selected Sites in Imo State." Research Journal of Environmental and Earth Sciences, 4(7), pp. 688-696.

Flammer, I., Blum, A., Leiser, A., Germann, P. (2001). "Acoustic Assessment of Flow Patterns in Unsaturated Soil." Journal of Applied Geophysics, 46(2), pp. 115-128.

Franks, C. D., K. A., Goings (2000). "Separating Roots from the Soil by Hand Sieving." Natural Resources Conservation Service, pp. 1-2.

Gao, W., Ren, T., Bengough, A. G., Auneau, L., Watts, C. W., Whalley, W. R. (2012). "Predicting Penetrometer Resistance from the Compression Characteristic of Soil." Soil Science Society of America Journal, 76(2), pp. 361-369.

Gao, W., Watts, C. W., Ren, T., Shin, H. C., Taherzadeh, S., Attenborough, K., Whalley, W. R. (2013). "Estimating Penetrometer Resistance and Matric Potential from the Velocities of Shear and Compression Waves." Soil Science Society of America Journal, 77(3), pp. 721-728.

Gassmann, F. (1951). "Elastic Waves through a Packing of Spheres." Geophysics, 16(4), pp. 673-685.

Gray, D. H., Ohashi, H. (1983). "Mechanics of Fiber Reinforcement in Sands." Journal of Geotechnical Engineering, 109(3), pp. 335-353.

MacDonald, A., Thomann, T., Blatz, I., Shields, F. D. (1991). "The Effects of Vegetation on the Structural Integrity of Sandy Levees." US Army Engineer Waterways Experiment Station, pp. 1-117.

Gray, D.H., Sotir, R.B. (1995). "Biotechnical Stabilization of Steepened Slopes." Transportation Research Record, 1474, pp. 23–29.

Gregory, A. S., Webster, C. P., Watts, C. W., Whalley, W. R., Macleod, C. J., Joynes, A., Matthews, G. P. (2010). "Soil Management and Grass Species Effects on the Hydraulic Properties of Shrinking Soils." Soil Science Society of America Journal, 74(3), pp. 753-761.

Gyssels, G., Poesen, J., Bochet, E., Li, Y. (2005). "Impact of Plant Roots on the Resistance of Soils to Erosion by Water: a Review." Progress in Physical Geography, 29(2), pp. 189-217.

Hanson, G. J. (1991). "Development of a Jet Index to Characterize Erosion Resistance of Soils in Earthen Spillways." Transactions of the ASAE, 34(5), pp. 2015-2020.

Hanson, G. J., Robinson, K. M. (1993). "The Influence of Soil Moisture and Compaction on Spillway Erosion." Transactions of the ASAE, 36(5), pp. 1349-1352.

Hanson, G. J. (1996). "Investigating Soil Strength and Stress-Strain Indices to Characterize Erodibility." Transactions of the ASAE, 39(3), pp. 883-890.

Hanson, G. J., Temple, D. M. (2002). "Performance of Bare-earth and Vegetated Steep Channels under Long-duration Flows." Transactions of the ASAE, 45(3), pp. 695-701.

Hanson, G. J., Cook , K. R. (2004). "Apparatus, Test Procedures, and Analytical Methods to Measure Soil Erodibility In Situ." Applied Engineering in Agriculture, 20(4), pp. 455-462.

Hanson, G. J., Hunt, S. L. (2007). "Lessons Learned Using Laboratory JET Method to Measure Soil Erodibility of Compacted Soils." Applied Engineering in Agriculture, 23(3), pp. 305-312.

Hertz, H. (1882). "On the Contact of Elastic Solids." Journal Für Die Reine Und Angewandte Mathematik, 92(110), pp. 156-171.

Hess, H. M., Attenborough, K., Heap, N. W. (1990). "Ground Characterization by Short-range Propagation Measurements." The Journal of the Acoustical Society of America, 87(5), pp. 1975-1986.

Hickey, C. J., Ekimov, A., Hanson, G. J., Sabatier, J. M. (2009). "Time-lapse Seismic Measurements on a Small Earthen Embankment During an Internal Erosion Experiment." Symposium on the Application of Geophysics to Engineering and Environmental Problems, Fort Worth, TX, pp. 144-156.

Hock, S., Ivanov, J., Miller, R.D. (2007). "Test for Detecting an Impermeable Water Barrier in an Earth- fill Dam in Austria Using MASW Method." Symposium on

the Applications of Geophysics to Engineering and Environmental Problems, Denver, CO, pp. 621–628.

Howard, W., Hickey, C. J. (2009). "Investigation of the Near Subsurface Using Acoustic to Seismic Coupling." Ecohydrology, 2(3), pp. 263-269.

Hung, M. H., Lauchle, G. C., Wang, M. C. (2009). "Seepage-induced Acoustic Emission in Granular Soils." Journal of Geotechnical and Geoenvironmental Engineering, 135(4), pp. 566-572.

Hubbard, J. L. (2010). "Use of Electrical Resistivity and Multichannel Analysis of Surface Wave Geophysical Tomography in Geotechnical Site Characterization of Dam." (Thesis). Print.

Hubble, T. C. T., Docker, B. B., Rutherfurd, I. D. (2010). "The Role of Riparian Trees in Maintaining Riverbank Stability: a Review of Australian Experience and Practice." Ecological Engineering, 36(3), pp. 292-304.

Ivanov, J., Miller, R. D., Stimac, N., Ballard Jr, R. F., Dunbar, J. B., Smullen, S. (2006). "Time-Lapse Seismic Study of Levees in Southern New Mexico." In SEG Expanded Abstracts, New Orleans, LA, pp. 3255-3259.

Kemper, W. D., Rosenau, R. C. (1984). "Soil Cohesion as Affected by Time and Water Content." Soil Science Society of America Journal, 48(5), pp. 1001-1006.

Kwong, A. K. L., Lau, C. K., Lee, C. F., Ng C. W. W., Pang, P. L. R., Yin, J. H., Yue, Z. Q. (2001). *Soft Soil Engineering*. In Proceedings of the Third International Conference on Soft Soil Engineering, Hong Kong, China

Lavender, E. A. (1992). "Genotypic Variation in the Root System of *Betula pendula*." (Dissertation). Print.

Leij, F. J., Alves, W. J., van Genutchen Th. M., Williams, J. R. (1996). *The UNSODA Unsaturated Hydraulic Database*. U. S. Environmental Protection Agency, Cincinnati, OH

Lu, Z., Hickey, C. J., Sabatier, J. M. (2004). "Effects of Compaction on the Acoustic Velocity in Soils," Soil Science Society of America Journal, 68(1), pp. 7-16.

Lu, N., Likos, W. J. (2006). "Suction Stress Characteristic Curve for Unsaturated

Soil." Journal of Geotechnical and Geoenvironmental Engineering, 132(2), pp. 131-142.

Lu, Z., Sabatier, J. M. (2009). "Effects of Soil Water Potential and Moisture Content on Sound Speed." Soil Science Society of America Journal, 73(5), pp. 1614-1625.

Lu, Z., Wilson, G. V. (2012). "Acoustic Measurements of Soil Pipeflow and Internal Erosion." Soil Science Society of America Journal, 76(3), pp. 853-866.

Marot, D., Regazzoni, P. L., Wahl, T. (2011). "Energy-based Method for Providing Soil Surface Erodibility Rankings." Journal of Geotechnical and Geoenvironmental Engineering, 137(12), pp. 1290-1293.

Mavko, G., Mukerji, T., Dvorkin, J. (2009). *The Rock Physics Handbook: Tools for Seismic Analysis of Porous Media*. Cambridge University Press, Cambridge, UK

Mindlin, R. D. (1949). "Compliance of Elastic Bodies in Contact." Journal of Applied Mechanics, 71(3), pp. 259-268.

Minnesota Department of Transportation, Pavement Design, 2007

Mualem, Y. (1976). "A New Model for Predicting the Hydraulic Conductivity of Unsaturated Porous Media." Water Resources Research, 12(3), pp. 513-522.

Oelze, M. L., Sabatier, J. M., Raspet, R. (2003). "Roughness Measurements of Soil Surfaces by Acoustic Backscatter." Soil Science Society of America Journal, 67(1), pp. 241-249.

Operstein, V., Frydman, S. (2000). "The Influence of Vegetation on Soil Strength." In Proceedings of the Institution of Civil Engineers-Ground Improvement, 4(2), pp. 81-89.

Pollen, N., Simon, A. (2005). "Estimating the Mechanical Effects of Riparian Vegetation on Stream Bank Stability Using a Fiber Bundle Model." Water Resources Research, 41(7), pp. 1-11.

Potts, D. M., Dounias, G. T., Vaughan, P. R. (1987). "Finite Element Analysis of the Direct Shear Box Test." Geotechnique, 37(1), pp. 11-23.

Powledge, G., Ralston, D., Miller, P., Chen, Y., Clopper, P., Temple, D. (1989). "Mechanics of Overflow Erosion on Embankments. I: Research Activities." Journal of Hydraulic Engineering, 115(8), pp. 1040-1055.

Powledge, G. R., Ralston, D. C., Miller, P., Chen, Y. H., Clopper, P. E., Temple, D. M. (1989). "Mechanics of Overflow Erosion on Embankments II: Hydraulic and Design Considerations." Journal of Hydraulic Engineering, 115(8), pp. 1056-1075.

Richardson, C. (2001). "Protecting Our Watersheds through Research and Management: Challenges and Opportunities." ARS National Program Staff, Temple, TX, pp. 1-16.

Rinehart, R.V., M. L. Parekh, J. B. Rittgers, M. A. Mooney, A. Revil, (2012). "Preliminary Implementation of Geophysical Techniques to Monitor Embankment Dam Filter Cracking at the Laboratory Scale." In Proceedings of the 6th Annual ICSE, Paris, France, pp. 756-770.

Sabatier, J. M., Hess, H., Arnott, W. P., Attenborough, K., Roemkens, M. J. M., Grissinger, E. H. (1990). "In Situ Measurements of Soil Physical Properties by Acoustical Techniques." Soil Science Society of America Journal, 54(3), pp. 658-672.

Sabatier, J.M., Frederickson, C.K., Hickey, C.J., Chambers, J.P., Romkens, M.J.M., (1996). "Interactions of Sound within Agricultural Soils." In Proceeding of the Sixth Federal Interagency Sedimentation Conference, Las Vegas, NV, pp. 8.

Seed, R. B., Bea, R. G., Abdelmalak, R. I., Athanasopoulos-Zekkos, A., Boutwell, G. P., Briaud, J. L., Wartman, J. (2008). "New Orleans and Hurricane Katrina I: Introduction, Overview, and the East Flank." Journal of Geotechnical and Geoenvironmental Engineering, 134(5), pp. 701-717.

Shaikh, A., Ruff, J. F., Charlie, W. A., Abt, S. R. (1988). "Erosion Rate of Dispersive and Nondispersive Clays." Journal of Geotechnical Engineering, 114(5), pp. 589-600.

Shields, F. D., Sabatier, J. M., Wang, M. (2000). "The Effect of Moisture on Compressional and Shear Wave Speeds in Unconsolidated Granular Material." The Journal of the Acoustical Society of America, 108(5), pp. 1998-2004.

Shin, H. C., Taherzadeh, S., Attenborough, K., Whalley, W. R. (2012). "Use of Short Range Outdoor Sound Propagation and Acoustic-to-seismic Seismic Coupling to Deduce Soil State." Acoustics, Nantes, France, pp. 201-PU202.

Simon, A., Collison, A. J. (2002). "Quantifying the Mechanical and Hydrologic Effects of Riparian Vegetation on Streambank Stability." Earth Surface Processes and Landforms, 27(5), pp. 527-546.

Song, Y. S., Hwang, W. K., Jung, S. J., Kim, T. H. (2012). "A Comparative Study of Suction Stress between Sand and Silt under Unsaturated Conditions." Engineering Geology, 124, pp. 90-97.

Swiss Standard SN 670 010b. "Characteristic Coefficients of Soils." Association of Swiss Road and Traffic Engineers

Temple, D. M., Hanson, G. J. (1994). "Headcut Development in Vegetated Earth Spillways." Applied Engineering in Agriculture, 10(5), pp. 677-682.

Tengbeh, G. T. (1989). "The Effect of Grass Cover on Bank Erosion." (Thesis). Print.

Terzaghi, K. (1943). *Theoretical Soil Mechanics*. John Wiley and Sons, New York City, New York

Trung, L. H. (2012). "Root Characteristics of Some Grass Species on the Sea Dikes in Viet Nam." Communications on Hydraulic and Geotechnical Engineering, Delft, Netherlands 2012(3)

Van Genuchten, M. T. (1980). "A Closed-form Equation for Predicting the Hydraulic Conductivity of Unsaturated Soils." Soil Science Society of America Journal, 44(5), pp. 892-898.

Velea, D. (2000). "Elastic Wave Velocities in Partially Saturated Ottawa Sand." Soil Science Society of America Journal, 64(4), pp. 1226-1234.

Wan, C. F., Fell, R. (2004). "Investigation of Rate of Erosion of Soils in Embankment Dams." Journal of Geotechnical and Geoenvironmental Engineering, 130(4), pp. 373-380.

Whalley, W. R., Jenkins, M., Attenborough, K. (2011). "The Velocity of Shear Waves in Saturated Soil." Soil Science Society of America Journal, 75(5), pp. 1652-

1657.

Whalley, W. R., Jenkins, M., Attenborough, K. (2012). "The Velocity of Shear Waves in Unsaturated Soil," Soil and Tillage Research, 125, pp. 30-37.

Whalley, W. R., Ober, E. S., Jenkins, M. (2013). "Measurement of the Matric Potential of Soil Water in the Rhizosphere." Journal of Experimental Botany, 64(13), pp. 3951-3963.

Wu, T. H., McKinnell III, W. P., Swanston, D. N. (1979). "Strength of Tree Roots and Landslides on Prince of Wales Island, Alaska." Canadian Geotechnical Journal, 16(1), pp. 19-33.

Yarbrough, L. D. (2000). "Channel Bank Stability Analysis and Design Considering the Effects of Riparian Vegetation and Root Reinforcement." (Thesis). Retrieved from author.

CHAPTER IX: APPENDIX

9.1 LITERATURE REVIEW

9.1.1 Geotechnical Engineering

There has been an increased interest in soil erodibility in the last three decades (Pollen et al., 2005). Field and laboratory methods have been developed to study soil erodibility. Models have also been constructed to predict erosion. The dominant parameters contributing to soil erodibility are the erodibility coefficient and the critical shear stress. The erodibility coefficient describes the rate of erosion due to hydraulic stress on the soil, and the critical shear stress is the shear stress applied to the soil to initiate erosion. A literature review presents a chronological history of research on geotechnical engineering properties that relate to soil erodibility and near surface phenomena.

The review begins with the research of Van Genutchen (1980) that described a relatively simple equation from the soil-water content-pressure head curve. The equation enables one to derive closed form analytical expressions for the relative hydraulic conductivity when substituted in the predictive conductivity models of N. T. Burdine or Y. Mualem (Burdine, 1953, Mualem, 1976). The expressions for relative hydraulic conductivity as a function of pressure head contain three independent parameters which can be obtained by fitting a soil-water retention model to experimental data. The unsaturated hydraulic conductivity is predicted well with the closed-form analytical expressions for four out of five cases with a wide range of hydraulic properties (van Genutchen, 1980).

Later Shaikh (1988) observed a slightly different phenomena of the erosion rate of dispersive clays and nondispersive clays by placing samples in a flume with flowing water. The samples were compacted to near optimum water content and then subjected to flowing water. The stress on the samples ranged from 1.67-12.9 Pa. The nondispersive clays had erosion rates that were two orders of magnitude greater than the dispersive clays'. Empirical equations were then developed to estimate the erosion rate of compacted unsaturated clays as a function of sodium adsorption and tractive stress (Shaikh et al., 1988).

The next year G. R. Powledge (1989) continued research on surface erodibility during overflow and published a tow part report. The mechanics of overflow on embankments were researched, or how overtopping erosion affects embankments for dams, levees, roadways, etc. The overflow rates were based on probable maximum flood events. Several types of tests were conducted: a small geotechnical centrifuge model, a full-scale hydraulic flume, and hydraulic field trials. The experiments were performed on several different surfaces including grass, geotextiles, gabions, riprap, cellular concrete blocks and soil cement. The study concluded that overtopping flow is a multivariable and multidisciplinary problem, and more tests should be conducted (Powledge et al., 1989)

In 1991, a jet erosion test (JET) was developed by Hanson to characterize erosion resistance on spillways. The erodibility of the soil is characterized by the critical shear stress and the erodibilty coefficient. The critical shear stress is the minimum stress that must be applied to a soil for erosion to take place. The erodibility coefficient describes

the rate of erosion due to hydraulic stresses in excess of the critical stress. During a JET, a submerged soil sample is impinged by a water jet at a constant head. Scour depth of the sample is measured as a function of time until an equilibrium depth is reached. The equilibrium depth is where the stress (i.e. critical stress) from the jet is no longer able to erode the soil sample. In most cases the test is terminated before the erosion ends and the equilibrium depth must be estimated using an analysis of the scour depth versus time plot. The critical shear stress is determined based on the equilibrium scour depth. The erodibility coefficient is determined based on an analysis of the measured scour depth versus time and the critical shear stress. The JET has been designed and tested for measuring erodibility on laboratory samples and in the field (Hanson, 1991).

Hanson (1993) continued to test soils over a range of dry unit weights and moisture contents. Moisture content at the time of compaction had a significant influence on soil erosion resistance. When water content was kept constant and dry unit weight increased, the soil's erosion resistance increased (Hanson et al., 1993). In 1994 D. M. Temple with Hanson utilized both field and laboratory data to improve the criteria for design and analysis of emergency spillways. The failure was broken down into three phases, vegetal cover failure, concentrated flow erosion, and headcut advance. A computational procedure was developed to estimate the time of headcut formation given flow and channel surface conditions (Temple et al., 1994).

Two years later Hanson (1996) investigated the effect of soil strength and stress-strain on erosion resistance. Cone penetrometer, pocket penetrometer, unconfined compressive strength (UCS) and stress-strain measurements were obtained as a function of compaction, water content and dry unit weight. The results revealed soil strength was not a good indicator of erosion resistance. Stress-strain characteristics, on the other hand, appeared to have potential to provide useful data on erosion resistance (Hanson, 1996).

Years later another apparatus was built to observe erosion of a different type. The erosion function apparatus (EFA) designed by Briaud et al. (2001) is a method used to predict erosion rates of fine-grained soils, specifically at bridges. A Shelby tube sample is fitted into the wall of a rectangular pipe. Water flows through the pipe and erodes the top of the sample. The erosion rate is measured as the decrease in height of the sample eroded per time. Different shear stresses are applied to the sample by varying the flow rate. The results are plots of erosion rate versus shear stress and/or erosion rate versus flow velocity. The end parameters are the critical shear stress, or the stress at which the sample begins to erode, and the rate of erosion after that critical stress has been surpassed. The parameters are used to predict the rate of scour at a bridge and have been adapted to overtopping erosion rates (Briaud et al., 2001).

Back to Hanson's et al. (2002) JET, earthen embankments three meters high were constructed into channels and tested for overtopping erosion resistance. Two channels were vegetated and two were not. Water surface, bed and velocity profiles and predicted hydraulic stresses are compared. The non-vegetative did not run as long as the vegetative embankments. The non-vegetative channel erosion rates were 25 and 50 times greater than the vegetative channel's rates. Erosion progressed into stair-stepped overfalls. JET analysis tests on laboratory samples showed that erosion

resistance varied up to three orders of magnitude due to variations of compaction, saturation and density. Excess stress parameters, erodibility coefficient and critical stress were predicted (Hanson et al., 2002).

The same year two other tests were developed to study internal erosion. The Hole Erosion Test (HET) and the Slot Erosion Test (SET) are laboratory tests developed by Wan and Fell (2002) to study erosion characteristics of soil associated with cracks in earthen dams. Results of these tests are used to predict rates of erosion and critical hydraulic shear stress required to initiate piping erosion. For the HET, a soil sample is compacted into a standard mold used for the standard compaction test. A six millimeter diameter hole is drilled through the sample to simulate a concentrated leak. The sample is submerged and subjected to water flow. Shear stress is calculated as a function of the eroding fluid density, hydraulic gradient across the sample, and diameter of the hole. The flow rate is used as an indirect measurement of the diameter of the hole. Erosion rate per unit surface area of the hole is calculated using the dry density of the soil and the hole diameter. Erosion rate per surface area is plotted against the hydraulic shear stress. The slope of a best fit straight line on the rising portion of this plot gives a coefficient of soil erosion per width eroded in the pipe (Wan and Fell, 2004).

The SET developed by Wan and Fell (2004) is similar to the HET, but the soil sample is much larger. A pre-formed slot 2.2 mm wide x 10 mm deep is built along the side wall of the sample instead of a circular hole. A fluid is passed through the sample to initiate erosion. The widening of the slot due to erosion is measured during the test. Estimation of the coefficient of soil erosion is calculated with a process similar to the one discusses in the HET section above. The coefficient of soil erosion may be used to predict the initiation and progression of internal erosion (Wan and Fell, 2004).

Focusing more on soil water to particle interaction under various stresses and saturations, Lu and Likos (2006) presented the concept of the suction stress characteristic curve (SSCC) for unsaturated soil. Analyses on the particle-scale were employed to distinguish three types of interparticle forces: active forces in the soil grains, active forces at or near interparticle contacts, and passive, counterbalancing forces at or near interparticle contacts. The second type of force includes physicochemical, cementation, surface tension, and negative pore-water pressure forces and can be combined into a macroscopic stress called suction stress. Suction stress depends on degree of saturation, water content, and matric suction. The SSCC parallels with well-established concepts of the soil-water characteristic curve (SWCC) and hydraulic conductivity function for unsaturated soils. The behavior of the SSCC is validated with a variety of soil types in the literature. The experimental evidence shows that both Mohr-Coulomb failure and critical state failure can be well represented by the SSCC concept (Lu and Likos, 2006).

Back to erodibility research Hanson et al. (2007) studied the effect compaction has on erodibility of soils. Samples were compacted with different water contents and compaction efforts. The JET was used to quantify erodibility. Erodibility varied up to six orders of magnitude dependent on soil gradation, plasticity, water content and compaction effort. Soil texture and plasticity are prominent factors in erosion resistance, as much or more than compaction. Preparing soil to optimum water content and making higher compaction efforts were noticed to increase erosion resistance

(Hanson et al., 2007).

After Hurricane Katrina in 2005 the quantity of research on levee erosion was increased. The erosion function has been developed by Briaud (2005) as the relationship between erosion rate per time and the shear stress developed by water at the water-soil contact. The erosion function is the parameter given from the EFA test. 23 samples were collected from 11 locations at the surface of levees around New Orleans, Louisiana. A large range of erosion resistance was measured, some eroding completely and some resisting well. Numerical simulations were performed for the distribution of velocity vectors during an overtopping event and for shear stresses at the soil-water interface. The simulations support the results of the EFA tests (Briaud et al., 2008). A case history was written by Seed et al. (2008) about New Orleans and the 2005 Hurricane Katrina event with emphasis on geotechnical lessons learned. The importance of including erodibility and foundation soils in levee design and construction was discussed (Seed et al., 2008).

Using 18 case histories, Bonelli et al. (2010) inferred the coefficient of erosion and erosion rate. A coefficient of piping erosion was developed to estimate the time to failure and flood of earthen dams. The HET was used to estimate a priori the coefficient of piping erosion. The radius evolution of the pipe followed a scaling law between critical stress and time of piping erosion, which were a function of the initial hydraulic gradient and the coefficient of erosion. The time of failure and peak flow were related to the coefficient of erosion and the maximum pipe diameter before breaching (Bonelli et al., 2010).

Two years later Benahmed et al. (2012) also used HET to classify soil erodibility. Benahmed carried out HET on cohesive soils to classify critical shear stress and the coefficients of erosion. The parameters that proved to play a key role in internal erosion are compaction energy, moisture content, degree of saturation and the percentage of fines (Benahmed et al., 2012). A new approach by Marot et al. (2001) was taken to consider fluid energy dissipation and the eroded mass for interpreting HET and JET. Different fine-grained soils were tested with varying erodibility. Erosion coefficient and average critical shear stress values were different for each test. Based on energy, an erosion resistance index was determined for both tests. Values of erosion resistance index were roughly the same for each apparatus and soil type. A single classification of soil erodibility was obtained (Marot et al., 2011).

Unlike Marot's fluid energy dissipation approach, Egwuonwu et al. (2012) investigated soil strength indices and stress-strain characteristics as potential indicators of erosion resistance in two compacted soils, a sandy clay loam, and a clay loam. Unconfined compressive strength (UCS) and stress-strain measurements as a function of moisture content and dry density were measured under varied applied loads. Initial soil strength alone was not a good indicator of erosion resistance. Strength and stress-strain characteristics were roughly inversely related to dry unit weight. The exponents of moisture content and dry unit weight for erosion resistance index, failure strain and the area under the failed stress-strain curve are opposite in signs. Results reveal if there is potential for an inverse relationship (Egwuonwu et al., 2012).

The same year Gao et al. (2012) studied the relationship between UCS,

penetrometer resistance and matric suction. Penetrometers can be used to measure the resistance of soil to root elongation. A function by Gao et al. (2012) was developed to estimate penetrometer resistance from soil compression characteristics. Five soils greater than -30 kPa matric suction and ranging from 30 to 1000 kPa in UCS were measured with a penetrometer to get soil resistance. Soil compression varied with texture, organic matter, and initial water content. Penetrometer resistance increased with decreasing void ratio (Gao et al., 2012).

Also regarding to varying matric suction, Song et al. (2012) estimated and compared suction stress between sand and silt. Water content and matric suction were examined using an automated SWCC apparatus based on the axis translation technique. Using the van Genutchen model SWCCs were estimated. The water content of silt was higher than sand at equal matric suctions. SSCCs were then estimated using the fitting SWCC parameters according to the method proposed by Lu and Likos (2006). The SSCC were different for sand and silt and significantly depended on pore size and pore size distribution. The suction stress showed rapid variation with change in matric suction for sand, but approached a constant value as matric suction increased for silt (Song et al., 2012).

The matric suction of soil depends on the soil moisture content, size of the pores, surface properties of the particles, and surface tension of the water (Whalley et al., 2013). The relationship of matric suction and moisture content was reviewed. Historically moisture content has been given much more attention than matric suction. Matric suction can be a very useful property for civil and agricultural engineers. The limitations and opportunities of methods to study matric suction were discussed as well as possible improvements to the equipment used (Whalley et al., 2013).

9.1.2 Root Reinforcement of Soils

Soils with under vegetation have been more resistant to soil erosion compared to bare soils (Pollen et al., 2005). Much research has been done to quantify the increase in slope stability due to riparian root reinforcement on stream banks. The roots add tensile strength to resist erosion of the soil which in turn increases the soil's shear strength(τ). Within the past 20 years work has been published to quantify the increase in shear strength of soils due to grass roots (τ_r). Models below utilize the tensile strength of roots (t_r), the root area ratio(RAR), and the root density (RD) to predict the increase in shear strength and cohesion (c) of soils. A chronological review of the literature pertaining to the effect of roots on soil will be discussed.

This area of research began to get some attention when Wu et al. (1979) investigated the stability of slopes before and after removal of forest cover. A simple perpendicular root model of the soil-root system was developed to evaluate the contribution of tree roots to shear strength of soils or cohesion due to roots (c_r). The tensile strength of tree roots per unit area and the angle of shear distortion (θ) are shown in Figure 2.2.

The tensile strength of tree roots is weighted by the RAR which is the area of

the roots divided by the total area of the sample. The internal friction angle of the soil is denoted by ϕ.

$$c_r = t_r RAR(sin\theta + cos\theta tan\phi)$$

Shear strength of the reinforced soil and tensile strength of roots were measured. A power law relationship was then established between the root diameter and the root's tensile strength

$$t_r = a{d_r}^{-b}$$

The values of the cohesion due to roots computed from Equation 8.1 showed small variation with a range of the shear distortion angle and internal friction angle. The term in parentheses was therefore assumed to be a constant of 1.2 giving the simplified Equation 2.15 (Wu, 1979).

$$c_r = 1.2 t_r RAR$$

In light of Wu's simple perpendicular model, Gray et al. (1983) conducted direct shear tests on dry sand reinforced with different fibers. The results showed that fiber reinforcement increased the peak shear strength and limited post peak reductions in shear resistance. A model was developed that predicts the influence of sand-fibers on shear strength. The concentration of fibers or RAR is directly proportional to the shear strength increase. Fiber orientation of 60° was most effective in increasing shear strength. Loose and dense states of the sand had similar effect on shear strength.

Years later Tengbeh (1989) conducted research on the effect of grass cover on bank erosion. Instead of using root area ratio to quantify the presence of roots, root density was used. Root density is the mass of dried roots divided by the volume of the soil-root matrix. The root density method is much more accurate when dealing with grass roots that are on the order of tenths of millimeters. Root density was related to cohesion of soil-root matrices in a clay soil using a logarithmic relationship. The root densities were compared to vane shearing strength and moisture content. A relationship between torsional box shearing strength and cohesion was developed at varied root densities. Other relationships established are between shoot density, root density, flow hydraulics, and scour resistance. The effect of shear strength due to grass roots on channel bank stability against slumping was observed (Tengbeh, 1989).

Again in 1991 Gray et al. (1991) studied the effects of fibers in sand on shear strength of soils. Instead of laboratory tests, insitu tests were performed on vegetated sandy channel levees. A profile wall method and other techniques were used to determine the distribution and concentration of roots (particularly woody vegetation) and biopores in levee structures. Grass and herbaceous ground cover provided large amounts of roots at depths less than six inches. Vegetation appeared to be effective in preventing shallow sloughing and surface raveling. The plant roots reinforced the soil and increased the shear strength of the surface layers (Grayet al., 1991).

Focusing strictly on the characteristics of roots, Lavender (1992) studied the genotypic variation of root systems of *Betula pendula*. Shoot variation of three root types, fine, woody, non-woody were assessed. The analysis consisted of measuring dry weights, lengths and various other ratios. For fine roots a good linear relationship between length and dry weight was established. The relationship makes it possible to

estimate root length from dry weight of roots (Lavender, 1992).

To get the bigger picture, Gray et al. (1995) discussed the basic principles of biotechnical stabilization and reviewed a case study of a repair to an unstable cut slope along a highway in Massachusetts. A stability analysis was performed. With environmental and scenic consideration, a composite, drained rock and earthen brushlayer fill was used. Biotechnical stabilization provided a satisfactory and cost effective solution. The treated slope has remained stable and blends naturally with its surroundings (Grayet al., 1995).

Years later more research was published on the effect of roots on slope stability. Operstein et al. (2000) investigated the influence of plant roots on the stability of slopes. The study described the determination of additional shear strength contributed to soil by roots. Three tests were conducted: tension tests on roots, pull-out tests of roots from the soil and direct shear tests on soil and root-reinforced soil. Alfalfa, rosemary, *Pistacia lentiscus*, *Meoporum parvifolium* and *Cistus* were tested in chalky soil. Like Pollen et al. (2005) Operstein et al. (2000) noticed that Wu's simple perpendicular root model overestimates cohesion due to roots. A liner relationship was then established between the increase in cohesion and the relative root tensile strength (Operstein et al., 2000).

A similar experiment conducted by Yarborough (2000) explored channel bank stability in attempt to quantify the effects of riparian vegetation and tree root reinforcement of the soil matrix. Unlike past research, the experiment was on tensile failure of silt-rich banks instead of slumping or sliding failures. Models from Wu et al., Gray, and Sotir were evaluated. Tensile strength in soil increased up to 245 kPa due to tree root reinforcement. Fast Lagrangian Analysis of Continua (FLAC) model was employed to show contrast in stability of a tree root reinforced slope and an unreinforced slope. The slope in the simulation was completely stable if the tree root reinforcement was set to 20 kPa (Yarborough, 2000).

Cheng et al. (2003) studied the mechanic function of soil reinforcement by herbaceous root systems but was only focused on tensile strength of herbaceous roots. An experimental comparison of the mechanics of soil-reinforcement of various herb roots was conducted. The comparison showed that various roots have different tensile strengths. Vetiver grass, common Centipede grass, White Clover, Late Juncellus, Dallis grass, Bahia grass, Manila grass and Bermuda grass were tested. The difference in tensile strengths is concerned with the gene variety and tissue structure of the various roots (Cheng et al., 2003).

Two years later Pollen and Simon (2005) noticed that as a soil-root matrix shears, the roots within the soil have different strengths and break progressively. The phenomena are associated with a redistribution of stresses. Progressive failure is well described by a fiber bundle model from material science. The fiber bundle root model was applied to 12 riparian species (particularly woody vegetation). The root reinforcement estimates were compared against direct shear test with root-permeated and non- root-permeated samples. Wu's simple perpendicular root model overestimated root reinforcement up to 50% in tests where all roots broke. Wu's model overestimated root reinforcement by an order of magnitude in tests where forces

did not exceed root strength (Pollen and Simon, 2005).

After Pollen and Simon's critique of Wu's simple perpendicular root model, De Baets et al. (2006) investigated the impact of root density and root length density of grass on the erodibility of root-permeated saturated top soils. Soil samples of varying root density were subjected to concentrated flow using a hydraulic flume. Root density, root length density, relative soil detachment rates, mean flow shear stresses and other properties were measured. The results indicated a negative exponential relation between the relative soil detachment rate and root density as well as root length density, independent of the applied flow shear stresses. Comparing the effects of vegetative cover on sheet and rill erosion rates and the effect of root area ratio of grass roots on relative soil detachment rates revealed that grass roots are very effective in reducing soil detachment rates.

De Baets et al. (2006) did not measure the root area ratio directly but calculated it using root length density (RLD) and the mean cross-sectional area of a single root ($RCSA$).

$$RAR = RLD \times RCSA$$

Root length density is the length of the root (L_R) divided by the volume of root permeated soil (V) (De Bates et al., 2006).

$$RLD = \frac{L_R}{V}$$

De Baets et al. (2008) assessed the root reinforcement effect of 25 Mediterranean matorral species using Wu's simple perpendicular root model. The power root tensile strength-root diameter relationships were determined. Wu's model was modified for a silt loam (ϕ=25°) with a fixed angle of shear distortion (θ=45°). Pollen and Simon showed that Wu's simple perpendicular model overestimates root reinforcement in grasses up to 100% compared to the fiber bundle model RipRoot. A reduction factor was added to account for the overestimation. (De Baets et al., 2008).

$$c_r = 0.5 t_r RAR$$

On a slightly different topic, Corriher et al. (2009) states fertility of grass is a very important factor in Forage production, yield, and persistence. Nitrogen is commonly the limiting factor, but phosphorous and potassium are also necessary. Lack of nitrogen will produce low protein levels. Potassium levels must be monitored to prevent reduced yields, poor stands, and winter-kill. Phosphorous helps the plant's root growth and development (Corriher et al., 2009).

Back to the effect of roots on soils, Gregory et al. (2010) conducted a study to explore the effect of roots of Forage grasses on hydraulic properties. Six different grasses were used. Tension infiltration measurements gave hydraulic properties and structure for two seasons. Shrinkage, water repellence, and water release characteristics were measured from soil samples. Tension infiltration measurements were made on fallow soil, permanent grassland and arable land for a long-term experiment. The data showed that the saturated hydraulic conductivity of the capillary matrix sown with grass is dependent on grass species. The pore size was affected by the grass. Grasslands showed evidence of macropore structure while the fallow did

not. In conclusion changes in soil structure were most likely due to shrinkage of soil particles and subsequent soil stress relaxation (Gregory et al., 2010).

The same year Hubble et al. (2010) presented a review of field and experimental studies that evaluate native vegetation's role in mass failure of riverbanks in eastern Australia. The presence of riparian forest on riverbanks reduces the likelihood of erosion by mass failure. The RAR method, Waldron's approach, and Wu's simple perpendicular root model lead to significant overestimation of the actual tree root-reinforcement. The overestimation is due to breakage and pull-out of tapered tree roots that have narrower roots below the shear plane. The roots do not achieve full tensile strength calculated on the basis of tree root diameter at the shear plane. The overestimation is also due to the fact that soil mass fails progressively along the length of the shear plane and not instantaneously (Hubble et al., 2010).

A couple years later Trung (2012) conducted a similar experiment but with grass roots on levees. A study was done to characterize roots of some grass species on sea dikes in Vietnam. Samples of grass root distributions with depth were taken by measuring grass root volume, weight, and number. Grass root number ratio was chosen to be more accurate than the traditional RAR. Root tensile strength tests were conducted for each grass type. The additional cohesion in the soil due to grass roots was calculated and compared to values obtained from direct shear tests (Trung, 2012).

Similarly Chen et al. (2015) characterized how a soil-root system under a Bermuda grass community responded to environmental changes and effects of the soil-root system on shallow soil conservation and riverbank reinforcement through field investigation and laboratory tests. Plants were sampled randomly to measure spatial structure and tensile strength of roots. Laboratory tests were conducted on soil-root systems and control soil to measure soil erosion resistance, soil scour resistance, and shear strength. The Bermuda grass roots increased soil erosion resistance, soil scour resistance, and shear strength. The grass root reinforcement enhanced the stability of shallow soil and the riverbank (Chen et al., 2015).

9.1.3 Acoustics of Soils

Acoustic waves have been utilized to evaluate and monitor ongoing internal changes of soil properties (Sabateir et al., 1996, Shields et al., 2000, Lu et al., 2004, Hickey et al., 2009). Acoustic waves, or elastic stress waves, traveling through the soil interact with soil particles and interstitial fluids. The acoustic response of the soil is affected by soil texture, structure, and variations in soil properties. Acoustic wave propagation through soils is a small strain phenomenon that introduces a small perturbation without altering the fabric of soils (Lu et al., 2009). Therefore acoustic parameters are constant-fabric characteristics and can be used to evaluate and monitor ongoing internal changes of soil properties. A chronological literature review of acoustic methods used in near-surface soils to predict soil properties will be discussed

Early research was conducted by Brutsaert et al. (1964) to measure the response of sound speed in soil as a function of moisture content. Electronic equipment was

designed to emit and receive ultrasonic pulses in unsaturated soil at shallow depths. Degree of saturation was plotted against capillary suction to show multiple drying cycles of the soil. The values were then compared to sound speed. The test was conducted in sand and silt loam. For both soil types the sound velocity increased as a function of capillary suction and decreased as a function of saturation. Even with greater soil capillary suction in the silt loam, the velocities in the sand were shown to be higher (Brutsaert et al.,1964).

Arnott et al. (1990) measured acoustic to seismic coupling using a laser-doppler vibrometer (LDV). Acoustic to seismic coupling is the transfer of atmospheric sound waves into poroelastic ground to excite ground motion (Arnott et al., 1990). The results using the LDV were compatible with results using geophones. Hess et al. (1990) conducted studies to characterize the ground by short-propagation measurements. Three properties were extracted: porosity, effective flow resistance, and tortuosity (Hess et al., 1990). Sabatier et al. (1990) also assessed the feasibility of using acoustic techniques such as acoustic reflection and transmission to characterize near-surface soil properties. The goal was to obtain surface air porosity (porosity minus volumetric water content), air permeability, and pore structure up to several centimeters deep. The air porosity obtained from acoustic reflection and transmission was within ten percent of the values gathered from gravimetric techniques (Sabatier et al., 1990).

Sabatier et al. (1996) also states that acoustic wave reflection and transmission, coupling and propagation through rough soils depends on air-porosity, pore tortuosity, air permeability, shape, size and packing density of the roughness elements, soil matrix elastic moduli, and bulk density. At The University of Mississippi National Center for Physical Acoustics (NCPA) the phenomena have been exploited in agricultural soils. The goal of the research is to be able to review and possibly produce in-situ images of the properties at a depth less than one meter. Acoustic attenuation was seen to be strongly dependent on contact strength between soil grains. Wave speed was more affected by soil compaction and shear moduli (Sabatier et al., 1996).

Two years late Berkenhagen et al. (1998) conducted investigations to clearly show that acoustic techniques are capable of measuring soil physical properties in-situ with minimal disturbance to the soil. A study was conducted to observe the sensitivity of seismic compressional waves to monitor structural and mechanical changes in soil. Clay was subjected to a wetting-drying cycle over a few months while acoustic measurements were taken. Large changes in mechanical and structural properties were noticed with changes in wave velocity and attenuation (Berkenhagen et al., 1998).

Instead of wetting and drying cycles, Shields et al. (2000) measured compressional and shear wave velocities in unconsolidated granular media as a function of water vapor content. The granular media chosen were two kinds of glass beads and Ottawa sand. Vapor had minimal effect on wave speed in the sand and glass beads made of titanium and barium oxides. Wave speeds in sodium oxide glass beads doubled with introduction of vapor pressure. The assumption was made that there was a chemical reaction that occurred between the lime glass and the water that formed a gel that in turn increased the velocity of the waves (Shields et al., 2000).

Compressional and shear waves were then measured by Velea (2000) in Ottawa sand in for a different experiment. The sand was placed in a cylindrical tank and velocities were measured horizontally as a function of depth while the zero tension level of water was raised. In the dry sand, velocities varied nonuniformly with depth with the maximum value occurring at about 2/3 the way to the bottom of the tank. After water was added to the bottom of the tank, the nonuniform depth dependence was removed. Velocities decreased at higher saturations until the zero tension level reached the top of the sand. The assumption was made that the nonuniform depth dependence in the dry sand was due to the tank wall supporting part of the gravitational stress in the sand. In conclusion the water-grain contact had little effect on the normal contact stiffness, but the water did reduce tangential contact stiffness to zero (Velea, 2000).

Like the previous two studies, Flammer et al. (2001) studied how water affects acoustic velocities, specifically how acoustics can be used to investigate transient and presumably heterogeneous water infiltration into and redistribution within soils. Spatial and temporal scale of pulse transmission through soils was measured. Using a ten kilohertz pulse with 50 mm wavelength, travel velocities were observed. Velocities and absorption rates behaved as expected with soil moisture variations, but the temporal reaction patterns differed considerably (Flammer et al., 2001).

Acoustics can also be used to predict surface roughness. Chambers et al. (2002) used acoustics to characterize surface roughness in agricultural settings. Sound propagation attenuates more rapidly in soil than in free space due to absorption. Rough surfaces have been known to have different attenuation phenomenon. Effective impedance or reflection coefficient had been used to quantify surface roughness. Experimental data and modeling results were presented over a variety of soil surfaces: impermeable, loosely packed, low sloped perturbations and steeply sloped wedges (Chambers et al., 2002).

Like Chambers, Oelze et al. (2003) measured surface roughness with acoustic backscatter. Four soil plots were constructed with variation in roughness. Acoustic backscatter and a laser microreliefmeter were used to measure the roughness power spectra of the surfaces. Both methods were in agreement for estimating surface roughness. The technique has the potential to evaluate the statistical properties quickly and inexpensively (Oelze et al., 2003).

The next year Blum et al. (2004) measured the spatial and temporal variations of soil water in a column using acoustic pulses emitted from transducers to form a 2D acoustic tomography. Water content was measured with a time domain reflectometer (TDR). Acoustic pulse travel times were converted into velocities distributions and then into water content distributions for two experiments. The preferential flow paths were moved between the two experiments (Blum et al., 2004).

Instead of predicting variations in soil water, Lu et al. (2004) measured acoustic velocity in a triaxial cell with varying compactions. Two air dried remolded soils and an undisturbed field sample were tested. Acoustic velocity and deviator stress both increased linearly in early stage of compaction and nonlinearly during intermediate compaction. Velocities changed little after soil was compacted to failure. Unload-reload cycles proved to have steeply varying velocities and deviator stresses. Hysteric

and load-history-dependent properties were observed (Lu et al., 2004).

For an insitu acoustic approach, Ivanov et al. (2005) conducted a geophysical survey on a single low-conductivity, highly fractured earthen levee in southern Texas. Compressional wave and shear wave refraction tomography and Rayleigh surface-wave analysis using multichannel analysis of surface waves (MASW) were developed. Compressional wave velocity gave reasonable results, but there was no change even after the dam was at full pool for two days. Shear wave velocity changed rapidly in an isolated area most likely due to swelling of the clay core after years of drought (Ivanov et al., 2005). Another survey was performed in southern New Mexico. Compressional wave velocities decreased rapidly during pooling, and the anomaly is isolated to one section where velocities had been unusually high before. The anomaly is likely due to burrowing animals in the dam. Shear wave velocity change was gradual and observed along the whole length of the pond width and below the levee. The change is consistent to shear wave velocity changes in sand due to saturation (Ivanov et al., 2006).

An earthen dam was surveyed by Hock et al. (2007) using MASW and refraction of seismic methods. The dam was built of homogeneous material. The goal was to detect an impermeable barrier (densely packed homogeneous material) in the upstream toe. Compressional and shear wave velocity profiles were collected. No abnormality had been detected using electromagnetic data. The only data that indicated any change was a slight increase in compressional wave velocity. The conclusion was the seismic data were consistent with the electromagnetic data which could not detect the impermeable barrier (Hock et al., 2007).

Other failure modes in earthen dams include piping, seepage and anomalous pore pressures. Seismic imaging could provide valuable preliminary information about the onset of these conditions. Time-lapse measurements taken by Hickey et al. (2009) were conducted on a small earthen dam while internal erosion was occurring. Several refraction surveys were carried out, and images were constructed using a finite-frequency seismic refraction tomography code. Significant temporal changes were observed. The weak zone in the dam was shown by a lower velocity. Passive seismic monitoring measures ambient seismic vibrations. The source of this seismic vibration in the dam was the internal zone of flow. The energy, magnitude and frequency of the source were dependent on the intensity of internal erosion (Hickey et al., 2009).

The same year a preliminary investigation was conducted by Howard et al. (2009) using acoustic to seismic coupling to measure the depth of the top of the fragipan horizon. Soils were analyzed at two sites with different fragipan depths. Acoustic to seismic coupling was shown to be sensitive to the spatial variability of the fragipan. Soil cores and other geophysical methods were used to calibrate the system (Howard et al., 2009).

Like Hickey, Hung et al. (2009) studied seepage-induced acoustic emission. Laboratory experiments were conducted, and the data were analyzed in amplitude, time and frequency domains. The most prominent frequency range was 0.8-10 kHz. The results were then subjected to dimensional analysis where a relationship was established between nondimensional sound pressure level and a nondimensional

frequency. Acoustic emission intensity, seepage velocity, soil and permeant properties were shown to be interrelated. The relationship provided a basis for detecting excessive seepage using monitored seepage-induced acoustic emission intensity (Hung et al., 2009).

Lu et al. (2009) conducted a long-term field survey to monitor and understand temporal variations of sound speed due to changes in physical properties of soils. Ten acoustic probes, five transducers, five tensiometers and five thermocouples were buried at the same depth in a trench of soil-sand mixture. Over two years sound speed, soil temperature, soil moisture, matric potential, surface temperature, and precipitation were measured continuously. Results revealed a power law relationship between matric potential and sound speed. Moisture content and temperature gave relatively minor contributions. The data were in good agreement with theoretical predictions (Lu et al., 2009).

Like Hickey, Hubbard (2010) characterized seepage by using electrical resistivity and MASW instead of geotechnical site characterization of a dam in East Texas. The results of geophysical testing are comparable to conventional geotechnical field and laboratory testing. Soil heterogeneity, resolution capabilities and data smoothing during interpretation can cause some dissimilarities, but low resistivity and low density corresponded with observations of seepage (Hubbard, 2010).

Similar to Lu, Whalley et al. (2011) measured shear wave velocities in three saturated soils as a function of consolidation in a triaxial cell. Plastic and elastic deformations were considered. Relationships between effective stress and shear wave velocities were similar for sand and silt, but the velocities were smaller in clay. No unique correlation was noticed between plastic and elastic deformations. Using empirical shear wave velocity, void ratio and effective stress with a normal consolidation curve, a common curve was constructed from the three soils whether subjected to plastic or elastic deformation (Whalley et al., 2011).

The next year active and passive acoustic techniques were used by Lu et al. (2012) to monitor and assess soil pipeflow and internal erosion. Soil with a six millimeter hole had a constant water head of two centimeters and constant flow rate. Sediment concentration, soil water pressure, and acoustic measurements were taken while the soil was subjected to pipeflow. Active measurements consisted of compressional wave velocities. P-wave velocities reflected the onset of pipeflow, increase in water pressure, saturation of soil around the pipe, variation of water pressure after head removal, and relaxation of soil. The processes can be understood by effective stress's relationship to compressional wave velocity. The passive measurements of ambient and water flow sounds were used to identify and assess pipeflow from time-domain RMS, frequency-domain RMS and contrasts in the power spectrum image (Lu et al., 2012). Passive acoustic emission, self-potential, and cross-hole tomography were assessed by Rinehart et al. (2012) for suitability to remotely and continuously monitor internal erosion and cracking of embankment dams over a long period. The acoustic techniques proved to be useful for monitoring cracking as a precursor to internal erosion (Rinehart et al., 2012).

Unlike the previous techniques, Shin et al. (2012) used acoustic-to-seismic

coupling to noninvasively deduce soil elastic properties. A microphone and LDV were used to get acoustic pressure and particle vibration. A modified Biot theory was used to make a wave propagation model. An optimization process was then used to minimize the difference between the data and model predictions (Shin et al., 2012).

The same year Whalley et al. (2012) discussed the use of shear wave velocities at different matric suctions and confining pressures to extract soil physical properties. Sandy clay loam and loamy sand were tested using a combination of a Bishop and Wesley tri-axial cell, Haines apparatus, and pressure plate apparatus. A single effective stress variable was used to relate shear wave velocities to soil's physical condition. Shear wave velocities were then related to void ratio, net stress, and matric suction by using a set of four parameters common to all soils at different states of saturation and consolidation (Whalley et al., 2012).

Like most of the papers discussed Gao et al. (2013) investigated the relationship between an engineering parameter, penetrometer resistance, and to a physical parameter, small strain shear modulus. Some published equations for predicting shear wave velocity were also tested. Samples were compacted, drained and then measured to get shear wave velocity, compressional wave velocity, and penetrometer resistance. Penetrometer resistance and small strain shear modulus were shown to have a linear relationship that was slightly sensitive to soil type. A possibility was also noticed for estimating matric suction from elastic wave velocity given the void ratio (Gao et al., 2013).

The background literature review reveals geophysical engineering has evolved to measure and model near-surface processes such as soil erodibility, soil stress distributions, soil wetting and slope stability. Root reinforcement of soils has been an active area of research that has accelerated since the 1990s. There are several methods to characterize root matrices and the contribution roots add to the stability of slopes and the erodibility of soil surfaces. Acoustic methods have also been developed to predict soil properties such as density, stress and porosity and to monitor internal changes in soil such as erosion, compaction, and stress redistribution. Research has shown that roots can increase the strength of soils, and acoustic methods have been developed to predict soil properties related to strength of soils. The literature has shown there is a lack of research on the acoustic behavior of soils reinforced with grass roots. The need exists for an acoustic method to predict grass roots' contribution to soil strength. The acoustic method could be used to monitor watershed processes such as levee and dam surface erodibility and slope stability of embankments and stream banks.

9.2 WAVEFORM WATERFALL PLOTS

Below are waterfall plots of the received waveforms from each pair of time of flight measurements. The measurements were taken from when the sod was planted on September 12, 2014 to October 26, 2015. The first arrival picks are shown.

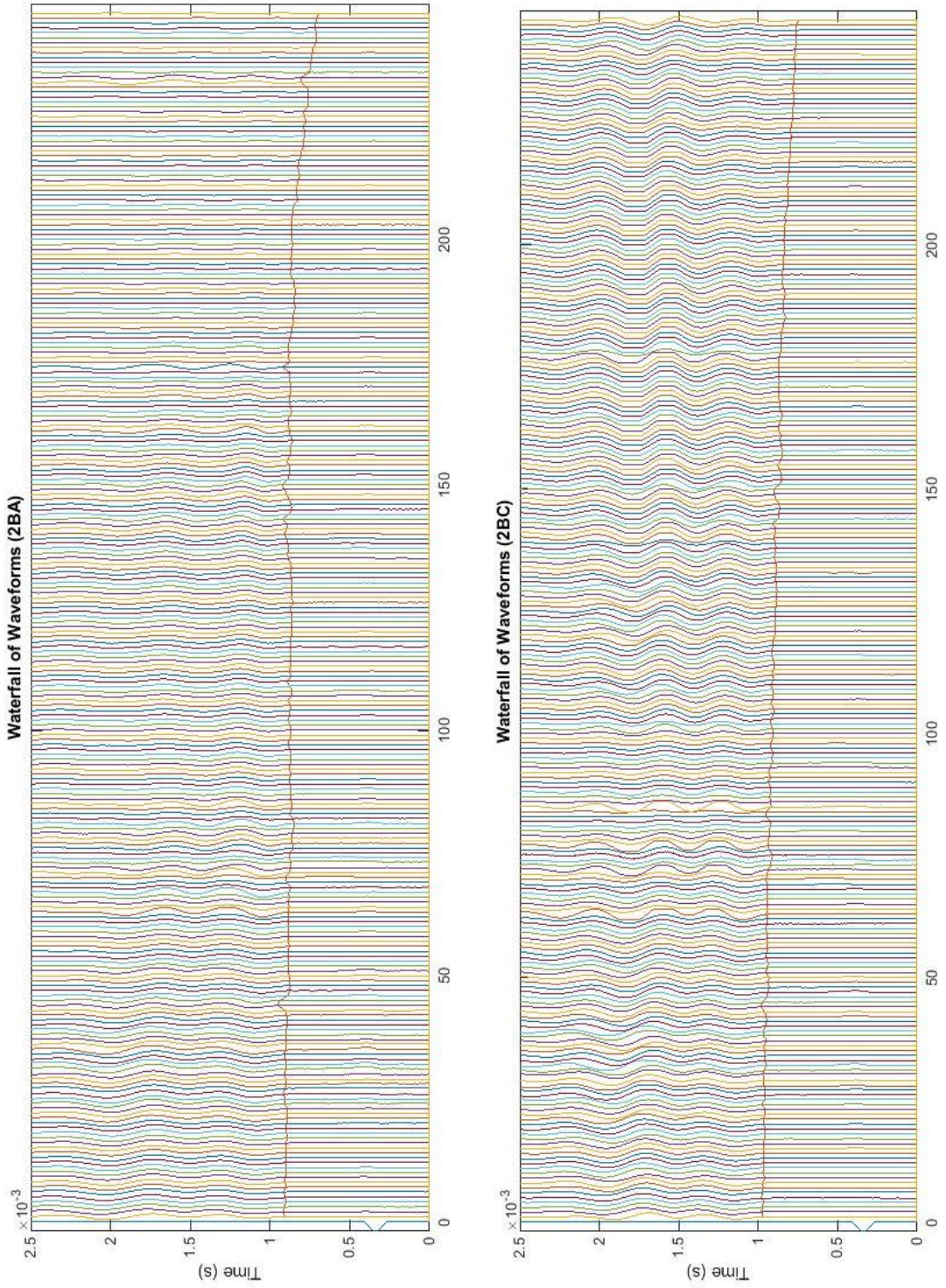

Figure 9.1 Bare soil waterfall plots of waveforms and first arrival picks

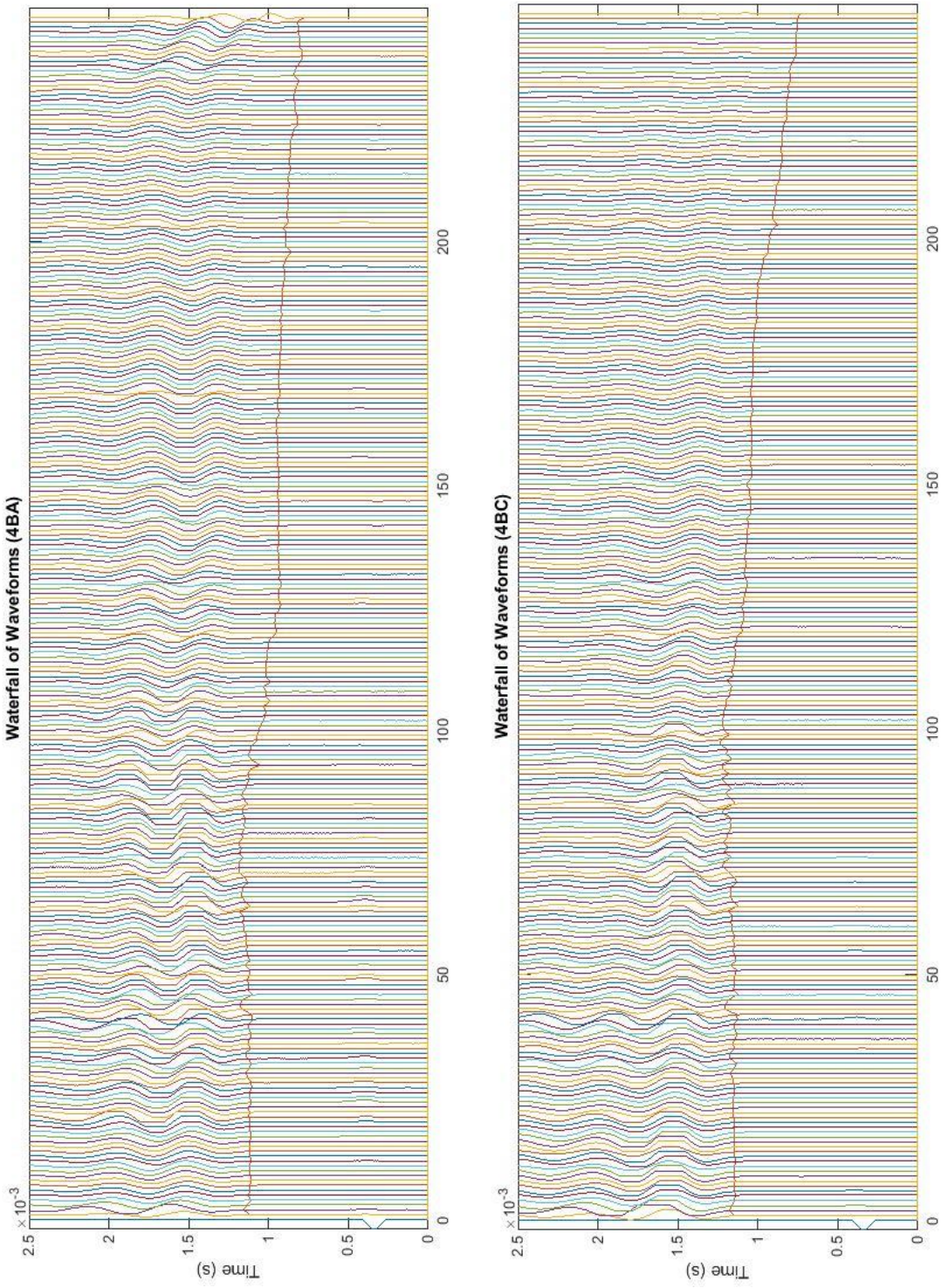

Figure 9.2 Common Bermuda waterfall plots of waveforms and first arrival picks

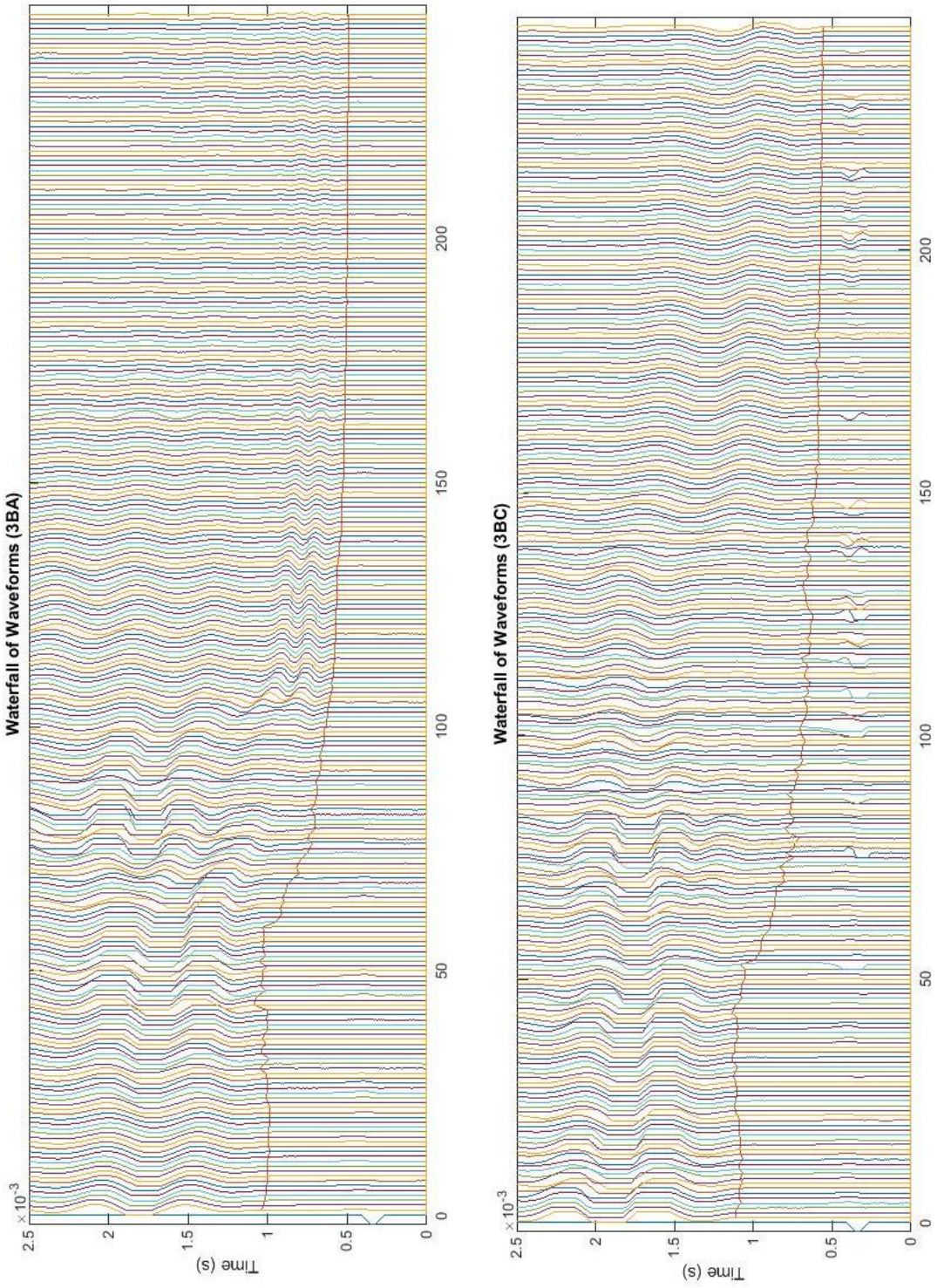

Figure 9.3 Forage Bermuda waterfall plots of waveforms and first arrival picks

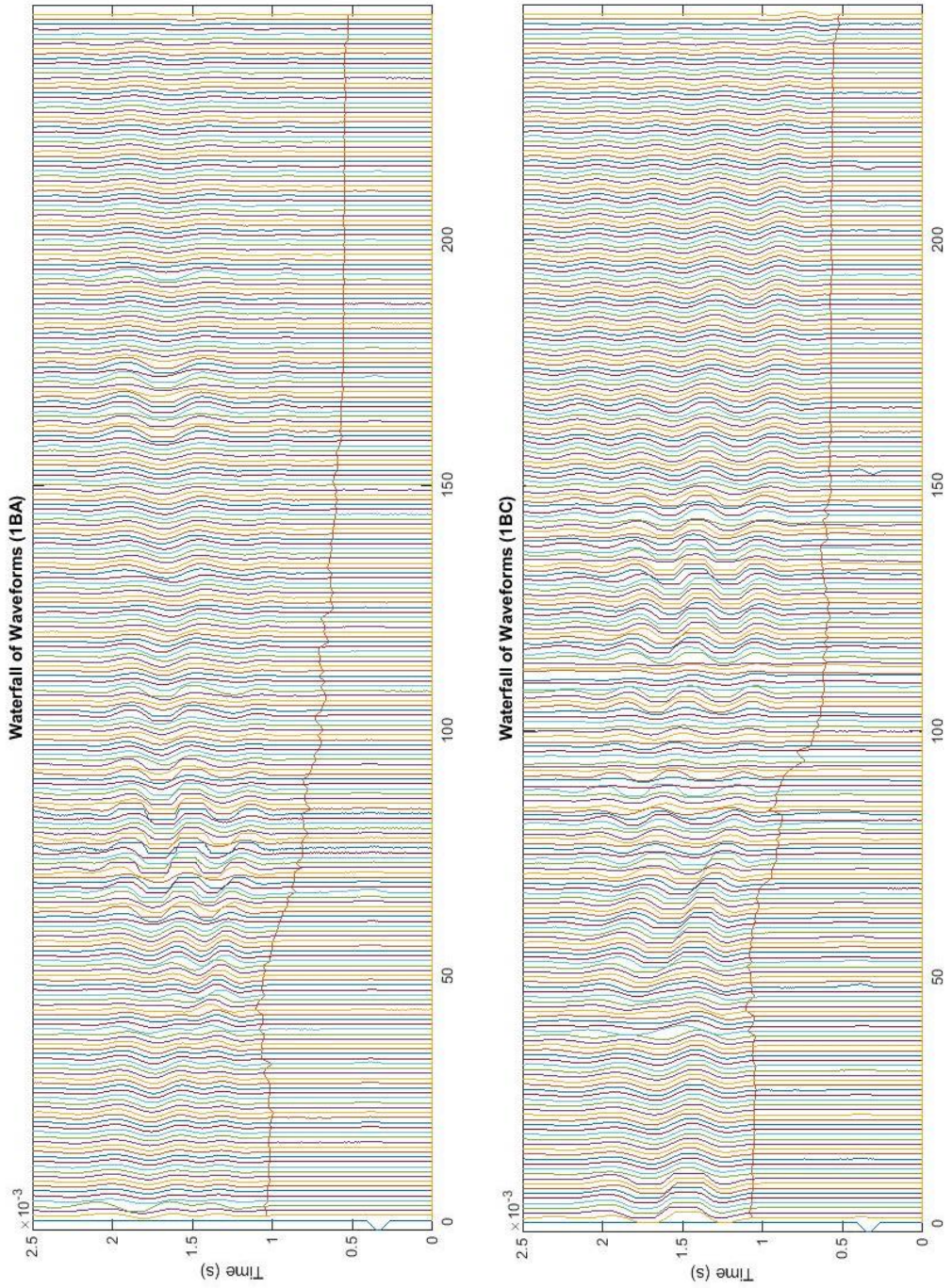

Figure 9.4 Bahia 1 waterfall plot of waveforms and first arrival picks

VITA

Blake Armstrong was born in Madison, MS, to the parents of Gary and Debby Armstrong. He is the younger brother to Brad Armstrong. He attended Madison Station Elementary and continued to Madison Central High School. After graduation, he moved to The University of Mississippi where he was introduced to Civil Engineering. While completing his undergraduate studies, he passed the Fundamental Engineering Exam to become an Engineer in Training. His senior year Dr. Sara Brown asked him if he were interested in enrolling in the Basic Acoustics Summer School under Dr. Craig Hickey of the Porous Media Group at National Center for Physical Acoustics (NCPA). He agreed and spent the summer learning, practicing, and presenting Geophysics. Still working at NCPA the next semester, Dr. Brown encouraged him to continue his education. He obtained a Bachelor of Science in Civil Engineering from The University of Mississippi in December of 2013. He accepted a research assistantship with Dr. Hickey of the Porous Media Group at NCPA. Blake graduated with a Master of Science in Geological Engineering in May of 2016. He is now pursuing a career in Engineering.